Investigation of NIR Dyes with Varying Anchoring Groups Aiming Towards Improved Stability and Efficiency by Rational Molecular Design

DISSERTATION FOR THE DOCTOR OF PHILOSOPHY

Ajendra Kumar Vats

STUDENT ID-18899015

GRADUATE SCHOOL OF LIFE SCIENCE AND SYSTEMS ENGINEERING

KYUSHU INSTITUTE OF TECHNOLOGY

WAKAMATSU, KITAKYUSHU, JAPAN

UNDER THE SUPERVISION OF

PROFESSOR SHYAM SUDHIR PANDEY

Dedicated to my Teachers, my family

And my late grandparents

Acknowledgments

My Dissertation for the Doctor of Philosophy would not have come to successful completion without the help of several people. I take this opportunity to express my sincere gratitude to all of them.

To begin with the deepest sense of gratitude, I wish to express my sincere thanks to my supervisor, **Prof. *Shyam Sudhir Pandey*** who believed in me and allowed me to work under his esteemed supervision for the doctoral program. He is the source of inspiration and enthusiasm and has always motivated me with his devotion, dedication, hard work, optimistic approach, and eagerness to learn new things. I will never forget his endless support and encouragement throughout my research period. I learned a lot from his knowledge, experience, and philosophy of life which molded me into a good human being. His scientific discussion, keen observation, analytical ability, critical comments have nurtured my scientific skill and also inspired me to strive to be a good researcher. I have been fortunate enough as he gave me complete freedom to execute and explore new ideas and assisted me throughout this time when I needed help. Besides as a dedicated guide, he has always come forward as a moral supporter, which has made my stay in Japan more comfortable.

I am also very grateful to *Professor Shuzi Hayase, Professor Tingli Ma, and Professor Tamaki Kato* for providing the excellently equipped laboratory facilities, which has helped me to learn more and get quick results for my research.

I am also very thankful to my University, *Kyushu Institute of Technology* for providing the facility and platform for my research and helping me in managing the necessary criteria for my graduation. In this context, I would like to thank *Masako Hayashi San, Tokuda san, Tamari san, and all the student section staff* for helping me in many ways. I am thankful to *Yukiko Shiraishi San* for managing many cultural events, which has helped me to learn more about the cultures of Japan and other countries. Her jovial nature has helped me in maintaining a good bond. I am highly grateful to *JASSO Foundation* for providing me the financial support for my stay in Japan in my early days.

I am also very thankful to *Dr. Gururaj Shivashimpi (Sr. Scientist in MERCK, India),* for introducing me to Prof Shyam S. Pandey and KIT. I am also thankful to *Dr. Anusha Pradhan*, *Dr. Gaurav Kapil* who have helped me a lot in my research work. I would like to thank full *Dr. Manish*

Pandey to help me stay in Japan. I am also thankful to the entire lab members *of Pandey lab Dr. Atul Shankar Mani Tripathi, Dr. Rakesh Kumar Gupta, Dr. Nikita Kumari, Miss. Pritha Roy, Miss Tang Linjun, Mr. Shubham Sharma, Mr. Balane Epifanio do Rosario, Miss Moulkia Desu, and Mr. Nitin Kumar Singh. I am also thank full to short term student of the* Pandey lab from different universities *Mr. Ali Khalifa, Mr. Ravi Prakash Ojha, Mr. Shubajit Jana, Miss Nidhi Yadav, and miss Yushnita and I am grateful to Hayase Lab members Mr. Kei Tanihira, Dr. Akmal, Dr. Ajay, Mr. Hirotani and all* for aiding me with both research and friendly environment. I am also very grateful to Prof Ma lab Students *Yu San, Yang San.*

I would like to thank full to all my leaders during my industrial tenure and my very close friends *Miss. Nisha, Dr. Amit Pundir, Mr. Yogesh Rajput, Mr. Mukul Chauhan, Mr. Darling Sajan*, and *Dr. Deepak Arora*.

Finally, my Ph.D. endeavor could not have been completed without the endless love, support, tolerance, and blessings from my family. I am also very grateful to my father *Shri Surendra Kumar Vats,* My mother *Mrs. Pushpa Vats*, *my elder sister Miss Minakshi Vats* and my younger brother *Mr. Anupam Vats* and the entire family for their unwavering love and moral support. I am also thankful *to Nilima Mam* for her motherly love and guidance.

Still, many names are missing whose contribution and help are worth mentioning.

Last but not the least, I owe my research to almighty God who has always provide me strength, Patient, wisdom, and calmness in adverse conditions.

ABSTRACT

Natural photosynthesis inspired dye-sensitized solar cell (DSSC) has attracted huge attentions amongst next-generation solar cells owing to their transparency, vivid colors for aesthetic beauty, and very high photo conversion efficiency (PCE) under indoor light conditions. Besides, the cost of fabrication is also envisioned due to the utilization of the low-cost raw materials and processes not demanding for use of high energy. Amongst the next generation, solar cells DSSCs have entered into commercial ventures for the production of solar cell products aiming towards low-end applications. In the last three decades of research and development, DSSCs have witnessed not only very high photon harvesting quantum yield in the visible region (>90%) but also the photo conversion efficiency (PCE) of 12-14 % despite photon harvesting mainly in the 400 nm -700 nm wavelength region. The visible region of the solar spectrum consists of only 45 % of the solar energy while 55 % is still available for energy harvesting. This offers good hope for the design and development of the novel near-infrared (NIR) dyes to have more photon flux harvested leading to further enhancement in the PCE. Besides this, the stability of the DSSCs is another bottleneck towards commercialization, which needs to be solved amicably.

My research was started with the design and development of novel sensitizers with different anchoring groups and having the capability of photon harvesting in the far-red to near infra-red (NIR) wavelength region. To investigate the explicit role of the anchoring groups, the main p-molecular framework of the dye was kept the same. Quantum chemical (QC) calculations utilizing the Gaussian G09 program has been used to design novel dyes suitable for DSSCs utilizing mesoporous TiO_2 and iodine based redox electrolyte. Several anchoring groups including the most commonly used carboxylic and cyanoacrylic acid were taken into consideration during QC calculations. Selection of the anchoring groups was made considering, mode of binding, the strength of binding, and control of dye aggregation behavior. QC calculation was conducted for the estimation of the energetics of dyes, charge distribution, electron density distribution in the highest occupied molecular orbitals (HOMO) and lowest unoccupied molecular orbital (LUMO),

and electronic absorption. A new approach was proposed to construct a theoretical energy band diagram for the sensitizers, which matches very well with the experimental band diagrams.

Based on QC calculations, unsymmetrical squaraine dyes bearing different anchoring groups for their binding on the surface of mesoporous TiO_2 were successfully synthesized, characterized, and subjected to photophysical investigations. Implications of the nature of the anchoring group on device performance and stability after DSSC fabrication were investigated in detail. Adsorption behavior of these dyes on the thin films of mesoporous TiO_2 was investigated and results indicated that the rate of dye adsorption follows the order $-COOH>-PO_3H_2>OH>SO_3H$. At the same time, dye desorption studies demonstrated that the stability of adsorbed dyes on the mesoporous TiO_2 follows the order $-PO_3H_2> >OH>-COOH>-SO_3H$. Despite enhanced dye loading, very high binding strength, and favorable energetic cascade, SQ-143 bearing Phosphonic acid exhibited greatly hampered PCE (0.8 %) compared to that of SQ-138 with carboxylic acid anchoring group (4.1%)

To address the poor photon harvesting issues of dyes with phosphonate anchoring group despite their very strong binding with TiO_2, six unsymmetrical squaraine dyes with varying anchoring groups were rationally designed. A perusal of the binding strength on TiO_2 corroborated that SQ-162 bearing double anchoring groups of phosphonic and acrylic acid exhibited >550 times stronger binding as compared to dye SQ-140 bearing cyanoacrylic acid as anchoring group. SQ-140 exhibited the best photovoltaic performance with very good photon harvesting mainly in far-red to NIR wavelength region with PCE of 5.95 % under 1 Sun solar irradiation. Newly designed dye SQ-162 not only solved the problem of very poor efficiency of dye bearing only phosphonic acid while keeping the high dye loading and extremely high binding strength opening the path of design and development of novel NIR dyes with improved efficiency and stability by further extending the π-conjugation of the main dye molecular framework.

Table of content

Chapter-1

Introduction

1. Introduction

The fast depletion of precious non-renewable energy resources owing to the speedy industrialization encompassing from developed nations to developing countries has brought us to the brink of global warming owing to the enhanced greenhouse gas emissions [1]. This has compelled us towards the utilization of renewable energy resources, amongst them solar energy is one of the plausible due to its huge availability as a gift from Mother Nature [2]. In this context, the utilization of solar cells to tap this immensely available solar energy is going to be a key player to circumvent the issues about the huge energy demands of the future. Even though solar energy is huge but it has to be implemented over a large area to provide sufficient usable energy imposes an obvious need for cost reduction to compete with the energy production cost of fossil fuels [3]. Owing to the utilization of cheap raw materials in combination with low-cost fabrication processes next-generation solar cells such as dye-sensitized solar cells, organic polymer solar cells and recently came in the limelight perovskite solar cells have got considerable attention. Amongst the next-generation solar cells, dye-sensitized solar cells (DSSCs) have attracted a good deal of attention of the material science community owing to the ease of fabrication, aesthetic variable color, transparency, and very high indoor light-harvesting capability [4].

1.1 Futuristic energy problems and solar cell

Scientists and many companies in all over the world are working on the high efficiency, stability, prolonging life time and replacing toxic materials of the solar cell. Lot of research and development has been going on the field of solar cell. Recently Perovskite solar cell comes in the picture and it is the good candidate of the PV technology.

1.2 Next-generation Solar cell: an overview

Next-generation solar cells are PV technology that are potentially able to overcome the Shockley–Queisser limit of 31–41% power efficiency for single bandgap solar cells. This includes semiconducting p-n junctions ("first generation") and thin-film cells ("second generation"). Common third-generation systems include multi-layer ("tandem") cells made of amorphous silicon or gallium arsenide, while more theoretical developments include frequency conversion, (i.e. changing the frequencies of light that the cell cannot use to light frequencies that the cell can

use - thus producing more power), hot-carrier effects and other multiple-carrier ejection techniques. [5-8]

Emerging photovoltaics include:

- Copper zinc tin sulfide solar cell (CZTS), and derivates CZTSe and CZTSSe
- Dye-sensitized solar cells, also known as "Grätzel cell"
- Thin-film organic/polymer solar cells
- Perovskite solar cells
- Quantum dot solar cells

1.2.1 Dye-sensitized solar cells

A dye-sensitized solar cell (DSSCs) as the name suggested solar cell made by dyes means a colored molecule which is the "Heart of the solar cell". The principle of the Dye-sensitized solar cell is based on the combination of photosynthesis and electrochemistry. DSSC mimics the procedure of photosynthesis and with the help of electrochemistry, chemical energy converts into electric energy. Since its inception in 1991 by Grätzel and O-Reagan [9] 1991 demonstrating photo conversion efficiency (PCE) of 7.8 % ignited the field of DSSC research which is proliferating to date. Since then several optimization and improvisation in DSSC and their components like mesoporous TiO_2 [10], redox electrolytes [11], counter electrodes [12], and last but not least sensitizing dyes [13] leading to the proposal of state-of-art DSSCs achieving the PCE of 10-13%, surpassing amorphous silicon solar cells [14-16]. Importance and the critical role of sensitizing dyes in the DSSC working cycle and controlling the PCE are undoubtedly un-questionable and a perusal of state-of-art DSSCs utilizing potential dyes have demonstrated the PCE of >13% despite the photon harvesting only in the visible reason (mainly 400-700 nm) with nearly quantitative photon harvesting [17]. This demonstrates that all of the components of such state-of-art DSSCs are functioning optimally. At the same time, this provides hope for further enhancement in the PCE by design and development of the near infra-red (NIR) sensitizers absorbing beyond 700 nm. Therefore, the logical design of efficient NIR sensitizers and their implementation with several already available efficient visible sensitizers for panchromatic photon harvesting utilizing hybrid and tandem device architecture are expected to further boost the achievable PCE [18-20].

Amongst the principal requirements for an optimal sensitizer of DSSCs such as energetic matching and high molar extinction coefficient, the presence of suitable anchoring is inevitable. Anchoring groups are involved in the fixation of the dye-molecules on the mesoporous wide bandgap semiconductor like TiO_2, ZnO, etc. The nature of the anchoring group affects the PCE by controlling the electron injection from excited dye molecules to the conduction band of TiO_2 depending on the effectiveness of electronic coupling between the excited dye molecules and vacant d-orbitals of the TiO_2 [21]. At the same time, they also control the stability of DSSCs by controlling the strength of binding with the mesoporous wide bandgap semiconductors [22]. Therefore, anchoring groups are highly responsible for controlling the PCE as well the stability of the DSSCs, which currently intriguing issues for the commercialization of the DSSCs. A perusal of the nature of anchoring groups of the dyes reported so far imparting appreciably good PCE, carboxylic and cyanoacrylic acid have shown their dominance and are preferred anchoring groups utilized extensively [23]. Contrary to this, in terms of the stability of DSSCs and their binding strength on the mesoporous TiO_2, they are far-behind the anchoring groups like silyl ester, silatrane, and phosphonic acids [24-26]. The extremely high binding strength of dyes bearing silyl ester anchoring group over the most commonly used carboxylic as well as cyanoacrylic acid functional group of sensitizers has been demonstrated by Kakiage et al and Higashino et al [27-28].

1.2.2 Organic solar cells

Organic photovoltaics (OPVs) has emerged as one of the potential alternatives of the photovoltaics considering the figure of merits like being solution processable, tunable electronic properties, fabrication at relatively low-temperature and low-cost raw materials. Many other PV technologies have higher efficiency as compare to OPVs but due to low material cost, low material toxicity and less environment impact OPVs are more useful technology. Their photoconversion efficiency have been surpassed 13%, which is higher than commercial amorphous silicon solar cells. [29-30]. An OPV cell is a type of solar cell utilizing organic semiconductors (OSC) – as photoactive layer typically either polymers or small molecules. Alternation of the bond i.e., conjugation is highly required for the material to be conducting. Conjugation in these materials leads to electronic delocalization over the entire length of the conjugated backbone. On the other hand, in the inorganic materials, these electrons are the part of the 'highest occupied molecular orbital'

(HOMO). Inorganic semiconductors, higher energy levels are empty and the first such orbital is known as lowest unoccupied molecular orbital (LUMO). The energy gap between the HOMO and LUMO of the OSC is known as the bandgap. Increase in the conjugation of the molecule there is lowering of the bandgap, which can ultimately become suitable for visible light to excite the electron from HOMO to LUMO. Similar to other PV technologies, OPV also generate electricity from light after absorbing photons followed by excitation of the electrons – from the HOMO to the LUMO leaving behind positively-charged 'hole'. These holes and electrons are bound together by Coulombic attractive force forming electron-hole pair, which are most commonly known as an 'exciton'. Dissociation of these photogenerated exciton leads to generation of free electrons and holes, which migrate towards opposite side and this is actually responsible for the flow of the current in the external circuit.

Exciton binding energy, (Eb) is the attractive energy responsible for binding the electron and hole, which is very small (approximately 26 meV) in the inorganic semiconductors owing to their relatively higher dielectric constant. On the other hand, dielectric constants OSCs are relatively lower resulting in to the Eb of 0.3-0.5eV, which makes difficulty in the exciton dissociation by simple thermal energy alone needing two or more OSCs (donor and acceptor molecules) in OPVs. Donor absorbs light followed by exciton generation, which then diffuse towards the interface with the acceptor leading to the exciton dissociation. Although the efficiencies of OPVs are increasing day-by-day after their inception, fundamental limits on their efficiency still remain. In the 1961 by Shockley and Queisser (SQ), [31] in his famous work concluded that for a general p-n junction solar cell, the maximum achievable efficiency is 30%, with an optimum bandgap of 1.1eV. Extension of this SQ models proposed in 1961 to OPVs has led to a range of proposed maximum efficiencies, varying from 15% [32] to beyond 20% [33].

1.2.3 Perovskite solar cells

Perovskites belongs to class of materials bearing crystal structure of $CaTiO_3$ exhibiting interesting properties like superconductivity, magnetoresistance, etc. Perovskite is easy to synthesized are considered the most popular material for solar cells. Due to their unique structure and property it makes them perfect for realizing low-cost and highly promising next generation solar cells. Perovskite solar cells are expected to play a dominant role in the next-generation electric vehicle

batteries, sensors, lasers, and much more. One the organic/inorganic hybrid perovskite material $CH_3NH_3PbI_3$ was first used as a sensitizer by Prof. Miyasaka research group in 2009 as inorganic sensitizer for DSSCs with a liquid electrolyte, which had then furnished an efficiency of 3.8 % [34]. Perovskite solar was reported by Nam Gyu Park group with 6.5 % efficiency, opened a new horizon for the development of efficient perovskite solar cells as the next generation low cost solar cells [35]. Lead (Pb) is the major atom of the perovskite solar cell. Nowadays major research has been focused on the substituting the Pb with other metals to make them stable, environment and human health friendly along with the low-cost for their commercialization.

However, the perovskite $CH_3NH_3PbI_3$ exhibits broad absorption up to 800 nm which is major factor for good light harvesting in the far-red region. Recently research suggest that by substituting the Sn by Pb not only widen the wavelength window up to 1060 nm but also provides the stability to the solar cell. [36]. Perovskites exhibit various properties like broad wavelength light absorption, fast charge carrier separation, long carrier diffusion length, long carrier lifetime, which make them very attractive for the solid-state solar cells. In spite of many existing challenges companies have already thinking about commercialization of this new kind of next generation solar cells. Currently the main target has shifted to improv the efficiency and lower the cost of solar energy harvesting. PbI is one of the biproducts of perovskite generated after decomposition, which known to be toxic and having adverse effect to the human health as well as the environment. Researchers Hebrew University of Jerusalem in Israel, have recently reported about the recoverable triple-oxide mesostructured perovskite solar cells aiming towards a "greener" future.

1.3 Dye-sensitized solar cell

1.3.1 Introduction

The dye-sensitized solar cell is composed of by major components like electrodes made-up of mesoporous semiconductor oxide like Titanium oxide, sensitizing dyes, redox electrolytes, counter electrodes, and transparent conducting glass as substrate. Photo anode made by the dye adsorbed Titanium oxide, platinum coated counter electrode, and electrolyte consisted of I_3^-/I^- redox couple is sandwiched to fabricate the dye-sensitized solar cells. The operating mechanism of the solar cells is shown in Figure 1.

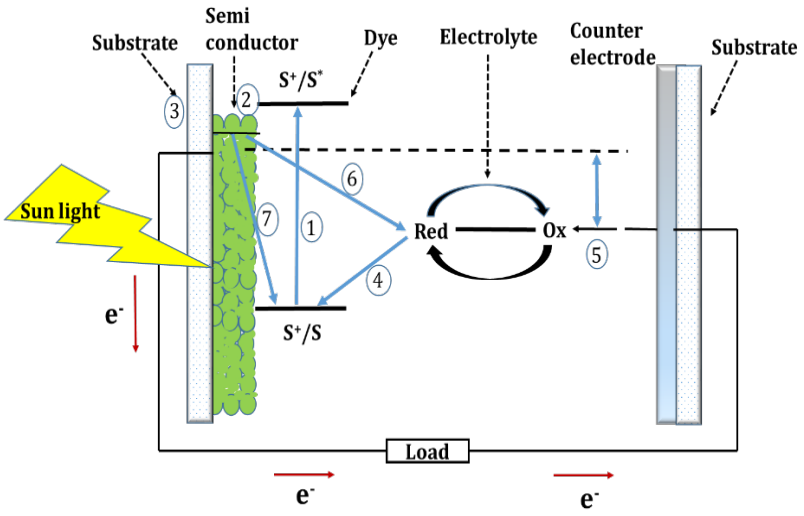

Figure 1. Structure and operating principle of dye-sensitized solar cells.

Upon light irradiation, the dye molecules gets excited and ultra-fastly injected an electron into the conduction band of the semiconductor electrode, then the vacate place in the HOMO of the dye was filled by electron donation from the electrolyte, I_3^-/I^- redox system. The dye regeneration is facilitated via the redox reaction between and by the iodide and triiodide ions with the help of incoming electrons from the counter electrodes completing the circuit.

1.3.2 State-of- art developments

1.3.2.1 Nanocrystalline semiconductor film electrode

Mesoporous semiconducting oxides TiO_2, ZnO, SnO_2, etc. used in DSSCs serve as not only the dye adsorption scaffold but also the carrier of the injected electrons from the sensitizer and transfer to the conducting substrate. Conducting substrate such as conducting glass, metal foil, and flexible polymer film are covered by Titanium dioxide films. There are two most commonly used deposition processes, called doctor-blading, and screen-printing for the preparation of photoanodes of the DSSCs. After deposition of the TiO_2 on the conducting glass sintered the substrate at higher temperature. Two types of the TiO_2 dispersions for making compact and mesoporous layer are being most widely used [37]. Compact layer is prepared by the sol-gel method using titanate as described by Grätzel et al. followed by the autoclaving at $450^0C \sim 500^0C$. After coating this colloidal solution on the conducting substrate followed by its calcination, a few monolayers of TiO_2 are formed. It can also be formed by the treatment with titanium tetrachloride aqueous solution followed by the sintering at $450^0C \sim 500^0C$. This treatment performs the several roles such

suppression of back electron transfer from the conducting glass substrate and increasing the surface area at the mesoporous TiO2 layer leading to enhanced dye loading resulting in to enhanced short-circuit photocurrent density (*J*sc) as well as the open-circuit voltage (*V*oc). Preparation of mesoporous films is most commonly conducted utilizing commercial TiO_2 (P25, Degussa AG, Germany) nanoparticle after making the printable ink. In order to prevent aggregate formation during making printable ink, the P25 powder is ground properly using a small amount of water and α-terpinol and other stabilizers.

Towards commercialization efforts of DSSCs, novel approaches for making thin film of TiO2 on flexible substrates was taken in to the considering. Flexible polymer substrate using conventionally prepared TiO_2 printable paste is un suitable for preparing the photoanode owing to the need for the high sintering temperature of 450^0C~550^0C [38-43]. In this context, different methods have been proposed in the recent past to circumvent this issue. Such methods include sintering of the TiO_2 at relatively lower temperature below 150^0C [44, 45] and a compressing method [46, 47] to achieve an electrically connected TiO_2 networks. Pichot et al. [44] reported the preparation of TiO_2 photoanode using TiO_2 without organic surfactant in order to lower sintering temperature around 100^0C leading to the PCE of 1.2%. Hagfeldt et al. [47] demonstrated a mechanically compressed nanostructured TiO_2 layer on a plastic film yielding PCE of 3.0%. Miyasaka et al. [48-49] demonstrated relatively high PCE up to 4.1% utilizing electrophoreticaly deposited TiO_2 layer followed by chemical treatment and heating at 150^0C for improved necking of the TiO_2 nanoparticles. D¨urr et al. [50] proposed a lift-off method, in which pre-sintered mesoporous layers on a suitable substrate is transferred to a flexible substrate and shown a PCE of 5.8% with flexible PET (polyethylene terephthalate) substrates. Kijitori et al. [51] prepared binder-free coating paste by using TiO_2 sol in acidic aqueous solution as the interconnection agent and coated the paste on ITO/polyethylene-naphthalate (ITO/PEN) film by doctor blading followed by heating at 150^0C to make the photoanode and demonstrated PCE >6% by their plastic DSSCs. Grätzel group [52] developed the high efficiency (7.2%) flexible solar cells based on a Ti-metal foil substrate for photoanode and a Pt-electrodeposited counter electrode on ITO-PEN, which is the highest efficiency for flexible DSSC reported so far.

1.3.2.2 Dye sensitizers

Dye sensitizers can be considered as "the Heart" of the DSSCs, being as the main absorber of the incoming light photons. It should strongly bound to the semiconductor surface and should be able inject the excited electrons efficiently to the conduction band (CB). They should make the favorable energetic cascade between the electron accepting wide band gap oxide semiconductor and redox electrode in order to have facile electron injection and the dye regeneration. Finally, it should be sufficiently stable in order to withstand very high ($>10^8$ redox cycles) upon the exposure to natural light [53]. The sensitizers mainly used in DSSC were divided into two types: organic dye and inorganic dye according to the structure. Inorganic dye includes metal complexes, such as polypyridyl complexes of ruthenium and osmium, metal porphyrin, phthalocyanine, and inorganic quantum dots, while organic dye includes natural organic dye and synthetically organic dye. Polypyridyl ruthenium sensitizers were widely used and investigated for their high stability and outstanding redox properties. The sensitizers must possess a suitable anchoring group such as carboxylate or phosphonate etc. at the right position of the dye molecular framework, which is not only responsible for their attachment on the semiconductor surface but also enable the facile electron injection.

1.3.2.3 Electrolytes

Redox electrolyte is one of the major components for dye-sensitized solar cells. The properties of the electrolyte affect the conversion efficiency and stability of the solar cells. Electrolytes used in DSC are mainly divided into three categories: liquid electrolyte, quasi solid-state electrolyte, and solid electrolyte. Liquid electrolytes are divided in to again of two types i.e., first organic solvent electrolyte and secondly, ionic liquid electrolyte. Due to low viscosity, fast ion diffusion, high efficiency, ease to be designed, and high pervasion into nanocrystalline film electrode [54-57], organic solvent electrolytes were widely used. The composition of the electrolytes includes an organic solvent, redox couple, and additive. Organic liquid electrolytes consist of solvents nitrile such as acetonitrile, valeronitrile, 3-methoxypropionitrile, and esters such as ethylene carbonate (EC), propylene carbonate (PC), γ-butyrolactone. The major and traditional redox couple electrolyte contained I_3^-/I^- couple. $SCN^-/ (SCN)_2$ couple, $SeCN^- / (SeCN)_2$ couple were also shown in the literature [59-60]. Sapp et al [61] although reported the Cobalt (III/II) based redox couple for DSSCs but PCE was far below the performance of that based on the I_3^-/I^- couple. Alkyl

imidazolium cation and lithium cations have been frequently used as the constituents of the I_3^-/I^- redox the couple in DSSC aiming towards forming the Helmholtz layer in order to restrict the direct contact of triiodide with semiconductor surface for hampering the charge recombination by back electron transfer leading to the improved fill factor and PCE. At the same time, high solubility of alkyl imidazolium cations in combination with high activity of iodide led to an increase in the light-harvesting efficiency and the stability of the sensitizer. 4-tert-butylpyridine (TBP) and N-methyl benzimidazole (NMBI) have been frequently used as electrolyte additives in order to suppress the dark current and improve the PCE. TBP has been found to reduce the charge recombination between the CB electrons and oxidized species of the electrolyte leading to remarkable enhancement in the Voc, fill factor and PCE. Due to good chemical and thermal stability, ionic liquids have been found to be better electrolyte as compared to organic solvent-based electrolyte. Kubo et al. [62] investigated the physical and physicochemical properties of 1-alkyl-3-methylimidazolium iodides (alkyl chain: C3–C9). To improve the mobility of the redox couple in the electrolyte and the photovoltaic performance, various ionic liquids with low viscosity were developed [63].

Apart from alkyl imidazolium cation, alkyl pyridinium salt and trialkyl methyl sulfonium-salt-based ionic liquid have also been successfully used making the redox electrolytes of DSSCs. Paulsson et al. [64] reported a PCE of 3.7% for DSSCs based on $(Bu_2Me)SI$ ionic liquid containing 1% iodine while a PCE of 2% was observed in the case of alkyl pyridinium cation-based ionic liquid [65]. Wang et al [66] reported an appreciably good PCE of 7.5% using solvent-free EMISeCN-based ionic liquid containing $(SeCN)_3^-$ /$SeCN^-$ electrolyte. The evaporation of the liquid electrolyte is one the serious problems towards the long-term operation and practical realization of DSSCs. Recently, efforts have been made to improve the long-term stability by using a p-type semiconductor [89, 90] or hole-transporting organic materials [91] to replace a liquid electrolyte. In general, quasi-solid-state ionic liquid electrolyte consisted of I_3^-/I^- couple such as 1-methyl-3- propylimidazolium iodine (MPII) and metal-oxide framework materials were also implemented in DSSC aiming towards forming a liquid channel for the I_3^-/I^- diffusion. Some polymers, [68] low-molecular-weight gelator, and silica nanoparticles have also been used to solidify ionic liquid-based electrolytes in DSSC.

1.4 Squaraine dyes

1.4.1 Introduction

Relatively thinner mesoporous TiO_2 electrodes are higher desired for DSSCs utilizing bulky and slow diffusing cobalt based redox electrolytes and transparent see-through solar cells. Therefore, there is a need for dyes with large molar extinction coefficient in order to tap sufficient photons in relatively thinner TiO_2 layers. Efficient organic dyes with donor-π-acceptor (D-π-A) structure have been proposed, developed and utilized as sensitizers of DSSCs in the recent past. Typically, a suitable anchoring group is introduced in the acceptor part of dye molecules for their attachment on the wide band gap mesoporous TiO_2 surface. The dye molecular structure plays a dominant role in controlling the overall DSSC performance. Good blocking behavior of dye molecules offered by introduction of multiple long alkyl chains as substituent is crucial for successful use in combination with the novel redox mediators based on cobalt redox shuttle-based electrolytes. Steric hinderance by alkyl groups can slow down the electron transfer between TiO_2 and oxidized redox mediator or hole conductor. Amongst various sensitizing dyes, squaraine dyes have attracted a good deal of attentions owing to very large molar extinction coefficient, huge structural variability and tailoring the light absorption window from visible to infra-red (IR) wavelength region of the solar spectrum. The squaraine dye takes its name from its central moiety `squaric acid` which was first introduced by Schmidt in 1980. The main dye molecular structure of the squaraine dyes consists of the central electron-deficient and four membered rings with electron-donating groups on either side and belongs to the class of polymethine Donor-π-Acceptor (D-A-D) dye with zwitterionic structure.

1.4.2 Background

The credit of first report on squaric acid goes to Cohen et al and dates back in 1959. This dibasic acid was prepared by the aqueous hydrolysis of 1,3,3,-triethoxy-2-chloro- 4,4-difluorocyclobutene while presence of the acidic carbonyl group of this molecule was verified since it does not respond to positively to the phenylhydrazine [69]. Synthesis of the first symmetrical squaraine dye was done by Treibs in 1965 by reaction between the squaric acid and pyrrole giving violet-red dye product [60]. Since then, a number of squaraine dyes with different donor groups aiming towards diverse applications in the area of electronics, optoelectronics and sensing came in to the light.

1.4.3 Synthesis and properties

Condensation reaction between the electron deficient squaric acid electron-rich aromatic or heterocyclic compounds like N, N-dialkylanilines, benzothiazoles, phenols etc. easily produces squaraine dyes, which enables synthetic diversity of this squaraine class of dyes aiming towards tuning the dye molecular framework as per the needed applications. In order to synthesize symmetrical squaraine dyes, 2 equivalents of the donor species are reacted with the equivalent of squaric acid. On the other hand, in the case of synthesis of the unsymmetrical dye, squaric acid is first converted to its monoester followed by its hydrolysis, 2nd desired donor moiety is reacted get final desired unsymmetrical squaraine dye [58]. At the same time, condensation of squaric acid with more than one active place with the highly electron-rich donors results in to the high molecular weight dyes with even more narrow bandgaps [70, 61]. Typically, squaraine dyes are planer molecules with extended π-conjugation, which is responsible for shifting the optical absorption window towards the higher wavelength region. Squaraine dyes exhibit sharp and intense light absorption in far-red to NIR wavelength region very high molar extinction coefficient (>10^5 dm^3 mol^{-1} cm^{-1}), which is associated with the Π- Π* electronic transition. Squaraine dyes are highly prone to aggregation due to their rigid and planar structure. They exhibit two types of aggregated species such as H-aggregates and J-aggregates in solutions as well as solid-state. Face-to-face to stacking of the dye molecules leads to the formation of the H- aggregates, while J-aggregates are formed by the head-to-tail stacking of the dye molecules. Formation of the J-aggregates leads lowering of the energy band gap as compared to the monomeric dye leading to the bathochromic shift in the absorption maximum [71]. On the other hand, H-aggregation results in to blue-shifted optical absorption as compared to that of dye monomer absorption. g properties Two-photon absorption (TPA) is another important physical characteristic exhibited by squaraine dyes. The squaraine with highly extended π-conjugation has been reported to show non-linear second-order optical absorption [63].

1.4.4 Applications

i) **DSSCs**: Squaraine dyes are highly suitable for enhancing the efficiency of DSSCs due to the capability of the NIR light harvesting in combination with very high extinction coefficient, which approximately 10-100 times higher than most commonly used ruthenium complex-based sensitizers. This high molar extinction coefficient is also highly suitable for the solid-state DSSCs,

requiring thin layer of dye-adsorbed TiO_2 layer. At the same time, NIR photon harvesting capability of squaraine dyes make them a desirable material candidate for smart windows and tandem DSSC applications [72].

ii) **Organic Light-emitting diode (OLED) and transistor:** NIR sensitive squaraine dyes have also shown their usefulness light sensitive OFETs and photodiodes. Apart from this, broad-band optical telecommunication and sensing are other areas of interesting applications for use of squaraine dyes might play an important role.

iii) **Biosensor and metal ion detector:** Squaraine dyes can also be designed to exhibit very high fluorescence quantum yield and are highly suitable for the application in the area of biosensor as fluorescence probes. Tailoring the molecular structure of the squaraine dyes by introducing suitable ion capturing or ion-coordinating sites make them suitable for the selective detection of metals ions, which in turn can use the health and environmental pollution monitoring.

iv) **Photodynamic therapy:** Squaraine dyes which are sensitive in the long wavelength NIR-IR region possess large penetration depth making them suitable for not only in-vivo bioimaging but also as a sensitizer to kill the living tumor cells. There are also some reports about singlet oxygen generation by squaraine dyes, which finds application in the area of cancer therapy [73-74].

1.5 Existing problems and research motivation

Considering all acute needs of renewable energy shortly and also the depletion of the existing fossil fuel, low-cost energy harvesting especially from renewable resources is inevitable. In this context, DSSCs are one of the potential contenders amongst the next-generation solar cells owing to the low-cost raw materials, processes not needing a clean room, high energy-consuming processes, and Equipment. In the last three Cades, huge efforts have been made in the DSSC research leading to the demonstration of the PCE surpassing amorphous silicon and the start of some commercial ventures. Although, state-of-art DSSCs have achieved PCE 13-14 % despite efficient photo harvesting in the visible wavelength region (400-700 nm), which is far beyond its theoretical limit of 32 % for single-junction solar cells. Therefore, further improvement in the PCE is envisioned by the development of a suitable sensitizer's cable of efficient light absorption and photon harvesting in the far-red to NIR wavelength region, since the visible wavelength region only constitutes 45 % of the solar spectrum. At the same time, to compete with currently available silicon solar cells with the stability of about 20 years, the stability of the DSSCs has to be much

improved from the existing report of about 2.5 years. This motivated me towards the design and development of novel NIR dyes with improved binding strength with TiO2 leading to enhanced DSSC stability.

1.5.1 Aim of the present research

Aim for the research for my doctoral thesis to contribute towards enhancement in the PCE and stability of DSSCs by designing novel sensitizers owing to my chemistry background. Therefore I decided to take the challenge for design novel NIR dyes with narrow and intense light absorption as a sensitizer for DSSC for wide wavelength region photon harvesting in combination with potentially visible light-harvesting dyes developed so far. Development of the visible light sensitive dyes is rather easy owing to their relatively higher band gap, which make rather easy to play with the energetic control requirements of the sensitizer. At the same time, designing NIR dyes needs more careful considerations owing to their small bandgap and there are relatively narrow room to play with the energetics. Therefore, the design of NIR dyes as sensitizers for DSSCs is a challenging task but success leads to break the current PCE bottleneck of 14 %. Implementation of the multiple dyes for DSSCs utilizing hybrid and tandem device architecture has successfully demonstrated, therefore, even the development of NIR dyes with only 5-6 % may lead to the attainment of PCE beyond 15-18 %, utilizing current state-of-art device fabrication, potentially visible sensitizers developed and commercialized so far in combination with the tandem/hybrid device architecture. At the same time, the anchoring group of the sensitizers plays a dominant role not only in controlling the PCE but also the DSSC stability by controlling the strength of binding of the dyes with the mesoporous TiO_2. Therefore, as a chemist not only I can make long-wavelength photon harvesting dyes but also judicious incorporation suitable anchoring group with strong binding. This may lead to the path for the development of stable DSSCs with improved PCE.

1.5.2 Organization of the thesis

The thesis consists of five chapters.

The first chapter deals with the general introduction, which bears the introduction to solar cells with emphasis on the next-generation solar cells considering their need towards the futuristic

energy crisis. The main emphasis has been given to components, fabrication, working principle, and application of dye-sensitized solar cells.

The second chapter comprises the technique used for quantum chemical calculations along with the synthesis/characterization of the novel sensitizers and fabrication of the dye-sensitized solar cells. In a nutshell, this chapter displays the general instrumentation, materials, and methodology adopted for the research theme.

The third chapter deals with the design and development of novel sensitizers with different anchoring groups and having the capability of photon harvesting in the far-red to near infra-red (NIR) wavelength region. Quantum chemical (QC) calculations utilizing the Gaussian G09 program has been used to design novel dyes suitable for DSSCs utilizing mesoporous TiO_2 and iodine based redox electrolyte.

Chapter four comprises the synthesis and photophysical characterizations of novel NIR dyes with varying anchoring groups along with their utilization as sensitizers of DSSCs. The implication of the nature of the anchoring groups on the dye adsorption behavior and their binding strength on the TiO_2 and PCE has been discussed in detail.

In chapter five, efforts have been taken to solve the bottleneck of poor PCE exhibited phosphonate anchoring group by rational molecular design utilizing combined experimental and theoretical approaches. It has been shown that newly designed dye with double anchoring groups consisted of acrylic acid and phosphonic acid exhibited not only very strong binding with TiO2 but also much improved PCE as compared to that dye with a single phosphonic acid anchoring group.

Finally, the last chapter carries the overall conclusion of my research along with prospects of the work carried out.

References

1. H. Lund and B. V. Mathiesen, *Energy*, 2009, 34, 524.
2. A. M. Omer, *J. Agric. Ext. Rural Dev*., 2010, 2, 001.
3. N. F. Voudoukis, *European Journal of Electrical and Computer Engineering*, 2018, 2, 1.
4. M. Freitag, J. Teuscher, Y. Saygili, X. Zhang, F. Giordano, P. Liska, J. Hua, S. M. Zakeeruddin, J-E. Moser, M. Grätzel and A. Hagfeldt, *Nature Photonics*, 2017, 11, 372.
5. *Shockley, W.; Queisser, H. J. (1961). "Detailed Balance Limit of Efficiency of p-n Junction Solar Cells". Journal of Applied Physics. 32 (3): 510. Bibcode:1961JAP....32..510S. doi:10.1063/1.1736034.*
6. *Green, M. A. (2001). "Third-generation photovoltaics: Ultra-high conversion efficiency at low cost". Progress in Photovoltaics: Research and Applications. 9 (2): 123–135. doi:10.1002/pip.360.*
7. *Martí, A.; Luque, A. (1 September 2003). Next Generation Photovoltaics: High Efficiency through Full Spectrum Utilization. CRC Press. ISBN 978-1-4200-3386-1.*
8. *Conibeer, G. (2007). "Third-generation photovoltaics". Materials Today. 10 (11): 42–50. doi:10.1016/S1369-7021(07)70278-X*
9. B. O'Regan and M. Grätzel, *Nature,* 1991, 353, 737-740.
10. M.S. Ahmad, A.K. Pandey, N. Abd. Rahim, *Renewable and Sustainable Energy Reviews*, 2017, 77, 89-108.
11. J. Wu, Z. Lan, J. Lin, M. Huang, Y. Huang, L. Fan, and G. Luo, *Chem. Rev.* 2015, 115, 2136–2173.
12. J. Wu, Z. Lan, J. Lin, M. Huang, Y. Huang, L. Fan, G. Luo, Y. Lin, Y. Xie and Y. Wei, *Chem. Soc. Rev.,* 2017, 46, 5975-6023.
13. A. Mishra, M.K.R. Fischer, P. Bäuerl, *Angew. Chem. Int. Ed. Engl*, 2009, 48, 2474–2499.
14. M. K. Nazeeruddin, F. De Angelis, S. Fantacci, A. Selloni, G. Viscardi, P. Liska, S. Ito, B. Takeru and M. Grätzel, *J. Am. Chem. Soc.* 2005, 127, 16835.
15. A. Yella, H.W. Lee, H. N. Tsao, C. Yi, A. K. Chandiran, Md. K. Nazeeruddin, E. W.G. Diau, C.Y. Yeh, S.M. Zakeeruddin, and M. Grätzel, *Science*, 2011, 334, 629-633.
16. K. Kakiage, Y. Aoyama, T. Yano, T. Otsuka, T. Kyomen, M. Unno and M. Hanaya, *Chem. Commun*., 2014, 50, 6379-6381.

17. S. Mathew, A. Yella, P. Gao, R. H. Baker, B. F. E. Curchod, N. A. Astani, I. Tavernelli, U. Rothlisberger, Md. K. Nazeeruddin and M.Grätzel, *Nature Chemistry*, 2014, 6 , 242–247.
18. L. Zhang, X. Yang, W. Wang, G. G. Gurzadyan, J. Li, X. Li, J. An, Z. Yu, H. Wang, B. Cai, A. Hagfeldt, and L. Sun, *ACS Energy Lett*. 2019, 4, 943–951.
19. A. Islam, Md. Akhtaruzzaman, T. H. Chowdhury, C. Qin, L. Han, I. M. Bedja, R. talder, K. S. Schanze, and J. R. Reynolds, *ACS Appl. Mater. Interfaces*, 2016, 8, 4616–4623.
20. A. Pradhan, MS. Kiran, G. Kapil, S. Hayase, SS. Pandey, *Solar Energy Materials and Solar Cells*, 2019, 195, 122-133.
21. AK. Baranwal, T. Shiki, Y. Ogomi, SS. Pandey, T. Ma, S. Hayase, *RSC advances*, 2014, 4, 47735-47742.
22. G. M. Shivashimpi, SS. Pandey, R. Watanabe, N. Fujikawa, Y. Ogomi, Y. Yamaguchi, S. Hayase, *Journal of Photochemistry and Photobiology A: Chemistry,* 2014, 273,1– 7.
23. T.N. Murakami, E. Yoshida, N. Koumura, *Electrochimica Acta,* 2014, 131, 174–183.
24. L. Zhang and J. M. Cole, *ACS Appl. Mater. Interfaces,* 2015, 7, 3427–3455.
25. B.J. Brennan, M.J.L. Portole's, P.A. Liddell, T.A. Moore, A.L. Moore, D. Gust, *Phys. Chem. Chem. Phys*., 2013, 15, 16605–16614.
26. K. Hanson, M.K. Brennaman, H. Luo, C.R.K. Glasson, J.J. Concepcion, W. Song, T.J. Meyer, *ACS Appl. Mater. Interfaces*, 2012, 4, 1462.
27. K. Kakiage, M. Yamamura, E. Fujimura, T. Kyomen, M. Unno, M. Hanaya, *Chem. Lett.,* 2010, 39(3), 260.
28. T. Higashino, S. Nimura, K. Sugiura, Y. Kurumisawa, Y. Tsuji, and H. Imahori, *ACS Omega*, 2017, 2, 6958−6967.
29. *Molecular Optimization Enables over 13% Efficiency in Organic Solar Cells*, W. Zhao et al., J. Am. Chem. Soc*.,* (2017), DOI:10.1021/jacs.7b02677.
30. Li, S. *et al.* A Wide Band-Gap Polymer with a Deep HOMO Level Enables 14.2% Efficiency in Polymer Solar Cells. *J. Am. Chem. Soc.* jacs.8b02695 (2018). doi:10.1021/jacs.8b02695
31. Shockley, W. & Queisser, H. J. Detailed balance limit of efficiency of p-n junction solar cells. *J. Appl. Phys.* 32, 510–519 (1961).
32. 22 Minnaert, B. & Burgelman, M. Efficiency Potential of Organic Bulk Heterojunction Solar Cells. *Prog. Photovoltaics Res. Appl.* 15, 741–748 (2007).

33. 23 Gruber, M. *et al.* Thermodynamic efficiency limit of molecular donor-acceptor solar cells and its application to diindenoperylene/C 60 -based planar heterojunction devices. *Adv. Energy Mater.* 2, 1100–1108 (2012).
34. Kojima, A.; Teshima, K.; Shirai, Y.; Miyasaka, T., Organometal Halide Perovskites as Visible-Light Sensitizers for Photovoltaic Cells. *Journal of the American Chemical Society* 2009, *131*, 6050-6051.
35. H. Lindstr¨om, A. Holmberg, E. Magnusson, S.-E. Lindquist, L. Malmqvist, and A. Hagfeldt, "A new method for manufacturing nanostructured electrodes on plastic substrates," *Nano Letters*, vol. 1, no. 2, pp. 97–100, 2001.
36. Ogomi, Y., et al., Ch3nh3snxpb(1–X)I3 Perovskite Solar Cells Covering up to 1060 Nm. *The Journal of Physical Chemistry Letters* 2014, *5*, 1004-1011.
37. M. K. Nazeeruddin, A. Kay, I. Rodicio, et al., "Conversion of light to electricity by *cis*-X2bis(2,2_ -bipyridyl-4,4_ - dicarboxylate)ruthenium(II) charge-transfer sensitizers (X = Cl−, Br−, I−,CN−, SCN−) on nanocrystalline TiO2 electrodes," *Journal of the American Chemical Society*, vol. 115, no. 14, pp. 6382–6390, 1993.
38. B. O'Regan and M. Gr¨atzel, "A low-cost, high-efficiency solar cell based on dye-sensitized colloidal TiO2 films," *Nature*, vol. 353, no. 6346, pp. 737–740, 1991.
39. M. K. Nazeeruddin, A. Kay, I. Rodicio, et al., "Conversion of light to electricity by *cis*-X2bis(2,2_ -bipyridyl-4,4_ - dicarboxylate)ruthenium(II) charge-transfer sensitizers (X =
40. Cl−, Br−, I−,CN−, SCN−) on nanocrystalline TiO2 electrodes," *Journal of the American Chemical Society*, vol. 115, no. 14, pp. 6382–6390, 1993.
41. M. K. Nazeeruddin, P. P´echy, T. Renouard, et al., "Engineering of efficient panchromatic sensitizers for nanocrystalline TiO2- based solar cells," *Journal of the American Chemical Society*, vol. 123, no. 8, pp. 1613–1624, 2001.
42. M. Gr¨atzel, "Photoelectrochemical cells," *Nature*, vol. 414, no. 6861, pp. 338–344, 2001.
43. J.-H. Yum, S.-S. Kim, D.-Y. Kim, and Y.-E. Sung, "Electrophoretically deposited TiO2 photo-electrodes for use in flexible dye-sensitized solar cells," *Journal of Photochemistry and Photobiology A*, vol. 173, no. 1, pp. 1–6, 2005.
44. F. Pichot, J. R. Pitts, and B. A. Gregg, "Low-temperature sintering of TiO2 colloids: application to flexible dye-sensitized solar cells," *Langmuir*, vol. 16, no. 13, pp. 5626–5630, 2000.

45. C. Longo, A. F. Nogueira, M.-A. de Paoli, and H. Cachet, “Solid-state and flexible dye-sensitized TiO2 solar cells: a study by electrochemical impedance spectroscopy,” *Journal of Physical Chemistry B*, vol. 106, no. 23, pp. 5925–5930, 2002.
46. H. Lindstr¨om, A. Holmberg, E. Magnusson, S.-E. Lindquist, L. Malmqvist, and A. Hagfeldt, “A new method for manufacturing nanostructured electrodes on plastic substrates,” *Nano Letters*, vol. 1, no. 2, pp. 97–100, 2001.
47. H. Lindstr¨om, A.Holmberg, E.Magnusson, L.Malmqvist, and A. Hagfeldt, “A new method to make dye-sensitized nanocrystalline solar cells at room temperature,” *Journal of Photochemistry and Photobiology A*, vol. 145, no. 1-2, pp. 107–112, 2001.
48. T. Miyasaka, Y. Kijitori, T. N. Murakami, M. Kimura, and S. Uegusa, “Efficient nonsintering type dye-sensitized photocells based on electrophoretically deposited TiO2 layers,” *Chemistry Letters*, vol. 31, no. 12, pp. 1250–1251, 2002.
49. T. Miyasaka and Y. Kijitori, “Low-temperature fabrication of dye-sensitized plastic electrodes by electrophoretic preparation of mesoporous TiO2 layers,” *Journal of the Electrochemical Society*, vol. 151, no. 11, pp. A1767–A1773, 2004.
50. M. D¨urr, A. Schmid, M. Obermaier, S. Rosselli, A. Yasuda, and G. Nelles, “Low-temperature fabrication of dye-sensitized solar cells by transfer of composite porous layers,” *Nature Materials*, vol. 4, no. 8, pp. 607–611, 2005.
51. T. Miyasaka and Y. Kijitori, "High efficient plastic dye-sensitized solar cell based on the low-temperature TiO2 coating method," in *The 16th International Conference of Photochemical Conversion and Solar Storage*, Uppsala, Sweden, July 2006, W4-P-15.
52. S. Ito, N.-L. C. Ha, G. Rothenberger, et al., “High-efficiency (7.2%) flexible dye-sensitized solar cells with Ti-metal substrate for nanocrystalline-TiO2 photoanode,” *Chemical Communications*, no. 38, pp. 4004–4006, 2006.
53. Hagfeldt and M. Gr¨atzel, “Molecular photovoltaics,” *Accounts of Chemical Research*, vol. 33, no. 5, pp. 269–277, 2000.
54. C. Shi, S. Dai, K. Wang, X. Pan, F. Kong, and L. Hu, “The adsorption of 4-*tert*-butylpyridine on the nanocrystalline TiO_2 and Raman spectra of dye-sensitized solar cells in situ,” *Vibrational Spectroscopy*, vol. 39, no. 1, pp. 99–105, 2005.
55. C.-W. Shi, S.-Y. Dai, K.-J.Wang, et al., “Application of 3-hexyl- 1-methylimidazolium iodide to dye-sensitized solar cells,” *Acta Chimica Sinica*, vol. 63, no. 13, pp. 1205–1209, 2005.

56. C. Shi, S. Dai, K.Wang, et al., “Influence of various cations on redox behavior of I^- and I_3^- and comparison between KI complex with 18-crown-6 and 1,2-dimethyl-3-propylimidazolium iodide in dye-sensitized solar cells,” *Electrochimica Acta*, vol. 50, no. 13, pp. 2597–2602, 2005.
57. C.-W. Shi, S.-Y. Dai, K.-J. Wang, et al., “I_3^- /I^- redox behavior of alkali-metal iodide complexes with crown ether/cryptand macrocycles and their applications to dye-sensitized solar cells,” *Chinese Journal of Chemistry*, vol. 23, no. 3, pp. 251–254, 2005.
58. Z.-S. Wang, K. Sayama, and H. Sugihara, “Efficient eosin Y dye-sensitized solar cell containing Br^-/Br^- 3 electrolytes," *Journal of Physical Chemistry B*, vol. 109, no. 47, pp. 22449–22455, 2005.
59. B. V. Bergeron, A. Marton, G. Oskam, and G. J. Meyer, "Dye-sensitized SnO2 electrodes with iodide and pseudohalide redox mediators," *Journal of Physical Chemistry B*, vol. 109, no. 2, pp. 937–943, 2005.
60. G. Oskam, B. V. Bergeron, G. J. Meyer, and P. C. Searson, “Pseudohalogens for dye-sensitized TiO2 photoelectrochemical cells,” *Journal of Physical Chemistry B*, vol. 105, no. 29, pp. 6867–6873, 2001.
61. S. A. Sapp, C. M. Elliott, C. Contado, S. Caramori, and C. A. Bignozzi, "Substituted polypyridine complexes of cobalt (II/III) as efficient electron-transfer mediators in dye-sensitized solar cells," *Journal of the American Chemical Society*, vol. 124, no. 37, pp. 11215–11222, 2002.
62. W. Kubo, T. Kitamura, K.Hanabusa, Y.Wada, and S. Yanagida, “Quasi-solid-state dye-sensitized solar cells using room temperature molten salts and a low molecular weight gelator,” *Chemical Communications*, no. 4, pp. 374–375, 2002.
63. H. Paulsson, A. Hagfeldt, and L. Kloo, "Molten and solid trialkyl sulfonium iodides and their polyiodides as electrolytes in dye-sensitized nanocrystalline solar cells," *Journal of Physical Chemistry B*, vol. 107, no. 49, pp. 13665–13670, 2003.
64. P. Wang, S. M. Zakeeruddin, J.-E. Moser, R. Humphry-Baker, and M. Gr¨atzel, “A solvent-free, $SeCN^-$/$(SeCN)_3^-$ based ionic liquid electrolyte for high-efficiency dye-sensitized nanocrystalline solar cells,” *Journal of the American Chemical Society*, vol. 126, no. 23, pp. 7164–7165, 2004.

65. H. Matsui, K. Okada, T. Kawashima, et al., “Application of an ionic liquid-based electrolyte to a to a 100 mm×100 mm sized dye-sensitized solar cell,” *Journal of Photochemistry and Photobiology A*, vol. 164, no. 1–3, pp. 129–135, 2004.
66. Q.-B. Meng, K. Takahashi, X.-T. Zhang, et al., “Fabrication of an efficient solid-state dye-sensitized solar cell,” *Langmuir*, vol. 19, no. 9, pp. 3572–3574, 2003.
67. U. Bach, D. Lupo, P. Comte, et al., “Solid-state dye-sensitized mesoporous TiO2 solar cells with high photon-to-electron conversion efficiencies,” *Nature*, vol. 395, no. 6702, pp. 583–585, 1998.
68. J. Kang, W. Li, X. Wang, Y. Lin, X. Xiao, and S. Fang, “Polymer electrolytes from PEO and novel quaternary ammonium iodides for dye-sensitized solar cells,” *Electrochimica Acta*, vol. 48, no. 17, pp. 2487–2491, 2003.
69. Y. Ren, Z. Zhang, S. Fang,M. Yang, and S. Cai, “Application of PEO based gel network polymer electrolytes in dye-sensitized photoelectrochemical cells,” *Solar Energy Materials and Solar Cells*, vol. 71, no. 2, pp. 253–259, 2002.
70. L.Wang, S. Fang, Y. Lin, X. Zhou, and M. Li, "A 7.72% efficient dye-sensitized solar cell based on novel necklace-like polymer gel electrolyte containing latent chemically cross-linked gel electrolyte precursors," *Chemical Communications*, no. 45, pp. 5687–5689, 2005.
71. F. Cao, G. Oskam, and P. C. Searson, "A solid-state, dye-sensitized photoelectrochemical cell," *Journal of Physical Chemistry*, vol. 99, no. 47, pp. 17071–17073, 1995.
72. J. Wu, Z. Lan, D. Wang, et al., “Gel polymer electrolyte based on poly (acrylonitrile-*co*-styrene) and a novel organic iodide salt for quasi-solid state dye-sensitized solar cell,” *Electrochimica Acta*, vol. 51, no. 20, pp. 4243–4249, 2006.
73 L. Guo, S.-Y. Dai, K.-J. Wang, X.-Q. Fang, C.-W. Shi, and X. Pan, "Dye-sensitized nano-TiO2 thin membrane solar cells based on P(VDF-HFP)-type gel electrolytes," *Chemical Journal of Chinese Universities*, vol. 26, no. 10, pp. 1934–1937, 2005.
74 S. Dai, J. Weng, Y. Sui, et al., “The design and outdoor application of dye-sensitized solar cells,” to be available online in *Inorganica Chimica Acta*.

Chapter-2

Experimental (Instrument and characterization)

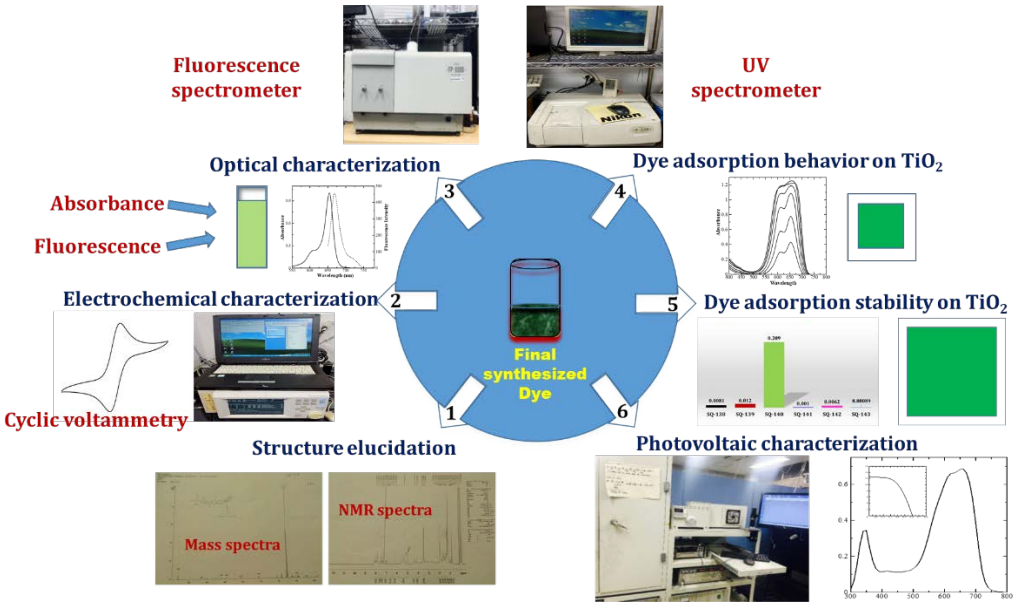

2.1 Synthesis and characterization

The production of a substance by the union of chemical elements, groups, or simpler compounds or by the degradation of a complex compound called synthesis. Electrons are involved in the formation of a bond. Bonds like a covalent bond, ionic bond, non-covalent bond like Vander-wall interaction, London forces, and hydrogen bond play an important role in molecule formation [1]. Molecular computational designing is the first step for getting the idea about the molecule, its energy, and quantum states. Then the synthesis part comes into the picture. On the initial level of the characterization, synthetic molecule confirmed by chromatographic techniques like TLC and HPLC, etc. after the confirmation of the reaction, phase separation comes into consideration followed by purification by different techniques like Precipitation, crystallization, and chromatographic technique like HPLC, Column chromatography, etc. as shown in the figure-1.

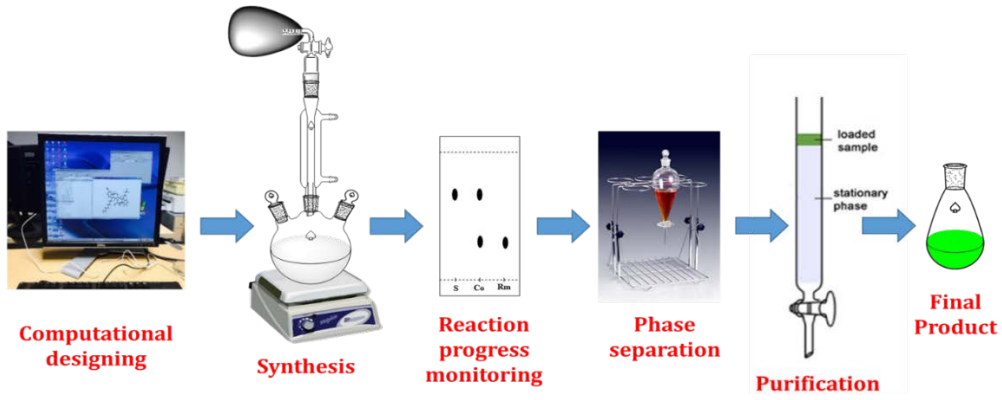

Figure-1. A Pictorial representation of the organic synthesis. MO calculation to the final product formation.

2.1.1 Theoretical Molecular Orbital Calculations

Wave-particle duality of electrons emanating from the combination of De-Broglie principle and Planks theory is one of the important discoveries in Physics. Later, concept of the wave function representing electron clouds [2] led Erwing Schrodinger to propose his famous 'Schrodinger's wave equation for a particle moving in the one-dimensional box, which was then extended to the motion in three dimensions. This equation describes the changes in wave function as a function of time and spatial position due to quantum effects.

The Hartree Fock method: This is an approximation proposed solve the Schrodinger wave equation for multi-electronic system. It is utilized to estimate the wave function and energy for electrons under consideration in molecular system consisted of the multiple number of electrons, which now most popular as the Self-consistent Field Method (SCF). In this method, Hartree proposed to solve the Schrodinger equation for Z/2 of one-particle in the potential zone contributed by the nucleus and the other electrons by charge density iteration in order to get the Z electron wave functions. Then from the potential of individual wave function contributed from both the nucleus and other electrons [3], the Z/2 Schrodinger equations are solved again. Fock then modified Hartree's method by the introducing anti-symmetry as required by fermions as well as Pauli's exclusion principle (Slater determinant) [1].

$$\boldsymbol{\epsilon i \Psi i}\ (\boldsymbol{r}) = (-\mathbf{1}\mathbf{2}\boldsymbol{\nabla}\mathbf{2}+\boldsymbol{vion}\ (\boldsymbol{r}))\ \boldsymbol{\Psi i}\ (\boldsymbol{r}) + \Sigma\int \boldsymbol{dx'j}|\boldsymbol{\Psi j}\ \boldsymbol{r'}|\mathbf{2}|\boldsymbol{r}-\boldsymbol{r'}|\boldsymbol{\Psi i}\ (\boldsymbol{r}) - \Sigma\boldsymbol{\delta\sigma i\sigma j}\int \boldsymbol{dx'j\Psi j}\ *\boldsymbol{\Psi i}\ (\boldsymbol{r'})$$
$$|\boldsymbol{r}-\boldsymbol{r'}|\boldsymbol{\Psi j}\ (\boldsymbol{r}) \ldots\ldots\ (\mathbf{1})$$

The first term represents the kinetic energy and electron-ion potential. The second term represents the "Hartree" term, which bears the electrostatic potential from the charge distribution of N electrons. The third term known as the "exchange" term, is implied only on electrons with the twin spin and is taken from the Slater determinant form of the wave function respectively.

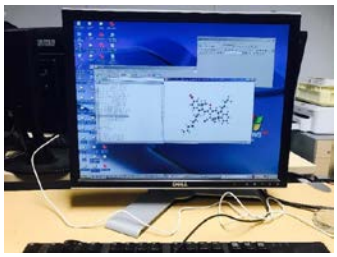

Figure-2. Gaussian program package utilized for the theoretical MO calculations

Density Functional Theory (DFT): Density Functional Theory was introduced by Koch and Holthausen. This theory eliminates the multi-body electronic wave functions as implemented in the Hartree Fock method considering the fact that electron density is rather more relevant [2]. Here it was considered that distribution of the energy is dependent on the electron density, which adopts the minima for the ground-state. Therefore, a modified version of DFT, Time-Dependent (TDDFT) calculation determines the more reliable transition energy rather than the excited state's total energy [4]. The time-dependent Kohn–Sham equation is given by

$$[-\mathbf{12}\nabla\mathbf{2}+\boldsymbol{veff}(\boldsymbol{r},\boldsymbol{t})]\boldsymbol{\Psi}(\boldsymbol{r},\boldsymbol{t})=\boldsymbol{i}\partial\partial\boldsymbol{t}\boldsymbol{\Psi}(\boldsymbol{r},\boldsymbol{t})\ldots..(\mathbf{2})\ \boldsymbol{veff}(\boldsymbol{r},\boldsymbol{t})=\boldsymbol{v}(\boldsymbol{t})+\boldsymbol{vSCF}(\boldsymbol{r},\boldsymbol{t})\ \boldsymbol{veff}(\boldsymbol{r},\boldsymbol{t})$$

And $\boldsymbol{\Psi}$ ($\boldsymbol{r}$, $\boldsymbol{t}$) are the potential and orbitals of an independent particle system where $\boldsymbol{\Psi}$ ($\boldsymbol{r}$,) yield the same charge density as in the interacting system. $\boldsymbol{v}$ ($\boldsymbol{t}$) and $\boldsymbol{vSCF}$ ($\boldsymbol{r}$, $\boldsymbol{t}$) is the applied field and the SCF field. In order to perform such mathematical calculations, a Gaussian program version G09 was used. In order to prepare the input file for calculation of the desired molecular structure and visualization of the calculated results, Gauss-view software (version-5) was used as graphical-user interface [2].

2.1.2 Electronic absorption spectra

In the electronic absorption spectra, electrons are excited from their lower energy level to a higher energy level by the photon energy provided by the spectrophotometer. The absorption of the radiations like UV-vis, Near Infrared, is measured concerning wavelength [5].

We have used the Jasco V-530 UV-VIS spectrophotometer for the absorption spectra analysis. 5µM ethanolic solution of the respective dyes in cell and glass substrate coated with TiO_2 for the solid-state absorption spectra have been used.

Figure -3. UV-Visible spectrophotometer used for measuring the electronic absorption spectra.

In the measured absorption spectrum, one can see a peak associated with d-d or Metal to Ligand transition in the case of transition metal complexes, while and π- π* transition is more prevalent in the organic compound [6]. Upon the absorption of the photons by a molecule they undergo excited state followed returning to the ground state in the absence some electron acceptors. Efficiency of light absorption by a molecule can be represented in terms of its molar extinction coefficient and the absorbance using the following relation:

$$A = \log I_0 / I$$

Where I_0 and I are the incident and transmitted light intensities, respectively.

$$A = \varepsilon cl$$

$$Or, \varepsilon = A/cl$$

Where, A, ε, c, and l are absorbances, molar extinction coefficient, concentration, and length of the cell respectively.

2.1.3 Fluorescence Spectroscopy

Fluorescence comes under category of photoluminescence, where optical excitation leads to boosting electrons in a molecule from their ground state to the singlet excited state. In this excited state molecules loose some energy by vibration relaxations as well as molecular collisions and returns back to the ground state by emitting photons of relatively higher wavelength [7-8]. This why emission spectrum just a mirror image of the electronic absorption spectrum. The shift in the maxima of absorption and emission spectra is most commonly known as Stokes shift. Rigid molecules show very small stokes shift, while molecules having free rotating groups or flexible polymers exhibit relatively large Stokes shift. Emission spectrum of molecules in solution or solid-state is measured by Fluorescence spectrometer and in my research I used a fluorescence spectrometer fluorescence and fluorescence lifetime measurement system (Quantarus Tau Model C-11370, Hamamatsu Photonics, Japan). Samples were excited by laser light source at wavelength of 470 nm and fluorescence was measured.

Figure-4. Fluorescence and fluorescence lifetime measurement system.

2.1.4 Nuclear Magnetic Resonance

2.1.4.1 ^{1}H NMR

Many nuclei have a spin and all nuclei are electrically charged, if the external field is applied, an energy transfer is possible between the base energy to a higher energy level. The energy transfer takes place at a wavelength that corresponds to radio frequencies and when the spin returns to its base level energy is emitted at the same frequency.[9] NMR spectroscopy is an excellent method and tool for the precise structure characterization and elucidation of organic and bio-molecules. NMR is most suited for the analysis of the pure compounds so we can say this technique is used for quality control. NMR can be used to determine the molecular conformation in the solution as well as studying the physical properties at the molecular level like a conformational exchange, phase changes, solubility, and diffusion.

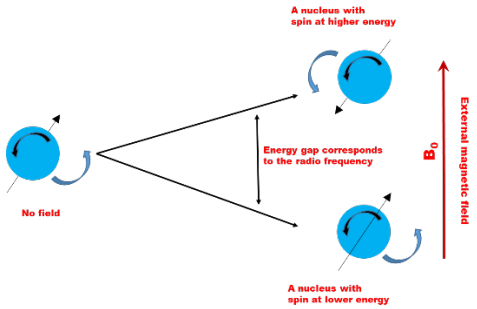

Figure-5. The basic principle of the NMR spectroscopy.

2.1.5 Mass Spectroscopy

To estimating the mass-to-charge ratio of the ions, mass spectrometry is a very important tool in the field of chemistry. This results in a typical spectrum called mass spectrum which is the plot presentation of the ion signal as a function of the mass-to-charge ratio. To elucidate the chemical structure, isotopic or elemental identification of the molecules, and other chemical compounds characterization, these spectrums are used [10].

2.1.5.1 Fast Atom Bombardment ionization mass spectrometer (FAB Mass spectrometer)

The concept and design of the FAB mass involve the bombardment of a solid spot of the analyte/matrix mixture on the end of a sample probe by a fast particle beam (figure-6). The matrix (a small organic species like Dithiodiethanol etc.) is used to keep a homogenous sample surface.

Some species are ejected (sputtered) from the surface as secondary ions by this process. These ions are then extracted and focused before passing to the mass analyzer [11].

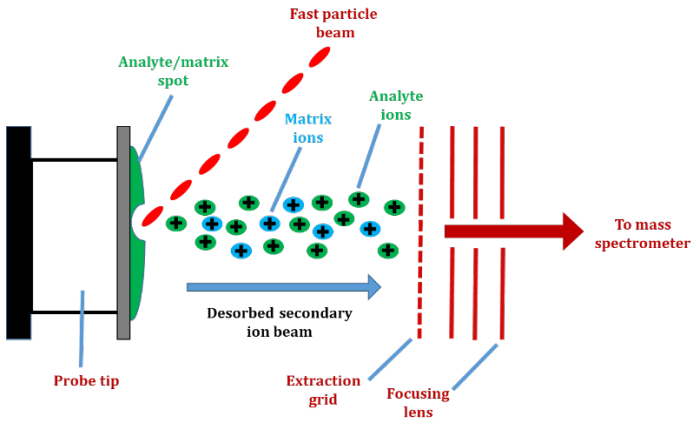

Figure-6. Principle of the FAB-Mass spectroscopy.

In FAB, the particle beam is a neutral inert gas (Ar or Xe) at 4-10 keV. This is the 'soft' ionization method. Very little residual energy is possessed by the ions after desorption - making them particularly suited to the analysis of low volatility analytes [12]. The resulting spectra were obtained in the form of molecular species (e.g. $[M+H]^+$ and $[M+Na]^+$) with some minor structural fragmentation. In the lower mass region of the spectra, matrix and matrix/salt cluster ions obtain. Fab mass techniques have been largely superseded by the superior techniques of electrospray ionization (ESI) and matrix-assisted laser desorption/ionization (MALDI).

2.1.5.2 Matrix-Assisted laser Desorption Ionization Time-of-Flight Mass Spectrometry (MALDI-TOF MS)

In mass spectrometry, MALDI-TOF also a soft ionization technique for the estimation of the mass-to-charge ratio. This technique works on the laser energy absorbing matrix to create ions from a large molecule with small fragmentation [13] Matrix for this technique should be chemically inert and should not be decomposed under analysis. The mechanism of MALDI consist of three steps [14]: Firstly, Formation of a 'Solid Solution' is essential for the matrix to be in excess thus leading to the analyte molecules being completely isolated from each other.

(ii) Matrix Excitation: The laser beam is focused on the surface of the matrix-analyte solid solution. The matrix chromophore absorbs the lase irradiation causing rapid vibrational excitation, bringing about localized disintegration of the solid solution.

(iii) Analyte Ionization: The photo-excited matrix molecules are stabilized through proton transfer to the analyte. Cation attachment to the analyte is also encouraged during this process. These ionization reactions take place in the desorbed matrix-analyte cloud just above the surface. For an experiment, the sample dissolves in any organic solvent-based on the solubility and mixes with the matrix. The mixture was then inserted on the MALDI-TOF plate which was then allowed for drying followed by inserted into the instrument and record the spectrum by running the program.

2.1.6 Cyclic voltammetry

Cyclic voltammetry (CV) is an important and widely used electroanalytical technique in the field of electrochemistry. CV is used for various purposes like redox processes, to determine the stability of reaction products, the presence of intermediates in redox reactions [15] electron transfer kinetics, [16], and the reversibility of a reaction [17]. Concentration is proportional to the current in a reversible, Nernstian system, the concentration of an unknown solution can be determined by generating a calibration curve of current vs. concentration. In the DSSC research CV is one of indispensable tool for characterization sensitizing dyes, redox electrolyte as well as counter electrodes. Apart from this, HOMO energy level of dyes can be easily estimated by CV from the 1st oxidation peak. Bis (cyclopentadienyl) iron (II) or ferrocene, Fe $(C_2H_5)_2$ is one of the most studied organometallic molecules. It bears a sandwich structure, where the iron sandwiched between two cyclopentadienyl rings (Figure-7). Additionally, it is a well-established [18] one-electron donor (n = 1). The discovery of ferrocene by Pauson and Miller revolutionized the area of organometallic chemistry [19].

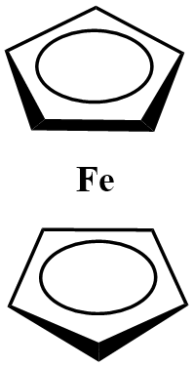

Figure-7. Structure of Ferrocene

It is well known that ferrocene easily undergoes one-electron oxidation to form ferrocenium cation in a reversible manner [20-22]. (Figure-8).

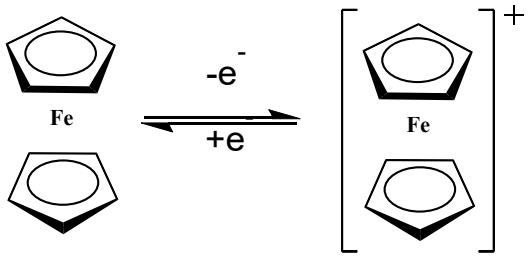

Figure-8. Reversible one electron redox reaction of the ferrocene molecule.

Thus, ferrocene has been widely used as the reference standard along with Tetrabutylammoniumhexaflourophosphate (NBu_4PF_6) as a supporting electrolyte for electrochemical characterization. Electrochemical characterization of the sensitizing dyes was carried out on an auto polarization system HSV-100, Hakuto Denko, japan as shown in (figure-9) by using 0.2 mM solution of the respective dye and Tetrabutylammoniumhexaflourophosphate NBu_4PF_6)(0.1M) as a supporting electrolyte in Dimethylformamide against Ferrocene (0.2 mM) as the reference standard and Tetrabutylammoniumhexaflourophosphate (NBu_4PF_6)(0.1M) as a supporting electrolyte in DMF.

Figure-9. An auto-polarization system (HSV-100) used for the CV measurement in this work.

CV measurement was carried out under different scan rates 100 mV/S or 20 mV/S. The concentration of the supporting electrolyte has been taken high as compare to dye to increase the conductivity in the solution. The first oxidation peak of the sample curve was considered as the HOMO value after calibration with the ferrocene. HOMO was estimated against the first oxidation peak of the ferrocene which is reported (-5.01) [23].

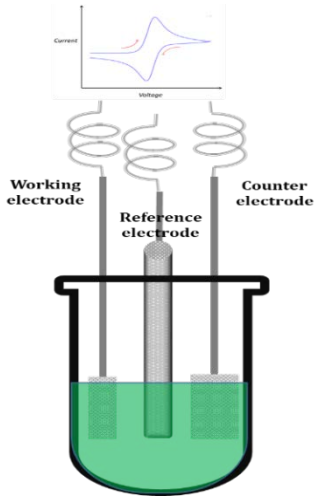

Figure-10. Electrochemical cell used for the cyclic voltammetry

The electrochemical cell for the cyclic voltammetry containing three-electrode, working electrode, the counter electrode, and the reference electrode is needed to dip in the analyte solution. In this work, Pt foil was used as working and counter electrodes, while saturated calomel electrode (SCE) has been used as reference electrode.

Commonly used counter electrode is made up of platinum and graphite. The counter electrode is also known as the auxiliary or second electrode. The counter electrode can be any material that can conduct the current easily. The counter electrode does not react with the solution this is the only source of the electrons to complete the circuit depending on the reaction happening on the working electrode. Supporting electrolytes is generally an ionic solution, a high concentration of the supporting electrolyte is used because it provides high conductivity to the solution. Electrolyte plays a very important role in the estimation of the HOMO-LUMO due to its high conductivity behavior resulting minimizes the IR drop such as record potentials correspond to the actual potentials.

2.2 Fabrication of Dye-sensitized Solar Cells (DSSCs)

Dye-Sensitized Solar Cell consists of three major components like photoanode (working electrode), a counter electrode, electrolyte and their optimum functioning is high desired for the fabrication of efficient DSSCs. Past three decades have witnessed the huge research and development on this aspects leading to modern state-of-art DSSCs surpassing the PCE of amorphous silicon solar cells.

2.2.1 Preparation of photoanodes

Fluorine-doped tin oxide (FTO) conducting glass substrate was first cut followed by washing in detergent and sonicated in distilled water, acetone, and isopropanol, respectively, for 10 minutes. UV-ozone treatment was ten performed for 10 min to clean the surface prior to dipping in 40 mM aqueous $TiCl_4$ at 80^0C for one hour. Surface treated substrates thus obtained were rinsed by in distilled water and the sintered at 500^0C for one hr. in a muffle furnace as shown in the Fig. 11.

Figure-11. Photograph of the muffle furnace used to prepare TiO_2 coated FTO glass substrate.

$TiCl_4$ surface treated substrates were then coated with the mesoporous TiO_2 paste (Solaronix Ti-Nanoxide D/SP) by screen printing as shown in the Figure-12 using a metal mask of pre-defined area. After screen printing of the mesoporous TiO2 layer, it was baked in the muffle furnace at 500^0C in order to remove binder and solvents present in the printable paste leaving pore TiO_2. The TiO_2 coated FTO substrates after getting the desired thickness by repeated coating and baking process was finally subjected $TiCl_4$ treatment followed by final sintering at 500ºC for 30 min. TiO_2 coated substrates thus obtained were taken out from the furnace and dipped in the dye solution while hot and then left at room temperature for the dye adsorption. After complete dye adsorption, the substrates are taken out and then rinsed in the respective solvent to remove the physically adsorbed dye molecules finalizing the working electrode.

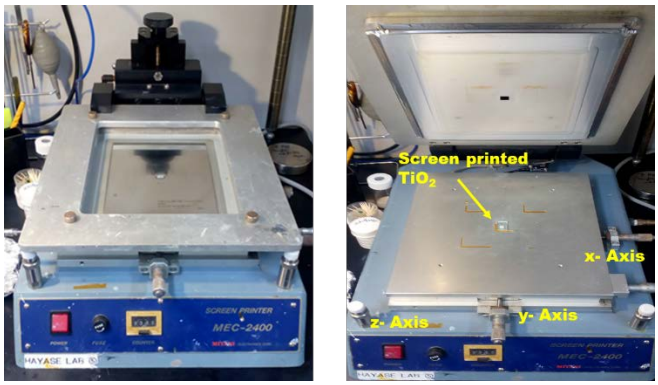

Figure-12. Screen printer used for the preparation of the working electrode

2.2.2 Preparation of photocathodes

The photocathode, which is most commonly known as counter electrode of the DSSC receives electrons from the external circuit and passes it towards electrolyte for further process. In my experiment, we had used sputtered and spin coated Platinum on the FTO as the counter electrode.

2.2.2.1 Sputtering

Sputtering is a very simple and fast method of depositing thin films a material from its target on a suitable substrate at room temperature. This convenient method for coating film of such materials with high MP like Pt, W or metal oxides, which are rather highly cumbersome using physical vapor deposition. In the sputtering process, very high energy using either DC or AC voltage is applied between the two electrodes.

2.2.2.2 Spin Coating

Cleaned FTO substrates used to spin-coat hexachloroplatinic acid to make the Pt coated counter electrode. 50 µL solution of the hexachloroplatinic acid (1 mM)in 2-propanol was placed on the FTOs substrate and used for the spin coating ultrathin films using a spin coater as shown in the Figure-13. It was then allowed to stand for 30 seconds and then spun for 400 rpm for 5 seconds and then 1400 rpm for 10 seconds. Finally, coated substrates were then sintered at 500^0C leading to ultrathin Pt on the substrate which are in a few nm thickness range.

Figure-13. Spin coater for preparing counter electrode.

2.3 Measurement and characterization

Current-voltage characteristics

The current and voltage (I-V) characteristics of a solar cell used to know solar energy conversion capability and photoconversion efficiency. I-V curves basically represent relationship between the current and voltage at the existing conditions the irradiated light intensity and temperature. It offers important information pertaining to the of a solar to electricity conversion close to its maximum optimal power point (MPP). The intensity of the incident sunlight controls the current (I), while the increases in the temperature of the solar cell reduce its voltage (V).

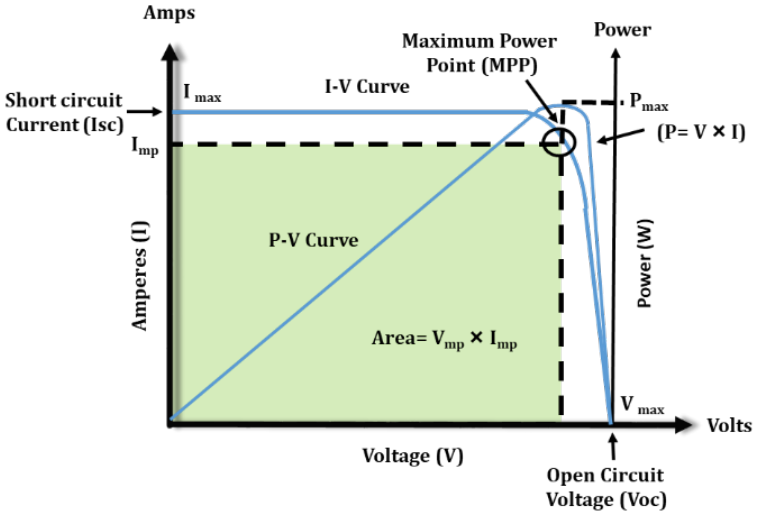

Figure-14. Solar cell I-V characteristic curve

The I-V characteristics of the DSSCs was measured with a solar simulator (CEP-2000 Bunko Keiki Co. Ltd, Japan) equipped with a xenon lamp (Bunko Keiki BSO-X150LC) as light source with irradiance of 1 Sun (100 mW/cm^2), which has been shown in the figure 15.

Figure-15. Photograph of the solar simulator utilized for photovoltaic characterization of the DSSCs fabricated in my research.

Photoconversion efficiency of a solar cell is governed by the photovoltaic parameters like short circuit current density (Jsc), open-circuit voltage (Voc), and the fill factor (FF) with the relation:

$$\eta = Jsc\ X\ Voc\ X\ FF/Pin$$

Where Pin is the intensity of the incident light. The standard AM 1.5 spectrum of sun falling on the earth surface have an intensity of 100 mW/cm^2.

Short Circuit Current Density (Jsc): It is basically the maximum current delivered solar cell, when solar cell is short circuited. Apart from this, charge injection and collection efficiency also make a significant contribution towards the finally observed Jsc.

Open Circuit Voltage (Voc): It is the maximum voltage obtained, when there is no net flow of current in the solar cell. In the DSSCs, it is controlled by difference in the energy of the conduction band of the wide band gap semiconductor and the redox potential of the electrolyte. In the case DSSCs, utilizing TiO_2 and iodine based redox electrolyte it is 0.9 V. Therefore, cobalt complex based redox shuttle with relatively deeper redox potential give higher Voc as compared to the most commonly used iodine based electrolyte. At the same time, it is also affected by charge carrier recombination due to back electron transfer, which lead to hampered Voc as well as Jsc.

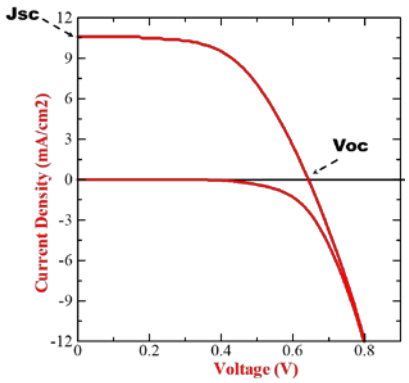

Figure-16. A typical I-V curve obtained after simulated 1 sun illumination and under dark.

Fill Factor (FF): It is basically the ratio of the maximum power output to the product of the Jsc and Voc. The FF can be calculated by the following relation:

$$FF=P_{max}/Jsc\ X\ Voc$$

Where, $Pmax$ is the maximum power, whose values range from 0 to 1. The FF is controlled by the shunt and series resistances. In order to have high FF, shunt resistance should be as much higher as possible while a lower series resistance leads to the higher FF.

Efficiency of the solar cell: The observed percentage photoconversion efficiency can be calculated by the following relation:

$$\eta=Jsc\ X\ Voc\ X\ FF/Pin$$

Where, Pin is the input power, which 100 mW/cm^2 for full bright 1 Sun irradiation.

Photocurrent action spectrum

Plot of the Incident photon conversion efficiency (IPCE) as function of the wavelength of light also known as photocurrent action spectrum gives the vital information about the efficiency of the conversion of photons in to electrons. Numerical value of IPCE is governed by several factors such as the efficiency of the photon harvesting, charge injection, and final charge collection. The equation which describes the IPCE can be mathematically represented as:

$$IPCE\ (\lambda) = LHE\ (\lambda) \times \Phi inj \times \eta c = LHE\ (\lambda) \times APCE$$

The light harvesting efficiency (LHE) depends on the wavelength irradiated photons and can be estimated by the relation:

$$LHE = 1 - 10^{-\varepsilon(\lambda) LnC}$$

Where ε (λ) is the molar extinction coefficient, C is the concentration (which is determined by the effective photoanode roughness) of the dye respectively and Ln is the diffusion length

.

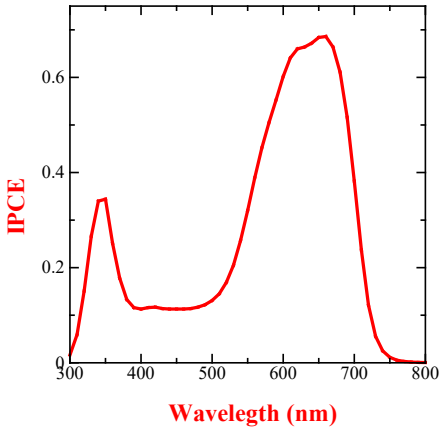

Figure-17. A typical photocurrent action spectrum for the DSSC utilizing a squaraine dye.

2.4 References

1. https://www2.ph.ed.ac.uk/~gja/qp/qp10.pdf
2. M.J. Frisch, G.W. Trucks, H.B. Schlegel, G.E. Scuseria, M.A. Robb, J.R. Cheeseman, G. Scalmani, V. Barone, B. Mennucci, G.A. Petersson, H. Nakatsuji, M. Caricato, X. Li, H.P. Hratchian, A.F. Izmaylov, J. Bloino, G. Zheng, J.L. Sonnenberg, M. Hada, M. Ehara, K. Toyota, R. Fukuda, J. Hasegawa, M. Ishida, T. Nakajima, Y. Honda, O. Kitao, H. Nakai, T. Vreven, J.A. Montgomery Jr, J.E. Peralta, F. Ogliaro, M. Bearpark, J.J. Heyd, E. Brothers, K.N. Kudin, V.N. Staroverov, R. Kobayashi, J. Normand, K. Raghavachari, A. Rendell, J.C. Burant, S.S. Iyengar, J. Tomasi, M. Cossi, N. Rega, J.M. Millam, M. Klene, J.E. Knox, J.B. Cross, V. Bakken, C. Adamo, J. Jaramillo, R. Gomperts, R.E. Stratmann, O. Yazyev, A.J. Austin, R. Cammi, C. Pomelli, J.W. Ochterski, R.L. Martin, K. Morokuma, V.G. Zakrzewski, G.A. Voth, P. Salvador, J.J. Dannenberg, S. Dapprich, A.D. Daniels, O. Farkas, J.B. Foresman, J.V. Ortiz, J. Cioslowski, D.J. Fox, Gaussian 09, Revision A.02,

3. http://vergil.chemistry.gatech.edu/courses/chem6485/pdf/basis-sets.pdf
4. Photosynthesis Research December 2009, Volume 102, Issue 2–3, pp 443–453
5. A. Pradhan, T. Morimoto, M. Saikiran, G. Kapil, S. Hayase, S.S. Pandey, Investigation of the minimum driving force for the dye regeneration utilizing model squaraine dyes for dye-sensitized solar cells, J. Mater. Chem. A 5 (2017) 22672–22682
6. Chi, Y.; Chou, P.-T., Transition-Metal Phosphors with Cyclometalating Ligands: Fundamentals and Applications. Chemical Society Reviews 2010, 39, 638-655
7. J.M. Lim, Z.S. Yoon, J.Y. Shin, K.S. Kim, M.C. Yoon, D. Kim, The Photophysical properties of expanded porphyrins: relationships between aromaticity, molecular geometry, and non-linear optical properties, Chem. Commun. (Camb.) 3 (2009) 261–273.
8. Lakowicz, Jr, Principles of Fluorescence Spectroscopy. Springer US, New York: 2006, 353-382.
9. Haruo Hayao, Pascal's Triangle, Non-Adjacent Numbers, and D-Dimensional Atomic Orbitals. *Hyperspace* 1999, *8*, 48-57.
10. K.D. MacFarlane and D.F. Torgerson, InternationaI Journal of Mass Spectrometry and Ion Physics, 21, 1976, p81.
11. Dass, C., *Fundamentals of Contemporary Mass Spectrometry*; John Wiley & Sons, 2007; Vol. 16.
12. A. Benninghoven and W.K. Sichtermann, Analytical Chemistry, 50, 1978, p1180.
13. *Hillenkamp, Franz; Karas, Michael; Beavis, Ronald C.; Chait, Brian T. (1991). "Matrix-assisted laser desorption/ionization mass spectrometry of biopolymers". Analytical Chemistry. 63 (24):1193A–1203A.* doi:10.1021/ac00024a002. ISSN 0003-2700. PMID 1789447.
14. K. Tanaka, et. al., Rapid Communications in Mass Spectrometry, 2, 1988, p151.
15. *Nicholson, R.S. (1965). "Theory and Application of Cyclic Voltammetry for Measurement of Electrode Reaction Kinetics". Anal. Chem. 37 (11): 1351–1355.* doi:10.1021/ac60230a016.

16. *DuVall, Stacy DuVall; McCreery, Richard (1999). "Control of Catechol and Hydroquinone Electron-Transfer Kinetics on Native and Modified Glassy Carbon Electrodes". Anal. Chem. 71 (20):4594–4602.* doi:10.1021/ac990399d.
17. Bond, Alan M.; Feldberg,Stephen (1998). "Analysis of Simulated Reversible Cyclic Volta metric Responses for a Charged Redox Species in the Absence of Added Electrolyte". J. Phys. Chem. 102(49): 9966–9974. doi:10.1021/jp9828437
18. Wilkinson G., Rosenblum M., Whiting M.C. and Woodward R. B. J. Am. Chem. Soc. 1952, 74, 2125- 2126. [2] Wilkinson G. J. Am. Chem. Soc. 1952, 74, 6149-6150. [3] Fischer E.O. and Pfab W.Z. Naturforsch. 1952, 76, 377-379.
19. Kealy T.J. and Pauson P.L. Nature. 1951, 168, 1039-1040. [5] Miller S.A., Tebboth J.A. and Tremaine J.F. J. Chem. Soc. (London) 1952, 632-635.
20. Molina P., Ta´rraga A., Curiel D. et. Vel M.D. Journal of Organometallic Chemistry. 2001, 258, 637.
21. Yamaguchi T., Takahashi K. et. Komura T. Electrochimica Acta. 2001, 46, 2527.
22. Vilas-Boas M., Pereira E. M., Freire C. and Hillman A. R. Journal of Electroanalytical Chemistry. 2002, 538, 47.
23. B. Su, H.H. Girault, Absolute standard redox potential of monolayer-protected gold nanoclusters, J. Phys. Chem. B 109 (2005) 11427–11431.
24. Lv., Z.; Yu, J.; Wu, H.; Shang, J.; Wang, D.; Hou, S.; Fu, Y.; Wu, K.; Zou, D., Highly Efficient and Completely Flexible Fiber-Shaped Dye-Sensitized Solar Cell Based on TiO_2 Nanotube Array. *Nanoscale* 2012, *4*, 1248-1253.

Chapter-3

Computational molecular design of dyes with varying anchoring groups

3.1 Introduction

Dye-sensitized solar cells (DSSCs) have currently become popular for the direct conversion of light into electricity with appreciably good efficiency at the same time, at relatively lower cost of production 1, 2]. In these cells, undoubtedly, sensitizing dyes that can also be considered as the "heart of the DSSCs" since it is directly involved in the absorption of light. The sensitizer dye, adsorbed on the TiO_2 surface. Upon light illumination, dye molecules absorb a photon and undergo photoexcitation boosting electrons from the ground state also known as the highest occupied molecular orbital (HOMO) to an excited state also known as the lowest unoccupied molecular orbital (LUMO). In the excited state, these electrons from the LUMO are then injected into the conduction band of the TiO_2 [3, 4]. The oxidized dye is subsequently returned to the ground state after reduction by the electron coming from the electrolyte via redox reaction. The electrons injected in to TiO_2 passthrough these nanoparticles finally reaching to the counter electrode via external load. To achieve efficient electron injection from the excited dye molecules, they are needed to be in intimate contact with the wide bandgap semiconductor surface [5, 6]. To attain the high photoconversion efficiency (PCE), several factors/parameters such as panchromatic light absorption, relatively long-lived excited states with energies matching with the TiO_2 conduction band, and redox energy level of the electrolyte along with the presence of a suitable anchoring group.

Anchoring groups play a dominant role in the DSSC working cycle since their presence in the dye molecular framework leads to the attachment of these molecules to the wide bandgap semiconductor surface making an intimate contact by suitable chemical bond formation [7]. To have facile electron injection, there should be sufficient electronic coupling between the excited dye molecule and vacant 3d-orbitals of the TiO_2. This can be ascertained by the presence of sufficient electron density in the LUMO of the dyes facilitated by intramolecular charge transfer (ICT). Therefore, the nature of the anchoring group is responsible for controlling the PCE by controlling the ICT and electron injection. By logical molecular design of organic sensitizers for DSSCs, Jia et al and Shivashimpi et al have demonstrated that the nature of the anchoring group has a profound influence on the PCE of the DSSCs and keeping the same molecular framework, only change in the anchoring group led to the drastically different PCE by controlling the electron injection [8-9]. At the same time, the nature of the anchoring group controls the stability of the

DSSCs by controlling the strength of binding of the dye molecules to the TiO_2 surface. In an interesting report, Kakiage et al have demonstrated that silyl-ester makes very strong binding with the TiO2 surface, where, only less than 10 % dye molecules were removed from TiO_2 surface in the water at 25ºC after 2000 hours, while more than 60 % dyes bearing –COOH anchoring was removed in less than 20 hours under the identical experimental condition as well as dye molecular framework [10]. Utilizing the organic as well inorganic sensitizers of DSSC, it has been demonstrated that changing the anchoring group from the most commonly used carboxylic acid to the phosphonic and cyanophosphonic acid led to the remarkably enhanced DSSC stability [11-12].

The past three decades of DSSCs research has seen huge research and development activities about the DSSC components leading to state-of-art DSSCs surpassing PCE exceeding amorphous silicon. Report of PCE >13 % with efficient incident photon to current conversion efficiency (IPCE) exceeding 90 % with photon harvesting mainly in the visible wavelength region (400 nm-700 nm) [13]. For commercialization further enhancement in the PCE in combination with device stability inevitable. In this context, more focus is needed to develop novel near-infra-red (NIR) sensitizers for panchromatic photon harvesting in combination with a suitable anchoring group to provide sufficient device stability. To design novel sensitizers for DSSCs, care should be taken about the required criteria such as high molar extinction coefficient, energetic band matching with wide bandgap semiconductor and redox electrolyte, presence of suitable anchoring group, and sufficient electronic coupling with excited dye molecule with TiO_2. There are in-numerable structural possibilities that exist for the organic molecules and some of the potential dyes developed exhibiting PCE >12 % required multiple-step synthesis and need sufficient time and efforts of the synthetic organic chemists [14]. Therefore, prior and reliable prediction of the suitability of the designed dye molecules for DSSCs is highly desired to save the time and efforts of the chemists and accelerate the research and development activities. To circumvent this issue, state-of-art theoretical calculations have now become a necessary tool and being developed and improvised day-by-day. The main aim of such calculations lies in the accurate prediction of the properties and many calculation techniques and methodologies have been developed. Computational chemistry map utilizes the expertise and power of both the computer as well as the chemists, which has been shown in Fig. 1.

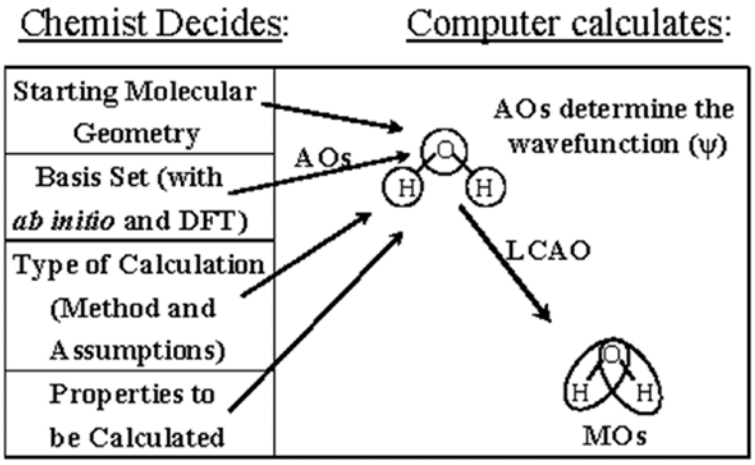

Figure. 1 Computational chemistry map exhibiting the roles of the chemists and computers

Despite utilization of calculation methods based molecular mechanics based on classical physics like Amber and MM2 treating large molecules but the limited prediction of properties, electronic structure calculation methods based on quantum mechanics have become more popular owing to the versatility for not only the molecular size but also prediction for a huge number of properties under investigation. Since quantum chemical (QC) calculations are based on the solution of the Schrodinger wave equation and it is well known that the exact solution of this especially for multi-atomic and multi-electronic systems is impossible needing mathematical approximations. Keeping this in mind, several methods based on semi-empirical and ab-initio calculations were developed in the past. The ab-initio method is good in a sense that they are more accurate, there is no need of experimental parameters but require high computational cost. On the other hand, semi-empirical methods like Austin model-1 (AM1), Parametric model-3 (PM3) and modified neglect of differential overlap (MNDO), etc., which are a simplified version of Hartree-Fock (HF) theory, although uses less computation cost but not only needs some experimental parameters but also predicted results are relatively less accurate as compared to that of ab-initio methods. In the various ab-initio methods, in terms different frequently utilized methods follows the order of (HF) < MP2 < MP4 < QCISD <<< Full CI in terms of the cost of computation and accuracy of the calculated results as shown in Fig. 2. Therefore, a judicious selection of a suitable basis set is highly desired since they basically represent atomic orbitals. In computation chemistry, density functional theory (DFT) has been most widely used as a reliable method for the prediction of the suitability of dye molecules as a photosensitizer [15]. On the other hand, Its time-dependent function, which is most widely known as (TD-DFT) is reported to give has been demonstrated to

give very reliable results pertaining to the excitation energies with the standard correlation functional and has been widely used in the DSSCs research [16].

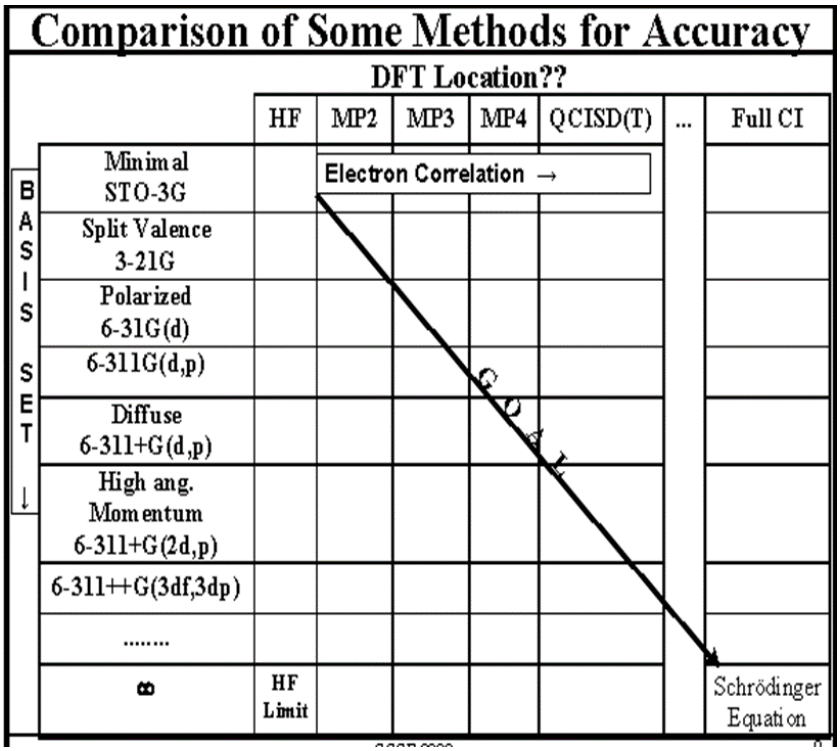

Figure. 2 Schematic representation for the correlation between the computational cost and accuracy of the calculated results.

In this work, we have selected the squaraine class of sensitizers having the same mother core but varying anchoring groups. Selection for this class of dyes is based on their capability of intense light absorption with a high molar extinction coefficient and the possibility to tune the light absorption window from the visible to IR wavelength of the solar spectrum, which is highly desired for the panchromatic photon harvesting [17]. At the same time, utilization of various anchoring groups to explore the search for optimum anchoring group with facile electron injection by improved ICT aiming towards improved stability along with the PCE. For this purpose, we selected unsymmetrical squaraine (SQ) dyes having the same main molecular framework and different anchoring groups (R and R'), the structure shown in Fig. 3. These designed molecules were subjected to the theoretical MO calculations to explore their suitability as a sensitizer for DSSC applications. Based on theoretical predictions, some of the potential newly designed dye molecules were synthesized, characterized, and subjected to photophysical investigations

including fabrication and characterization of DSSCs, and discussed in detail in the coming chapters 4 and 5.

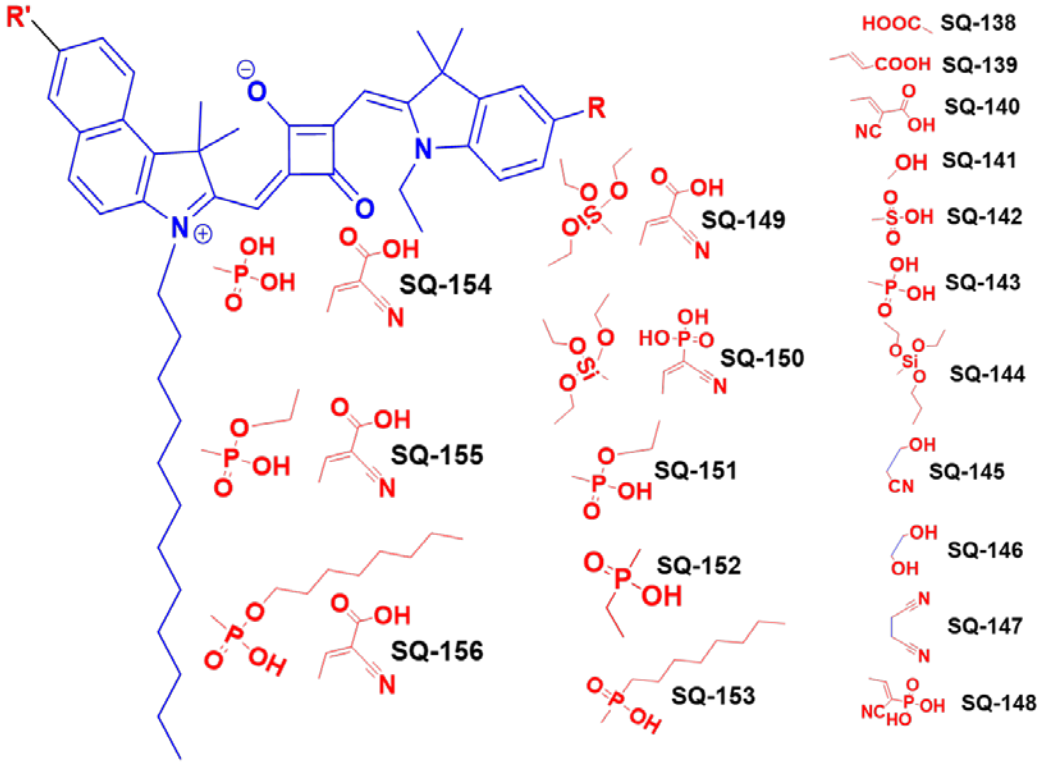

Figure 3. Chemical structure of the unsymmetrical squaraine dyes bearing different anchoring groups. R and R' represent different anchoring groups considered for theoretical investigations.

3.2 Experimental

Theoretical QC calculations were conducted on 6 core multi-processor Dell work-station using the Gaussian G09 program package [18]. Gauss View 5 was used as a graphical user interface to generate the initial molecular structure, preparation of Gaussian input files (gif), running the calculation using the G09 program, and visualization of the calculated results. Calculation was performed in the gas state and solution both utilizing the self-consistent reaction field polarizable continuum model (PCM) [19] and ethanol solvent. Selection of the ethanol solvent under PCM was made because an experiment about the optical characterization as well as DSSC fabrication using some of the potential sensitizers was done in the same solvent. Previous works have also clearly demonstarted that use of this solvent model give relatively better results for the calculation of the electronic absorption spectra [20].

In this work, 3D structural optimization in the ground state of the dye molecules was first conducted utilizing the 6-311G basis set and DFT in the presence as well as an absence of the PCM model. The energy of the HOMO and LUMO along with electron density distribution was then estimated after the structural optimization. Structural optimization in ground state was followed by excited-state TD-DFT calculation for the electronic structure calculations. In the Gaussian under the calculation by DFT, it is necessary to incorporate a suitable functional after the selection of the basis set. Different kind of functionals like exchange, correlation, standalone functionals, hybrid, and long-range corrected functionals are available under Gaussian program. Exchange functional of Becke and correlation functional of Lee, Yang, and Parr (B3LYP) is one of the most versatile functional utilized so far towards the structural optimization and calculation of the absorption spectra [21]. Other functionals like PBE, MPW1, and BPW91 have also been used for the calculation of visible light absorbing organic dyes for DSSCs [22]. Using combined theoretical and experimental approaches based on his model squaraine dye SQ-A, Yamaguchi et al demonstrated that even under a common basis set of 6-311G using DFT and TD-DFT, utilization of suitable function plays a dominant role for reliable prediction of energetics and absorption spectra [23]. They have clearly shown that functionals like Functional like B3PW91, MPWPW, B3LYP, and B3PW91are relatively better for predicting the HOMO energy level, while HCTH, LSDA, and B3PW91with PCM model are better for predicting the electronic absorption spectra. Including energy band gap, HOMO energy level, and absorption spectra, B3PW91 with PCM solvent model is the best for the reliable prediction of these parameters, which are relatively much closer to the experimental values. Similarly, using different symmetrical as well as unsymmetrical squaraine dyes, Pandey et al and Pradhan et al have also demonstrated the suitability of B3PW91 with the solvent model under TD-DFT for the reliable prediction of HOMO energy level and electronic absorption spectra [24-25].

3.3 Results and Discussion

3.3.1 MO calculation using model squaraine dye

3.3.1.1 Ground-state structural optimization

First, a model unsymmetrical squaraine dye **SQ-140** bearing Benzo indole-SQ-Indole as the main π-conjugated dye-molecular framework and cyanoacrylic acid as anchoring group with the molecular structure as sown in Fig. 4 was selected and subjected to 3D structural optimization

followed by MO calculation using Gaussian G09. The selection of cyanoacrylic acid as an anchoring group was made because carboxylic and cyanoacrylic acid has shown their dominance and is preferred anchoring groups utilized extensively for potential sensitizers of the DSSCs [7]. In parallel to the theoretical calculation, this dye was also chemically synthesized and characterized to test the reliability of the theoretically calculated results. Structure optimization was done utilizing 6-311G as basis set and functionals like DFT and P3PW91 in combination with the PCM model utilizing ethanol solvent, where calculated results are shown in the Fig. 4.

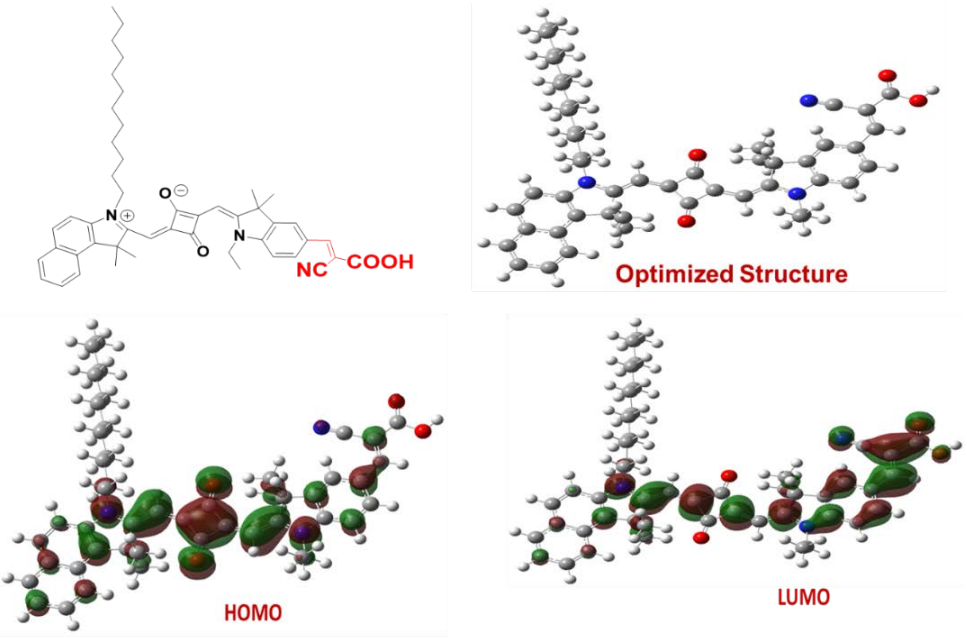

Figure 4. Molecular structure and theoretically calculated results about the optimized structure of SQ-140 along with the electron density distribution in HOMO and LUMO.

It is clear from this figure that in the HOMO electron clouds associated with the π-framework of the dye are principally located on squaraine unit, while electron density in LUMO corresponding to the π* MO exhibit a dramatic reduction of electron density at the central squaric acid core and benzoindole unit along with the sufficient diversion of electron density at the cyanoacrylic acid anchoring group. Such a shift in the electron density distribution is associated with the intramolecular charge transfer (ICT) and the presence of the sufficient electron density at the anchoring group indicates the good electronic coupling between the photoexcited dye and vacant 3d orbitals of the TiO_2 upon the attachment of this dye leading to the facile electron injection. It is worth mentioning here that the theoretically calculated value of HOMO energy level was found to

be -5.21 eV, which matches very well with the experimentally determined value of this dye (-5.17 eV) using cyclic voltammetry (chapter-4) validating the reliability of the theoretically calculated result.

3.3.1.2 Calculations for electronic absorption spectra

After successful structural optimization of the geometry in the ground state for SQ-140, which was then used for the excited-state calculation using TD-DFT at B3PW91/6-311G and PCM solvent model in ethanol to calculate the excitation energies from the ground state to the excited states. From the excited-state TD-DFT calculations, we can get several parameters such as electronic transitions, molar extinction coefficients, and oscillator strength along with the relative distribution of Mulliken charges as shown in Fig. 5. A perusal of the theoretically calculated electronic absorption spectrum of SQ-140 in ethanol solvent under the PCM model exhibited intense electronic absorption at 660 nm having oscillator strength of 1.7822 and a very high epsilon of about 7.2 X 10^4 associated with main π-π* electronic transition from the HOMO-LUMO. It can be seen from the experimentally measured electronic absorption spectrum of this dye (5 μM solution in ethanol) as shown in Fig. 4(b) also exhibiting a narrow and intense absorption mainly in the far-red wavelength region with absorption maximum (λ_{max}) at 670 nm with a very high molar extinction coefficient of 3.4 x 10^5 $dm^3.mol^{-1}.cm^{-1}$. This such a very small difference in the calculated λmax and epsilon values between the experimentally observed and theoretically calculated results indicates the potentiality of such methodology towards the theoretical prediction of absorption spectra for the design and development of novel NIR sensitizers. At the same time, charge distribution as shown in figures 4(c, d) exhibits more concentration of the negative charges towards the anchoring region responsible for pronounced ICT. Such analysis helps to compare the relative ICT depending on the nature of anchoring and helps to understand their relative adsorption behavior on to the TiO_2.

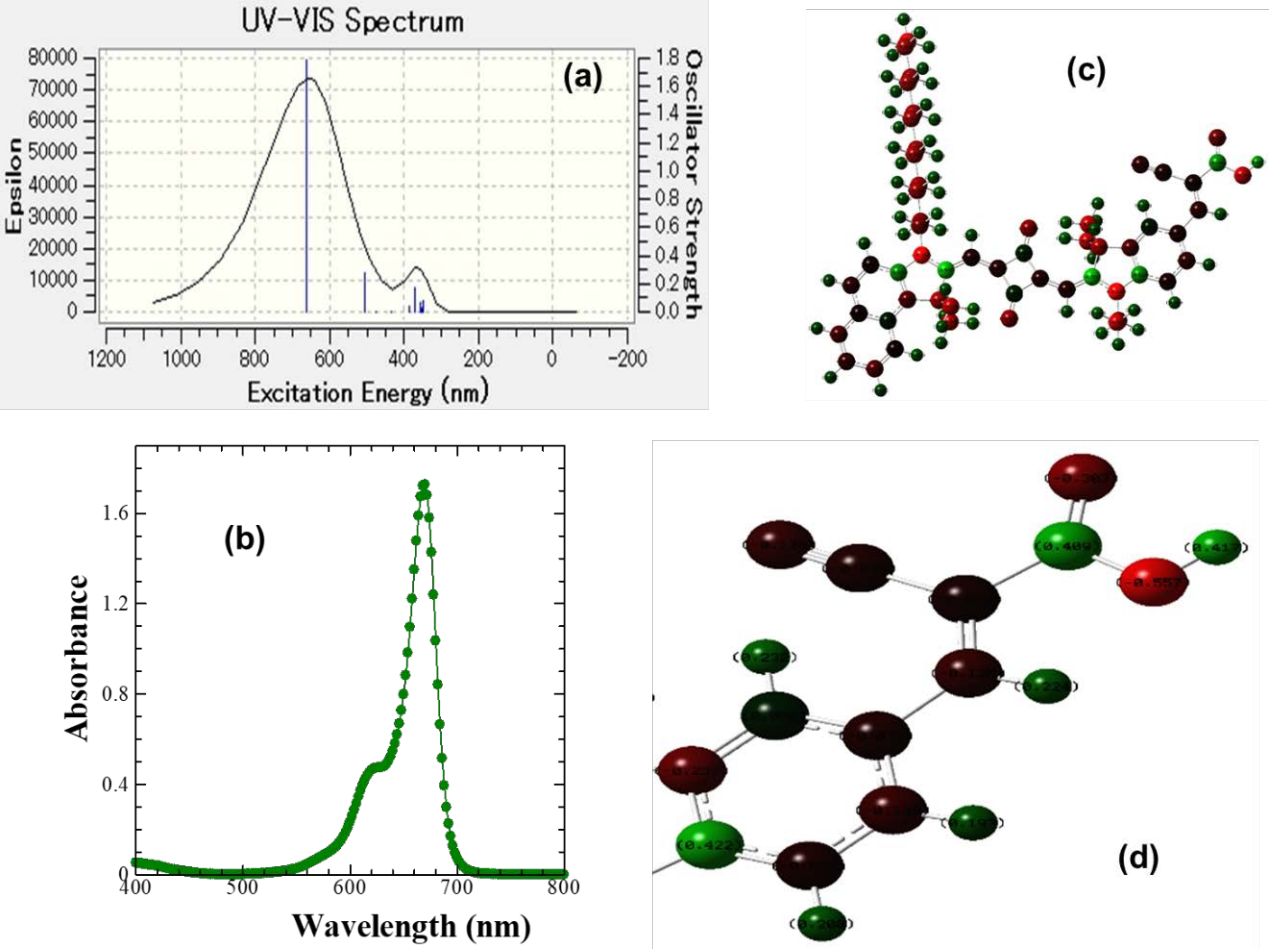

Figure 5. Theoretically calculated (a) and experimentally measured (b) electronic absorption spectra of SQ-140 in ethanol. Mulliken charge distribution and its expanded version near the anchoring group have been shown in the (c) and (d), respectively.

3.3.1.3 Construction of the energy band diagram for SQ-140 as a representative dye.

Dye molecule adsorbed on the surface of TiO_2 gets excited from their ground energy state to excited state upon light illumination resulting from the intramolecular π-π* electronic transition [20]. An energetic cascade between the conduction band of the TiO_2, dye sensitizer, and electrolyte necessary for successful completion of the DSSC working cycle. Theoretical energy band diagram of the unsymmetrical squaraine dye SQ-140 along with the energy level of the TiO_2 and (I^-/I_3^-) redox couple has been shown in Fig. 6. Redox energy level of I^-/I_3^- at -4.90 eV and conduction band energy of TiO_2 having a value of -4.0 eV were taken from the reported literature [26-27]. In the most common practices of the construction of the experimental energy band diagram of a functional organic material, its HOMO energy level is generally estimated by either photoelectron

yield spectroscopy (PYS) and most commonly using cyclic voltammetry their 1st oxidation potential from its relative shift concerning the standard ferrocene (Fe/Fe+) redox peak measured under similar experimental conditions. LUMO energy level is then estimated using the relation LUMO = HOMO + Eg, where, Eg corresponds to the energy bandgap. In most cases, Eg is experimentally estimated from the optical absorption edge (E_{opt}) of electronic absorption spectra. As it can be seen from Fig. 4 that despite a very good match between the theoretical and experimental λ_{max} of SQ-140, calculated absorption spectra are extremely broader as compared to that of the experimentally measured absorption spectrum.

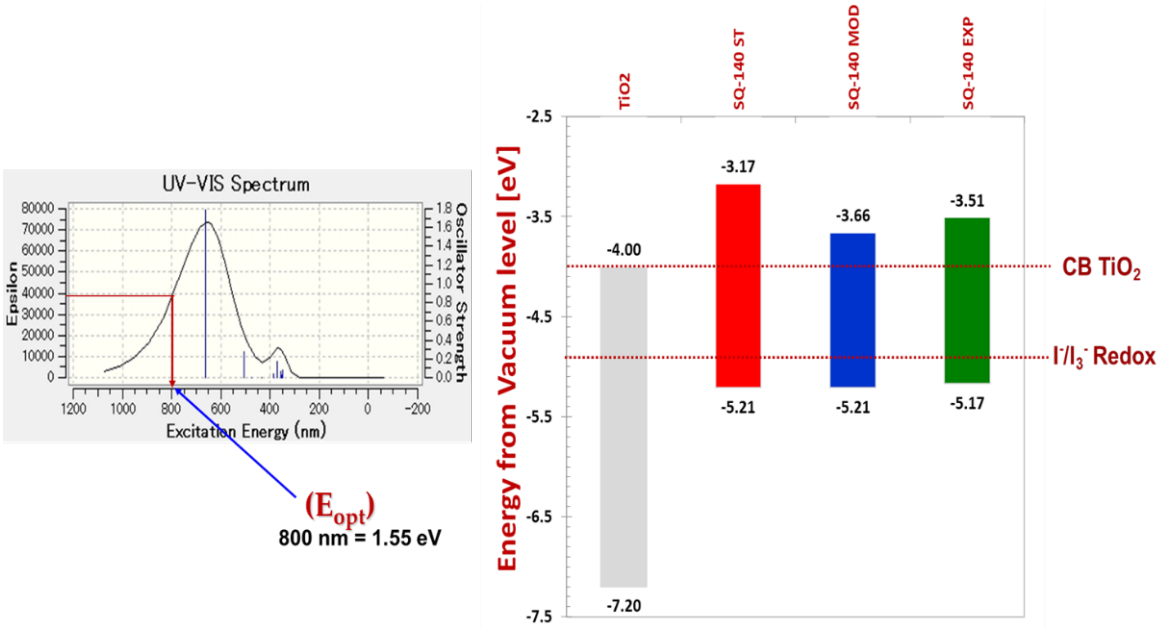

Figure 6. Theoretically calculated electronic absorption spectra (left) and energy band diagram (theoretical and experimental) of SQ-140 (right) along with the energy level of TiO_2 and iodine-based redox electrolyte.

This poses an obvious question on taking the absorption edge of calculated spectra for the estimation of the Eopt. Therefore, energy corresponding to the full width at half maximum (FWHM) of the calculated absorption spectrum was considered to be a better way to define it as E_{rupt} and estimate the calculated Eg. This calculated Eg has been used to construct the theoretical energy band diagram using this modified and Eg, which has been inspired from the experimental approach and has been named as modified theoretical energy band diagram. Therefore, three types of energy band diagrams for SQ-140 such as purely calculated adopting TD-DFT calculated (SQ-140 ST), purely experimentally measured (SQ-140 EXP), and using the newly proposed modified approach (SQ-140 MOD) were constructed as shown in Fig. 6. A perusal of the energy band

diagram of the SQ-140 reveals that although the calculated value of HOMO is very near to its corresponding experimental value, while calculated LUMO energy level is far from the experimental value. At the same time, utilization of our newly proposed modified method taking modified Eg via proposal of theoretical estimation of the Erupt seems to be a good and plausible strategy. This exhibits very close values of HOMO and LUMO energies along with the Eg compared to that of the experimentally determined value. Therefore, such a strategy for the prediction of the energy band diagram seems to be highly suitable for the design and development of novel NIR sensitizers. At the same time, this newly design dye seems to a potential NIR sensitizer compatible for DSSCs utilizing mesoporous TiO_2 as a wide bandgap semiconductor and dye adsorbing scaffold in combination with iodine based redox electrolyte.

3.3.2 MO calculation using unsymmetrical squaraine dyes with varying anchoring groups

3.3.2.1 Ground-state structural optimization

Encouraged from the very good match between the experimental and theoretically calculated values of HOMO for SQ-140, using DFT, 6-311G basis set and B3PW91 functional with PCM model, structural optimization of a series of unsymmetrical squaraine bearing different mono as well as bi-functional anchoring group were also conducted under similar conditions. To predict the explicit role of the anchoring group main p-conjugated mother core was kept the same (as shown in Fig. 3) for all of the newly designed dyes. Selection of anchoring group for the dyes under investigation was logically made taking their several advantageous futures as summarized in table 1.

Table 1. Summarization of various anchoring groups used the design of novel unsymmetrical squaraine dyes for present theoretical calculations.

Sensitizing Dye	Anchoring group	Reason for selection
SQ-138	Carboxylic acid	Most commonly used anchoring group
SQ139	Acrylic acid	Carboxylic acid extended π-conjugation
SQ-140	Cyanoacrylic acid	Extended π-conjugation with strong electron-withdrawing effect
SQ-141	Hydroxy	Electron donating effect
SQ-142	Sulfonic acid	Multidentate ligation
SQ-143	Phosphonic acid	Multidentate ligation and strong binding with TiO_2
SQ-144	Silyl ester	Very strong binding with TiO_2
SQ-145	Cyanophenol	Strong binding and electron-donating effect
SQ-146	Catechol	Strong binding with TiO_2
SQ-147	Dicyano	Strong electron-withdrawing effect

SQ-148	Cyanophosphonic acid	Strong binding with electron-withdrawing effect
SQ-149	Silyl ester and Cyano acrylic acid	Double anchor, very strong binding with electron-withdrawing effect
SQ-150	Silyl ester and Cyano phosphonic acid	Double anchor, very strong binding with electron-withdrawing effect
SQ-151	Phosphonic acid ethyl ester	Strong binding with suppressed dye aggregation
SQ-152	Ethyl phosphonate	Strong binding with suppressed dye aggregation
SQ-153	Hexyl phosphonate	Strong binding with enhanced suppression of the dye aggregation
SQ-154	Cyanoacrylic and phosphonic acid	Double anchor, very strong binding with electron-withdrawing effect
SQ-155	Cyanoacrylic acid and ethyl-phosphonate	Double anchor, strong binding with electron-withdrawing effect, suppressed aggregation
SQ-156	Cyanoacrylic acid and hexyl-phosphonate	Double anchor, strong binding with electron-withdrawing effect, much-suppressed aggregation

Electron density distribution of these designed sensitizers in their respective HOMO and LUMO was calculated, which is shown in Fig. 7. It can be seen from this figure that electron density in the HOMO, mainly lies on squaric acid unit, while in the LUMO it is more diverted towards the anchoring group. This diversion of electron density from the central squaraine unit of HOMO towards the anchoring group in the LUMO indicates the possibility of ICT leading to the feasibility of facile charge separation upon the photoexcitation. It can be seen from Fig. 6 that electron density in the LUMO of the dyes SQ-138, SQ-139, SQ-140, SQ-142, and SQ-148, where anchoring groups not only lies in the same plane of the main molecular framework and exhibit good ICT but also diversion of sufficient electron density at the anchoring group. This suggests their suitability as a sensitizer of DSSC, provided that they exhibit sufficient driving force for

electron injection in the CB of TiO_2, which will be discussed later.

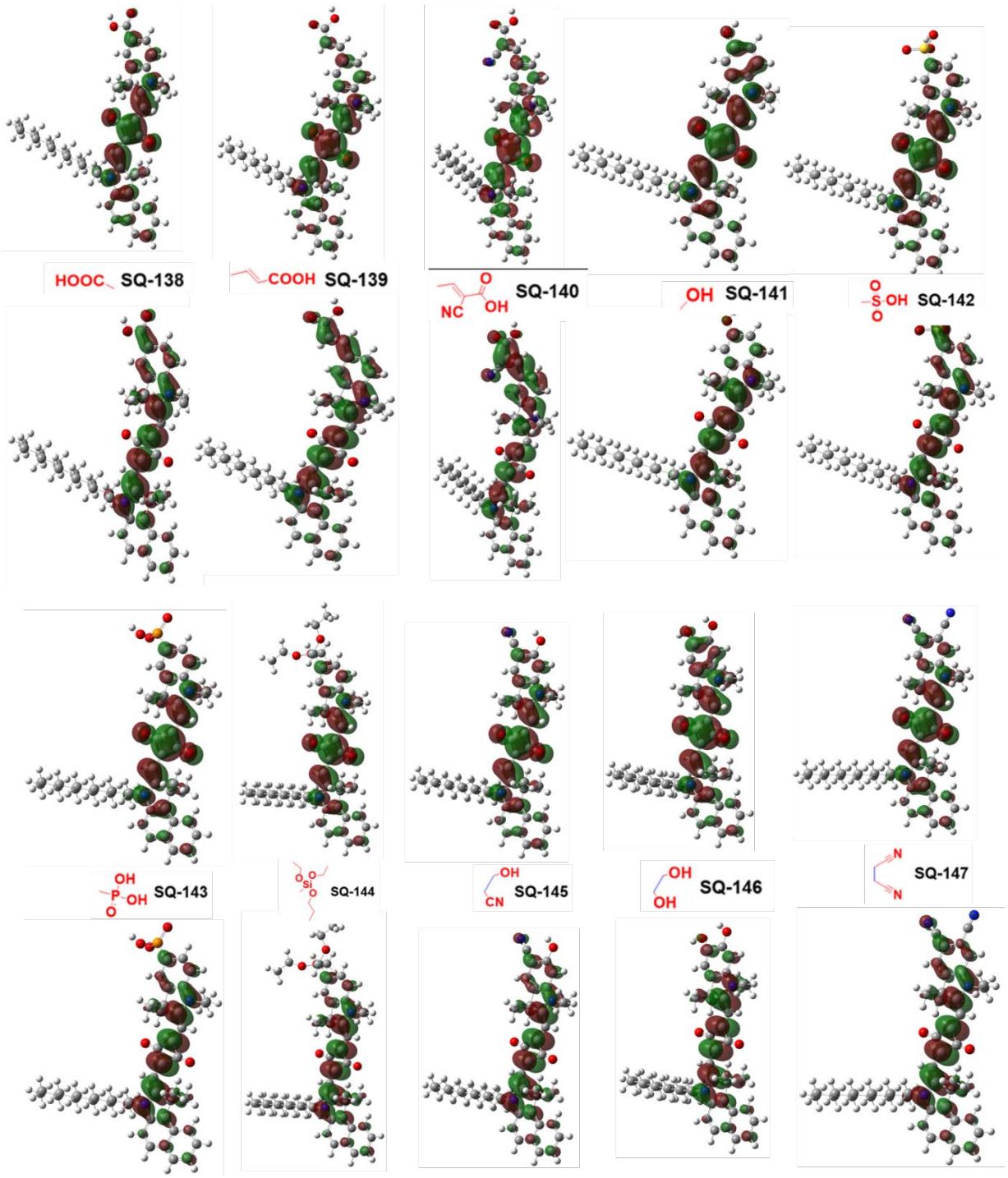

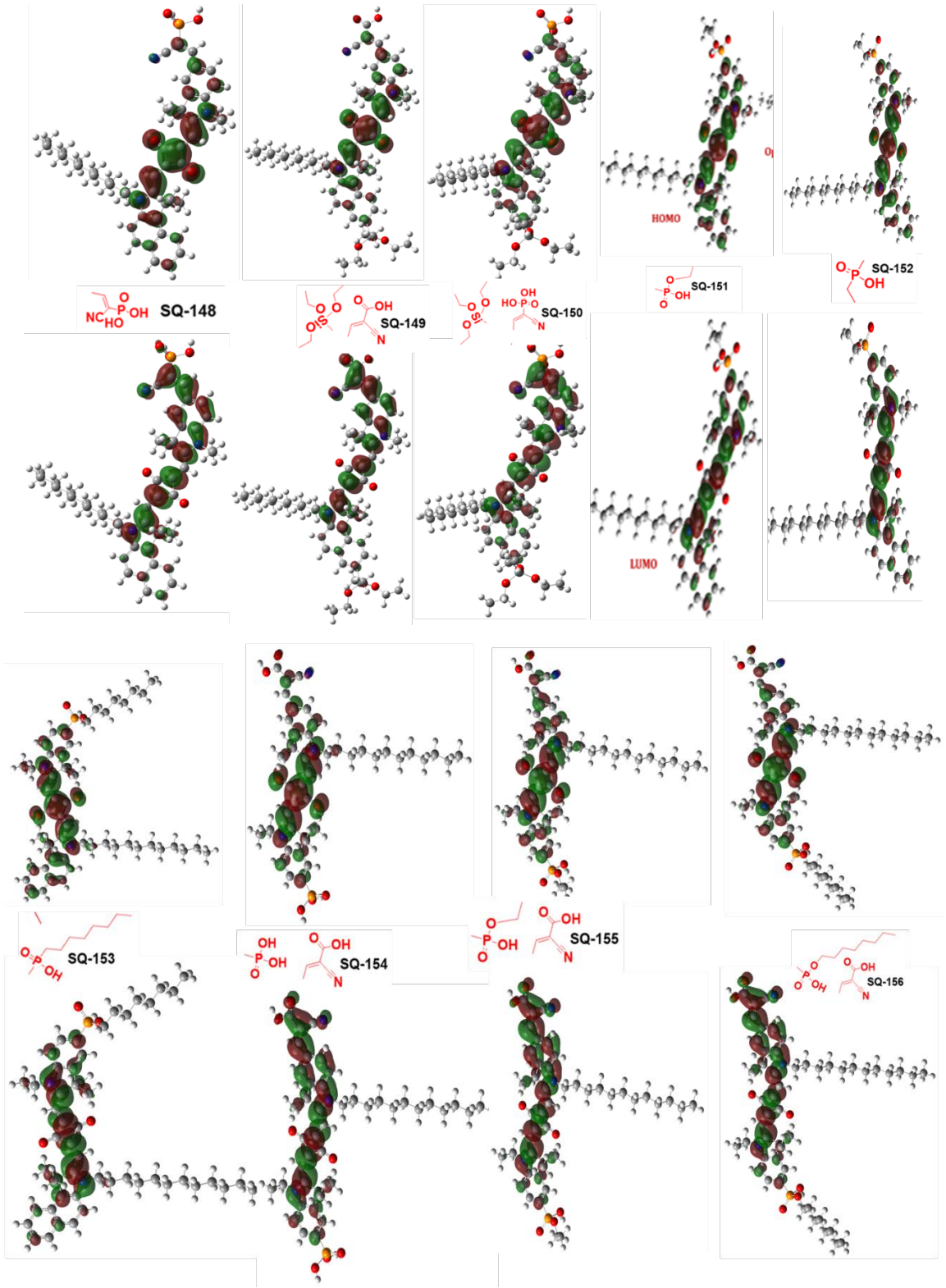

Figure 7. Calculated electron clouds in the HOMO (top) and LUMO (bottom) for the various unsymmetrical squaraine dyes bearing different anchoring groups.

On the other hand, the other sensitizing dyes like SQ-141 and SQ-143, SQ-144, SQ-145, and SQ-146 lack prominent ICT and are expected to face hindrance in the electron injection due to the low electron density on LUMO. This could be attributed to the electron-donating nature of the anchoring group in the case of SQ-141, SQ-145, and SQ-146, while in the case of SQ-143 and SQ-144 non-planarity of the anchoring group restricts the diversion of electron density at LUMO. Interestingly, the introduction of electron-withdrawing cyano group in the cyanophosphonic anchoring of dye SQ-148 leads to sufficient diversion of the electron density at LUMO as compared to only phosphonic acid in the case SQ-143 suggesting their suitability as a sensitizer. More importantly, SQ-149, SQ-150, and SQ-154 bearing double anchoring groups appear to be potential dyes in terms of not only the enhanced ICT but also they are expected to exhibit strong binding with TiO_2 to making them good sensitizer leading stable DSSCs.

3.3.2.2 Calculations for electronic absorption spectra

After successful structural optimization of the geometry in the ground state, all of the designed dyes were subjected to the excited-state calculation using TD-DFT at B3PW91/6-311G level of theory in combination with PCM solvent model using ethanol for the calculation of the electronic absorption spectra, which has been shown in Fig. 8. A perusal of the electronic absorption spectra reveals although all of the dyes under investigation exhibit intense light absorption in the far-red to NIR wavelength region associated with the □-p* electronic transition with high epsilon values but there is a differential shift depending on the nature and extent of □-conjugation associated with the anchoring group. There is a gradual red-shift in the calculated λ_{max} values for the SQ-138, SQ-139, SQ-140, and SQ-148 bearing carboxylic acid, acrylic acid, cyanoacrylic acid, and cyanophosphonic acid anchoring groups, respectively, which is attributed to their relative contribution of □-electron density from the anchoring group to main p-molecular framework of dye mother core. Amongst the dyes bearing phosphonic acid-based single and double anchoring groups, it can be seen that dyes with single phosphonate anchoring groups such as SQ-151, SQ-152, and SQ-153 exhibit relatively blue-shifted compared to that of analogous dyes with double anchoring group SQ-154, SQ-155, and SQ-156. This is attributed to the incorporation of the cyanoacrylic acid anchoring group having extended □-conjugation along with the phosphonate anchoring groups. It is interesting to note that in the case of the dyes bearing phosphonates and cyanoacrylic acid, calculated values of λ_{max} are slightly blue-shifted as compared to that SQ-140

bearing single cyanoacrylic acid anchoring group, which is attributed to the fact that introduction of non-planer phosphonate anchoring group creates some overall non-planarity of the dyes by slight twisting leading to this observed blue-shift. Theoretically calculated values of the λ_{max} obtained from the calculated electronic absorption spectra have been summarized in table 2.

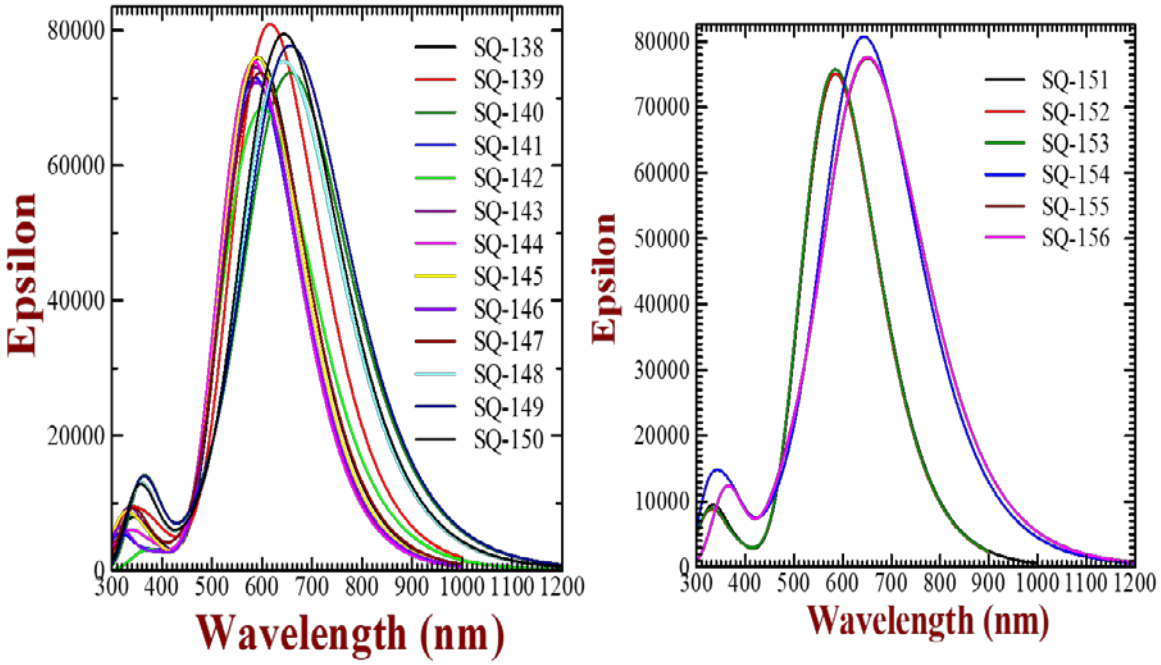

Figure 8. Theoretically calculated electronic absorption spectra of unsymmetrical squaraine dyes bearing different anchoring groups.

Table 2. Summarization of various anchoring groups used the design of novel unsymmetrical squaraine dyes for present theoretical calculations. Values shown in the parentheses are experimentally determined values of some synthesized dyes.

Sensitizing SQ-Dyes	Anchoring groups	Calculated $_{max}$ (nm)	Calculated HOMO (eV)
SQ-138	Carboxylic acid	595 (654)	-5.15 (-5.10)
SQ139	Acrylic acid	616 (665)	-5.11 (-5.08)
SQ-140	Cyanoacrylic acid	660 (670)	-5.17 (-5.21)
SQ-141	Hydroxy	584 (660)	-4.97 (-4.90)
SQ-142	Sulfonic acid	601 (652)	-5.24 (-5.22)
SQ-143	Phosphonic acid	587 (652)	-5.17 (-5.05)
SQ-144	Silyl ester	586	-5.08
SQ-145	Cyanophenol	591	-5.18
SQ-146	Catechol	589	-4.98
SQ-147	Dicyano	598	-5.26
SQ-148	Cyanophosphonic acid	643 (666)	-5.21 (-5.12)
SQ-149	Silyl ester and Cyano acrylic acid	660	-5.24
SQ-150	Silyl ester and Cyano phosphonic acid	649	-5.24
SQ-151	Phosphonic acid ethyl ester	586 (652)	-5.16 (-5.15)

SQ-152	Ethyl phosphonate	584	-5.14
SQ-153	Hexyl phosphonate	585	-5.13
SQ-154	Cyanoacrylic and phosphonic acid	647	-5.36
SQ-155	Cyanoacrylic acid and ethyl-phosphonate	656	-5.27
SQ-156	Cyanoacrylic acid and hexyl-phosphonate	656	-5.27

A perusal of the results shown in table 2 about the λ_{max} of the calculated absorption spectra and HOMO energy values after the TD-DFT calculation corroborates that introduction of electron-donating anchoring group leads to an upward shift in the HOMO energy level contrary to the downward shift exhibited by the dyes with electron-withdrawing anchoring groups. Introduction of short or long-chain alkyl groups in the phosphonic acid anchoring group neither alters the λ_{max} nor the HOMO energy values suggesting they can only control the dye aggregation without any detrimental impact on the Photophysical properties. It is interesting to note that the theoretically calculated results of the HOMO energy and λ_{max} for some of the dyes, which have been already synthesized and characterized, there is only a difference of about ± 0.06 eV in the λ_{max} and ± 0.05 eV in the HOMO energy level validating the reliability of the theoretical prediction.

3.3.2.3 Construction of the theoretical energy band diagram

Energetics of dye sensitizer and its cascade formation concerning the conduction band energy of the wide bandgap semiconductor and energy level of the redox electrolyte plays a pivotal role in the proper functioning of the DSSCs. In this calculated energy band diagram, we have considered the most commonly used TiO_2 as a wide bandgap semiconductor and I^-/I_3^- as redox electrolyte and explored the suitability of the newly designed sensitizing dyes for DSSCs using these systems. As discussed for SQ-140 in section 3.3.1.3 that owing to relatively much wider theoretically calculated absorption spectra, utilization of hybrid approach for energy band diagram of dyes considering defining Eg from Eopt at FWHM of the calculated electronic absorption spectra exhibits a very good correlation between the experimentally determined as well as theoretically calculated energy level of the dyes. Utilizing this approach, the energy of the HOMO and LUMO for all the unsymmetrical squaraine dyes under investigation was calculated and has been shown in Fig. 9 along with the energy of the CB of TiO_2 and energy level of the iodine-based redox electrolyte.

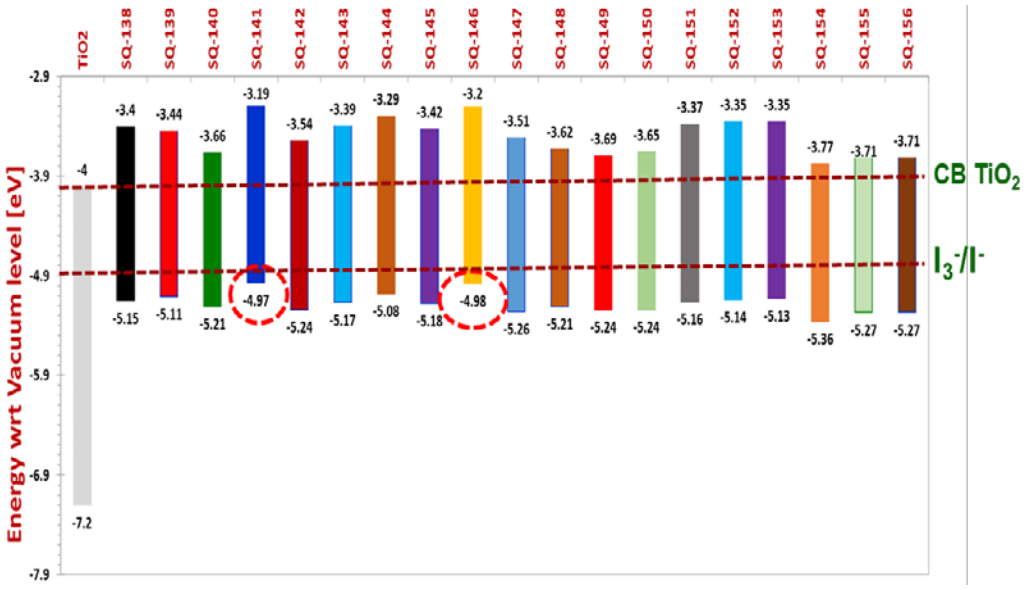

Figure 9. Theoretically calculated energy band diagram for unsymmetrical squaraine dyes bearing different anchoring groups. The energy of the conduction band of TiO_2 and redox energy level of the iodine-based electrolyte are reported values taken from the literature.

It can be seen from Fig. 9 that except few proposed sensitizers, all of the dyes exhibit an energetic cascade concerning the energy level of the conduction band of the TiO_2 and iodine-based redox electrolyte necessary of the electron injection and dye regeneration, respectively. Sensitizing dyes SQ-141 and SQ-146 bearing electron-donating hydroxyl and catechol anchoring groups respectively shifts the HOMO energy too much upwardly making them difficult for dye regeneration after the photoexcitation. Similarly, dyes SQ-154, bearing cyanoacrylic and phosphonic acid double anchoring group may face difficulty in the electron injection owing to the very small driving force for the electron injection.

3.4 Conclusions

Computational molecular design is a fast-growing area having potential applications in the area of drug design of pharmaceutical industries, materials discovery, and the design and development of functional materials for research and development. In the DSSC research, it has now emerged as a powerful tool for the development of sensitizers making speedy development of the novel materials and saving the precious time of the material scientists leading to the fast growth of this field. In this context, Gaussian has emerged as a powerful tool for the computational molecular design for the prior prediction of the various physicochemical properties of materials. It has been demonstrated that as a judicial selection of the computational cost and accuracy of the predicted results, 6-311G as a basis set, DFT for electron-pair correlation, and B3PW91 as functional using PCM solvent can reliably predict the energetics, electronic absorption spectra, and energy bandgap in the case of NIR dyes based on squaraine class of dyes. Using unsymmetrical squaraine dyes bearing varying functional group, it has been shown that there is an excellent correlation between the energy of the HOMO and absorption maximum with only a difference of ± 0.06 eV in the λ_{max} and ± 0.05 eV in the HOMO energy level between the theoretically predicted and experimentally observed values validating the reliability of the theoretical prediction for the design and development novel functional dyes.

References

1. M. Grätzel, "Photoelectrochemical cells", *Nature*, *414*, 338-344, (2001)
2. M. K, Nazeeruddin, *"*Special Issue: Michael Grätzel Festschrift, A Tribute for his 60th Birthday: Dye Sensitized Solar Cells", Ed.; Elsevier:
3. Tian, Yang, X.; Chen, R.; Hagfeldt, A.; and Sun, L. "A metal-free black dye for panchromatic dye-sensitized solar cells". Energy and Environmental Science, 2, 674-677 (2008).
4. S. Altobello, R., Argazzi, S. Caramori, C. Contado, S. Da-Fre, P. Rubino, C. Chone, G. Larramona, and C.A. Bignozzi, "Sensitisation of Nanocrystalline TiO2 with black absorbers based on Os and Ru Polypyridine complexes". Journal of American Chemical Society, 127(44), 15342-15343 (2005).
5. M. Grätzel, "Solar Energy Conversion by Dye-Sensitized Photovoltaic Cells" Inorg. Chem., 44, 6841–6851, (2005).

6. W. Zhao, Y. Hou, X. Wang, B. Zhang, Y. Cao, R. Yang, W. Wang, X. Xiao, "Study on squarylium cyanine dyes for photoelectric conversion" Sol. Energy Mater. Sol. Cells, 58, 173, (1999).

7. L. Zhang and J. M. Cole, "Anchoring Groups for Dye-Sensitized Solar Cells" ACS Appl. Mater. Interfaces, 7, 3427–3455, (2015).

8. H. Jia, K. Shen, X. Ju, M. Zhang, and H. Zheng, "Enhanced performance of dye-sensitized solar cells with Y-shaped organic dyes containing di-anchoring groups" New J. Chem.,40, 2799-2805,(2016).

9. G. M. Shivashimpi, SS. Pandey, R. Watanabe, N. Fujikawa, Y. Ogomi, Y. Yamaguchi, S. Hayase, "Effect of nature of anchoring groups on photosensitization behavior in unsymmetrical squaraine dyes" Journal of Photochemistry and Photobiology A: Chemistry, 273,1– 7, (2014,).

10. K. Kenji, Y. Masaki, F. Emi, K. Toru, U. Masafumi, H. Minoru "High Performance of Si–O–Ti Bonds for Anchoring Sensitizing Dyes on TiO_2 Electrodes in Dye-sensitized Solar Cells Evidenced by Using Alkoxysilylazobenzenes", Chem. Lett., 39(3), 260 (2010).

11. Y.H. Chen, L.W. Qi, F. Fang, and B. Tan, "Organocatalytic Atroposelective Arylation of 2-Naphthylamines as a Practical Approach to Axially Chiral Biaryl Amino Alcohols", Angew. Chem., 56, 16308-16312, (2017).

12. T.N. Murakami, E. Yoshida, N. Koumura, "Carbazole dye with phosphonic acid anchoring groups for long-term heat stability of dye-sensitized solar cells", Electrochimica Acta, 2014, 131, 174–183.

13. L. Zhang, X. Yang, W. Wang, G. G. Gurzadyan, J. Li, X. Li, J. An, Z. Yu, H. Wang, B. Cai, A. Hagfeldt, and L. Sun, "13.6% Efficient Organic Dye-Sensitized Solar Cells by Minimizing Energy Losses of the Excited State", *ACS Energy Lett*., 4, 943–951, (2019).

14. S. Mathew, A. Yella, P. Gao, R. H. Baker, B. F. E. Curchod, N. A. Astani, I. Tavernelli, U. Rothlisberger, Md. K. Nazeeruddin and M. Grätzel, "Dye-sensitized solar cells with 13% efficiency achieved through the molecular engineering of porphyrin sensitizers", Nature Chemistry, 6, 242–247, (2014).

15. M. Pastore, S. Fantacci and F. D. Angelis, “Modeling Excited States and Alignment of Energy Levels in Dye-Sensitized Solar Cells: Successes, Failures, and Challenges”, J. Phys. Chem. C, 117, 3685–3700, (2013).

16. M. K. Nazeeruddin, F. D. Angelis, S. Fantacci, A. Selloni, G. Viscardi, P. Liska, S. Ito, B. Takeru, and M. Grätzel, "Combined Experimental and DFT-TDDFT Computational Study of Photoelectrochemical Cell Ruthenium Sensitizers”, J. Am. Chem. Soc., 127,16835–16847, (2005).

17. S.S. Pandey, R. Watanabe, N. Fujikawa, G. M. Shivashimpi, Y. Ogomi, Y. Yamaguchi, S. Hayase,” Effect of extended π-conjugation on the photovoltaic performance of dye-sensitized solar cells based on unsymmetrical squaraine dyes”, Tetrahedron, 69, 2633, (2013).

18. M.J. Frisch, G.W. Trucks, H.B. Schlegel, G.E. Scuseria, M.A. Robb, J.R. Cheeseman, G. Scalmani, V. Barone, B. Mennucci, G.A. Petersson, H. Nakatsuji, M. Caricato, X. Li, H.P. Hratchian, A.F. Izmaylov, J. Bloino, G. Zheng, J.L. Sonnenberg, M. Hada, M. Ehara, K. Toyota, R. Fukuda, J. Hasegawa, M. Ishida, T. Nakajima, Y. Honda, O. Kitao, H. Nakai, T. Vreven, J.A. ontgomery Jr, J.E. Peralta, F. Ogliaro, M. Bearpark, J.J. Heyd, E. Brothers, K.N. Kudin, V.N. Staroverov, R. Kobayashi, J. Normand, K. Raghavachari, A. Rendell, J.C. Burant, S.S. Iyengar, J. Tomasi, M. Cossi, N. Rega, J.M. Millam, M. Klene, J.E. Knox, J.B. Cross, V. Bakken, C. Adamo, J. Jaramillo, R. Gomperts, R.E. Stratmann, O. Yazyev, A.J. Austin, R. Cammi, C. Pomelli, J.W. Ochterski, R.L. Martin, K. Morokuma, V.G. Zakrzewski, G.A. Voth, P. Salvador, J.J. Dannenberg, S. Dapprich, A.D. Daniels, O. Farkas, J.B. Foresman, J.V. Ortiz, J. Cioslowski, D.J. Fox, Gaussian 09, Revision A.02, Gaussian, Inc., Wallingford CT, 2009.

19. J. Tomasi, B. Mennucci, and R. Cammy, “Quantum mechanical continuum solvation models”. Chemical Reviews, 105, 2999-3093, (2005).

20. S. Fantacci, D.F. Angelis, J.J. Wang, S. Bernhard, and A. Selloni, "A combined computational and experimental study of polynuclear Ru-TPPZ complexes: Insight into the electronic and optical properties of coordination polymers". Journal of American Chemical Society, 126(31), 9715-9723, (2004).

21. C. Lee, w. Yang, and R.G. Parr, “Development of the Colic-Salvetti correlation-energy formula into a functional of the electron density”. Physical Review B, 37(2), 785-789, (1988).
22. M. Pastore, E. Mosconi, D.F. Angelis, and M. Grätzel, "A computational investigation of organic dyes for dye-sensitized solar cells: benchmark, strategies, and open issues". Journal of Physical Chemistry C, 114(15), 7205-7212, (2010).
23. Y. Yamaguchi, S. S. Pandey, N. Fujikawa, Y. Ogomi, S. Hayase, “A combined theoretical and experimental approaches towards designing NIR dyes for dye-sensitized solar cells”, Journal of Engineering Science and Technology, 9, pp. 51-65, (2014).
24. SS. Pandey, T. Morimoto, N. Fujikawa, and S. Hayase, "Combined theoretical and experimental approaches for the development of squaraine dyes with small energy barrier for electron injection”, Sol. Energy Mater. Sol. Cells, 159, 625–632, (2017).
25. A. Pradhan, T. Morimoto, M. Saikiran, G. Kapil, S. Hayase and SS. Pandey, “Investigation of the minimum driving force for dye regeneration utilizing model squaraine dyes for dye-sensitized solar cells”, J. Mater. Chem. A, 5, 22672, (2017).
26. Z. X. Li, Y. L. Xie, H. Xu, T.M.Wang, Z. G. Xu, H.L. Zhang, “Expanding the photoresponse range of TiO_2 nanotube arrays by CdS/CdSe/ZnS quantum dots co-modification”, J. Photochem. Photobiol. A, 224, 25-30, (2011).
27. Y. Ogomi, T. Kato, S. Hayase, “Dye-Sensitized Solar Cells Consisting of Ionic Liquid and Solidification”, J. Photopolym. Sci. Technol., 19, 403–408, (2006).

Chapter-4

Influence of the Nature of Anchoring groups on photovoltaic Performances and stability

Contents of this chapter have been published in Photochemistry and Photobiology-A, A. K. Vats, A. Pradhan, S. Hayase, SS. Pandey, *Journal of Photochemistry & Photobiology A: Chemistry,* 2020, 394,112467. The material of the chapter has been reproduced with the permission of the *Journal of Photochemistry & Photobiology A: Chemistry*

4.1 Introduction

Day by day increasing world population and changing the life style encouraged the world's researches and scientist to design and development of novel organic photo functional materials for the various electronic devices like field-effect transistors [1,2], sensors [3,4], and solar cells [5,6], etc. To avoid energy demands in the future, solar cells is the best alternate and has got an enormous attention amongst them [7]. Dye sensitized solar cell (DSSC) one of the strong candidates among all the Next-generation solar cells due to their relatively low-cost raw materials resulting low-cost of fabrication procedure, their esthetic color beauty, and transparency [8]. Functional dye molecules can be considered as the "heart of Dye-Sensitized Solar Cells" considering its prevalent role as a sensitizer in photon harvesting [9]. Efforts of various optimizations for different components of DSSCs and the design and development of novel efficient sensitizers in the last two decades resulted in the demonstration of power conversion efficiency (PCE) surpassing amorphous silicon [10-11]. Moreover, this PCE has been achieved for efficient photon harvesting (>90 %) by photon harvesting only in the visible region (< 700 nm) of the solar spectrum [12-13]. A perusal of the solar spectrum reveals that about more than 50 % of solar energy emanates from the photon flux beyond the visible wavelength region [14]. This provides hope for further enhancement in the PCE by the design and development of novel sensitizing dyes with the capability of light absorption beyond the far-red to near-infrared (NIR) wavelength region. Amongst various components involved in the construction of DSSCs, sensitizing dyes play a very important role not only in controlling the overall efficiency but also responsible for the stability of the solar cell. To function optimally in DSSC, sensitizing dyes must fulfill certain criteria. These dyes should energetically favorable concerning the conduction band of the wide bandgap mesoporous titanium dioxide semiconductor and iodine redox couple electrolyte for facile electron injection and dye regeneration respectively, after the photoexcitation. Apart from this, these sensitizers should also exhibit a high molar extinction coefficient and bear a suitable anchoring group at the right position of the main molecular framework. These anchoring groups not only responsible for the electron density in the LUMO after excitation of the dye molecule but also their nature decides the binding stability of DSSCs [8-10]. Ruthenium complex dye was the first reported dye for DSSC, which had exhibited 7% Photoconversion efficiency [11]. To avoids this, development of metal-free dyes owing to the fine-tuning of the energetics, ease of synthesis, and less toxicity comes into the consideration [12]. Dyes with extended π-

conjugation based on triarylamine [13, 14], carbazole [15,16], indoline, etc., are the metal-free dyes exhibiting efficient photon harvesting in the visible spectral region to near-infrared (NIR) region. Huge structure flexibility and synthetic manipulation make unsymmetrical squaraine more promising as compared to other classes of squaraine. Due to unidirectional flow of electron from one donor to another through central acceptor unsymmetrical dyes possess intense and sharp absorption with in the NIR wavelength window with high molar extinction coefficient. [17, 18]. Besides, these sensitizers tend to aggregation and quenching of fluorescence in the emission spectra which can be seen by their shoulder peak in the absorption spectra [19]. In this work, six new unsymmetrical NIR squaraine dyes as shown in figure-1 having sharp and intense light absorption in the NIR wavelength region were designed, synthesized, and characterized. After successful synthesis, these dyes were subjected to their Photophysical, photovoltaic characterizations and investigation of their anchoring binding behavior on the mesoporous TiO_2. Combined computational and experimental approaches have been applied to design these dyes keeping the same main π-framework with varying different anchoring groups.

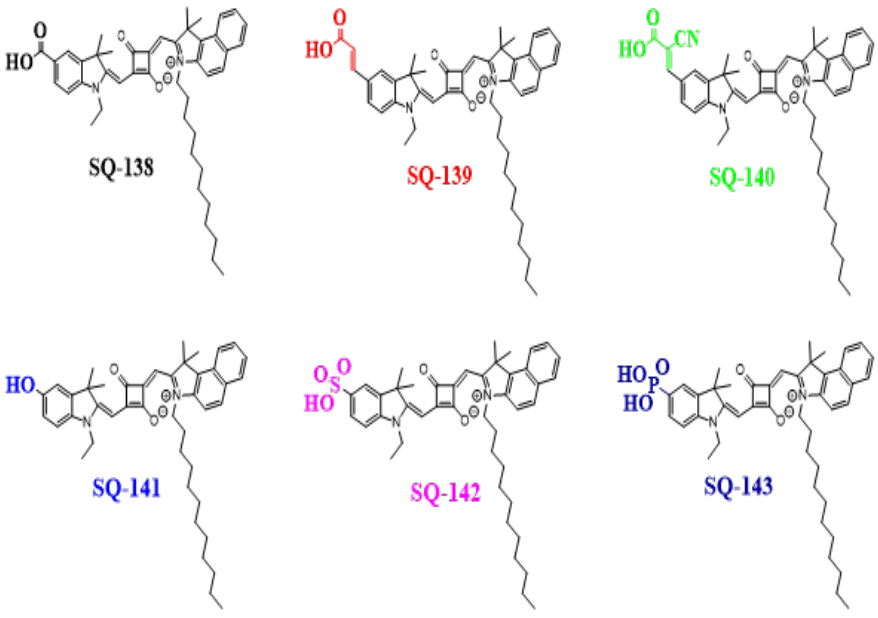

Figure-1. Chemical structure of the unsymmetrical squaraine dyes with varying anchoring groups used in the present investigation.

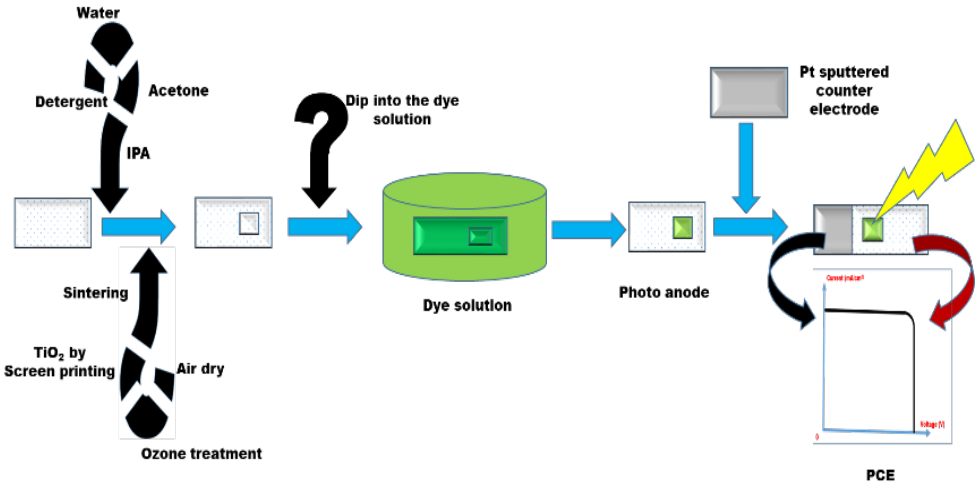

Figure-2 Device fabrication process

4.2 Experimental

Versatile application and tunable Photophysical properties of the Squaraine dyes make the research interesting of the squaraine chemistry and mainly of the unsymmetrical Squarine dyes. However, complicated synthesis of unsymmetrical dyes makes them more challenging as compare to the symmetrical dyes.[20].

4.2.1 Synthesis of unsymmetrical squaraine dyes

Keeping the same π-conjugated mother core and varying different Anchoring groups, Unsymmetrical squaraine dyes and their corresponding intermediates were synthesized as per the route of synthesis as shown in scheme-1 and scheme-2. Starting compound 1, 1, 2-trimethylbenzo (e) indole [1] was purchased from Sigma-Aldrich and another Starting compound 4-Bromoaniline [5], 4-hydrazineylbenzonitrile hydrochloride [11] were purchased from Tokyo Chemical Industry and used without further purification. The intermediate 5-carboxy-1-ethyl-2, 3, 3-trimethyl-3H-indolium iodide (i) was synthesized and characterized as per our previous publication [21].

4.2.1.1 Synthesis of 3-dodecyl-1,1,2-trimethyl-1H-benzo[e]indol-3-umiodide [2]

5 g (28.7 mmol) of 1, 1, 2-trimethyl-2, 3-dihydro-1H-benzo[e]indole [1] was taken in a round bottom flask with Propionitrile (40 mL) as the solvent. Then 12 g (43 mmol) of 1-Iodododecane (1.5 equivalent) was added to it. The mixture was then subjected to reflux at 110 °C for 26 h.

Reaction monitoring was done by TLC in a 15 % ethyl acetate: Hexane solvent system. After the completion of the reaction, the reaction mixture was cooled to room temperature followed by solvent evaporation. After complete evaporation of the solvent, ample diethyl ether was added to it followed by thorough ether washing. The residue was collected as a light pink solid to give the titled compound in 78 % yield (11.2 g). FAB mass (measured m/z: 378.3164 [M] +; calculated m/z: 378.3161).

4.2.1.2 Synthesis of (E)-4-((3-dodecyl-1,1-dimethyl-1H-3l4-benzo[e]indol-2-yl) methylene)-2-ethoxy-3-oxocyclobut-1-en-1-olate [3]

In a round bottom flask fitted with a condenser, 1 equivalent of compound [2], (5 g, 9.9 mmol) and 1 equivalent of 3, 4-Diethoxy-3-cyclobutene-1, 2-dione 1.6 g (9.9 mmol) was taken in 25 mL ethanol. To it, 5 equivalent of trimethylamine (7.0 ml) was added. The reaction mass was then subjected to reflux for 6 h, which soon turned to yellow color. Solvent was evaporated under a vacuum. Reaction mass was then extracted with ethyl acetate followed by thorough washing with distilled water and brine. The obtained ethyl acetate layer was subjected to vacuum evaporation and performed column chromatography with 10 % Ethyl acetate: Hexane. The solvent was removed to get the titled compound as a yellow powder in 77 % yield (3.8 g). FAB-mass (measured m/z: 502.0 $[M+H]^+$; calculated m/z: 501.3).

4.2.1.3 Synthesis of (E)-4-((3-dodecyl-1,1-dimethyl-1H-benzo[e]indol-3-ium-2-yl) methylene)-2-hydroxy-3-oxocyclobut-1-en-1-olate [4]

5 g (6.0 mmol) of compound [3] was dissolved in 15 mL ethanol in a 50 mL round bottom flask. To this solution 5 equivalent 4 N NaOH was added and refluxed for 2 hr. The reaction mixture was cooled and the solvent was evaporated under a vacuum. Reaction mixture was acidified by diluted HCl and extracted in chloroform and subjected to thorough washing by brine. The final hydrolyzed product was obtained as a red solid in 88 % yield (2.5 g).

4.2.1.4 Synthesis of 1-ethyl-5-hydroxy-2,3,3-trimethyl-3H-indol-1-iumiodide (ii)

The intermediate 5-hydroxy-2, 3, 3-trimethyl-3H-indole was synthesized following our previous work [22]. 1 equivalent 4 g (21.1 mmol) of 5-methoxy-2, 3, 3-trimethyl-3H-indole was dissolved in 20 mL dichloromethane. It was then cooled to 0°C. To the cooled solution, 4 ml (2 eq.) of Boron tribromide was added dropwise followed by the continuation of reaction at room

temperature. After 8 hrs. reaction progress was monitored by TLC. the reaction mass was quenched by sodium thiosulphate, and reaction mass was using ethyl acetate and thorough washing with distilled water followed by brine. The organic layer was evaporated under vacuum and the crude product was purified by column chromatography using 50 % Ethyl acetate: Hexane. The desired product was obtained in 72 % yield (2.66g). The obtained precursor 2.0 g (11.42 mmol) was dissolved in 10 ml acetonitrile. Then 2 equivalent (1.8 ml, 22.8 mmol) of 1-Iodoethane was added to it. The reaction mixture was then refluxed for 18 hr. while monitoring the progress by TLC. On completion, the solvent was evaporated under vacuum and the product was precipitated out adding diethyl ether. It was then filtered and the titled compound was obtained as pinkish solid in 63 % yield (2.3 g).

4.2.1.5 Synthesis of 5-sulfo-1-ethyl-2,3,3-trimethyl- -3H-indol-1-ium iodide (iii)

The intermediate was synthesized following the report by Park et al. [23]. 5-Sulfo-2, 3, 3-trimethyl-3H-indole was synthesized by the reaction of 4-Hydrazino-benzenesulfonic acid hemihydrate 4 g (21.3 mmol) with 5 mL of 3-methyl-2-butanone in 20 mL acetonitrile under reflux for 7 h. Reaction progress was monitored by TLC and upon completion of the reaction, the solvent was evaporated and performed column chromatography to give the product in 75 % yield. 2.5 g (10.4 mmol) of this compound was dissolved in 15 ml of acetonitrile and 2 equivalents of 1-Iodoethane (4 ml, 20.8 mmol) were added. The mixture was then refluxed for 12 h while monitoring the reaction progress by TLC. The solvent was evaporated under vacuum and product was precipitated by diethyl ether. which was filtered to get the titled compound as pinkish solid in 68 % yield (2.8 g).

4.2.1.6 Synthesis of 5-(diethoxyphosphoryl)-1-ethyl-2,3,3-trimethyl-3Hindol-1-ium iodide (iv)

After a slight modification in the procedure as reported by Archer et al. [24], compound (iv) was synthesized. To a solution of 4-Iodoindole (1 g, 3.5 mmol) in toluene was added Tetrakis (triphenylphosphine) palladium (0) (0.18 mmol), and trimethylamine (12.4 mmol) followed by the addition of Diethylphosphite (0.31 mmol), and the reaction mixture was refluxed for 12 h. Upon completion of the reaction as monitored by TLC, the solvent was evaporated. The product was extracted with ethyl acetate and washed with water and brine. Finally, purification was done by column chromatography giving desired compound diethyl (2, 3, 3-trimethyl-3H-indol-5-yl)

phosphonate as a colorless liquid. To a solution of this compound acetonitrile followed by ethyl iodide was added and reflux the reaction mass for 12 h. Upon completion of the reaction, the solvent was evaporated, and product was precipitated out by using diethyl ether. It was then filtered, washed with diethyl ether, and dried under vacuum to obtain the titled compound 5-(diethoxyphosphoryl)-1-ethyl-2,3,3-trimethyl-3H-indol-1-ium iodide (iv).

4.2.1.7 Synthesis of SQ-138

To a 50 mL round bottom flask, 1 equivalent of 5-carboxy-1-ethyl-2,3,3-trimethyl-3H-indol-1-ium iodide (i), (300 mg, 1.3 mmol), 1 equivalent (559 mg, 1.3 mmol) of hydrolyzed semi squaraine dye intermediate [4] were added in 30 mL of 1:1 toluene/n-butanol. The reaction mixture was refluxed for 12 h, which soon turned greenish. Reaction progress monitored by TLC, solvent was evaporated under vacuum after completion and purification was done by column chromatography using 5% methanol: chloroform solvent. Pure fraction afforded the titled 450 mg of the compound as a vibrant blue color in 51 % yield. Results of HR-FAB-MS (measured m/z: 686.4114 [M]+; calculated m/z: 686.4084) and 1H NMR (500 MHz, CDCl3): δ/ppm = 8.15(dd,H-44); 8.05(dd,H-41); 7.9(dd,H-8); 7.86 (dd,H-9); 7.55(dd,H-45); 7.41(t,H-6); 7.39(t,H-5); 7.27(d, H-7); 6.9(d,H-4); 6.08(s,H-33); 5.9(s,H-28); 4.14 (m,H-46); 3,98(t,H-16); 2.10(t,H-47); 1.82(m,H-17); 1.77(s,H39 + 40); 1.56(s,H14 + 15); 1.40(m,H-18), 1.39 (m,H-19); 1.38 (m,H-20),1.37(m,H-21), 1.34(m,H-22);1.33 (m,H-23); 1.31 (m,H-24);1.29 (m,H-25); 1.28(m, H-26), 1.22(t,H-27) confirms the structural identity of this dye.

4.2.1.8 Synthesis of SQ-141

To a 100 ml round bottom flask, 1 equivalent of 1-ethyl-5-hydroxy-2,3,3-trimethyl-3H-indol-1-ium iodide (ii) 300 mg (0.91 mmol) of and 1 equivalent (392 mg) of semi squaraine dye intermediate [4] was dissolved in 30 mL of 1:1 toluene/ n-butanol. The reaction mixture was refluxed for 18 h. After evaporation of the solvent under vacuum, crude product was purified by column chromatography by using chloroform methanol as the mobile phase to obtain a vibrant blue solid (285 mg) in 43 % yield. HR-FAB-MS (measured m/z: 658.4131 $[M]^+$; calculated m/z: 658.4134). 1H NMR (500 MHz, CDCl3): δ/ppm = 9.74.15(dd,H-43); 8.12(dd,H-41); 7.82(dd,H-8); 7.79 (dd,H-9); 7.51(dd,H-44); 7.49(t,H-6); 7.48(t,H-5); 7.20(d, H-7); 6.8(d,H-4); 5.9(s,H-33); 5.89(s,H-28); 4.02(m,H-45); 3.58(t,H-16); 2.10(t,H-46); 1.98(m,H-17); 1.78(s,H39 + 40); 1.50(s,

H14 + 15); 1.41(m,H-18), 1.40(m,H-19); 1.38(m,H-20); 1.37(m,H-21), 1.34(m,H-22); 1.32(m, H- 23); 1.31(m,H-24); 1.29(m,H-25); 1.28(m, H-26), 1.21(t,H-287).

4.2.1.9 Synthesis of SQ-142

400 mg (1.5 mmol) of 5-sulfo-1-ethyl-2,3,3-trimethyl-3H-indol-1-ium iodide and 1 equivalent (646 mg) of semi squaraine dye intermediate [4] was dissolved in 30 mL of 1:1 toluene/n-butanol in round bottom flask fitted by condenser. Reflux the reaction mass for 18 hr. After evaporation of the solvent under vacuum, crude product was purified with column chromatography using chloroform methanol as mobile phase. 400 mg of the desired compound was collected as a blue solid in 40 % yield. HR-FAB-MS (measured m/z: 722.3759 $[M]^+$; calculated m/z: 722.3753). 1H NMR (500 MHz, CDCl3): δ/ppm = 9.73(dd,H-44); 8.12(dd,H-41); 7.81(dd,H-8); 7.79(dd,H-9); 7.50(dd, H- 45); 7.39(t,H-6); 7.35(t,H-5); 7.19(d,H-7); 6.9(d,H-4); 4.04(s,H-33); 4.02(s,H-28); 3.67(m,H-46); 3.63(t,H-16); 2.14(t,H-47); 2.06(m,H-17); 1.84(s,H39 + 40); 1.56(s, H14 + 15); 1.44(m,H-18), 1.42(m,H-19); 1.39(m,H-20); 1.36(m,H-21), 1.34(m,H-22); 1.33(m,H-23); 1.31(m,H-24); 1.29(m,H-25); 1.28(m,H-26), 1.27(t,H-27).

4.2.1.10 Synthesis of SQ-143

In a 100 ml round bottom flask, 315 mg of 5-(diethoxyphosphoryl)-1-ethyl-2, 3, 3-trimethyl-3Hindol- 1-ium iodide (iv) and 302 mg of semi squaraine dye intermediate [4] was dissolved in 1:1 toluene/n-butanol. The reaction mixture was then refluxed for 18 h. The solvent was evaporated and the crude product was purified by column chromatography using chloroform methanol as the eluting system. After the evaporation of the collected pure fraction, 220 mg of compound was obtained in the ester form as a blue solid in 54.3 % yield. Ester was hydrolyzed by using TMS-Br as per the report [25] in DCM at room temperature for 6−8 hrs. Reaction progress was monitored by TLC using Methanol chloroform as mobile phase and column chromatography was performed by using Methanol chloroform as mobile phase. After the evaporation of the collected pure fraction, 130 mg of the titled compound was obtained as a blue solid in 63.7 % yield. HRFAB- MS (measured m/z: 723.3938 $[M+H]^+$; calculated m/z: 722.3849). 1H NMR (500 MHz, CDCl3): δ/ppm = 9.73(dd,H-44); 8.07(dd,H-41); 7.85(dd,H-8); 7.82(dd,H-

9); 7.53(dd,H-45); 7.40(t,H-6); 7.37(t,H-5); 7.29(d,H-7); 6.97(d,H-4); 6.43(s,H-33); 6.14(s,H-28); 4.24(m,H-46); 3.9(t,H-16); 3.79(t,H-47); 3.45(m,H-17); 1.57(s,H39 + 40); 1.38(s, H14 + 15); 1.26(m,H-18), 1.20(m,H-19); 1.18(m,H-20); 1.17(m,H-21), 1.15(m,H-22); 1.13(m,H-23); 1.14(m,H-24); 1.04(m, H- 25); 1.03(m,H-26), 0.82(t,H-27).

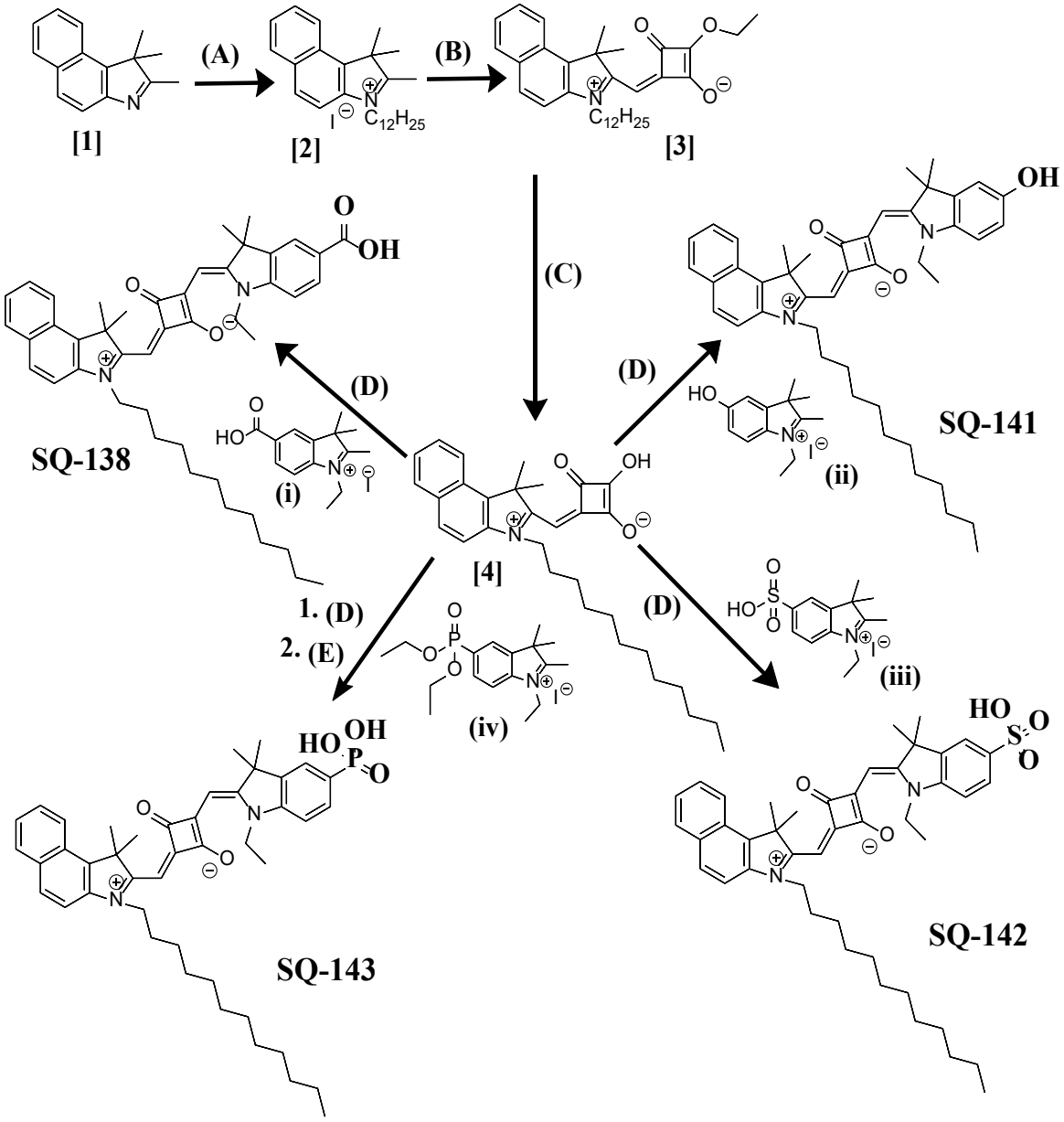

Scheme-1. Synthetic scheme for the preparation of unsymmetrical squaraine dyes bearing different anchoring groups. (A) 1-Iodododecane, Propionitrile, Reflux/ 26 h. (B) 3, 4-Diethoxy-3-cyclobutene-1, 2-dione, Triethylamine, Ethanol, Reflux/15 h. (C) 4 N NaOH, Ethanol, Reflux/2 h. (D) n-Butanol: Toluene (1:1). (E) TMS-Br, DCM, RT.

4.2.1.11 Synthesis of intermediate (4-bromophenyl) hydrazine hydrochloride [6]

To a round bottom flask, 5 g (29.0 mmol) 4-bromoaniline [5] was dissolved in 25 ml conc. HCl 25 ml. after cooling the reaction mass at 0^0C, Sodium nitrite 2.4 g (35 mmol) was dissolved in 2 V of water and added to the reaction mass slowly. Stirred the reaction mass at the same temperature for 30 min and then dissolved Tin chloride 13.74 g (72 mmol) in 3 V of water and added slowly. After complete addition, allow the reaction mass to room temperature and stirred overnight at the same temperature. Reaction monitoring was done by TLC. Thereafter filtered the reaction mass and dry under vacuum and Proceed for the next step. 5.8 g of the titled solid compound was collected as solid in 90.6 % yield.

4.2.1.12 Synthesis of intermediate 5-Bromo-2, 3, 3-trimethyl-3H-indole [7]

The compound was synthesized by the slightly modified procedure as reported by [26] (4-bromophenyl)hydrazine hydrochloride [6] 5 g (22.5 mmol) and 3-Methyl-2-Butanone 5.5 ml (51.8 mmol) was dissolved in 30 ml acetic acid and reflux the reaction mass for overnight. Reaction monitoring was done by TLC. Dry the reaction mass by evaporating the solvent the Thereafter solvent was evaporated and the crude was purified with column chromatography using ethyl acetate-hexane as a solvent system. 4.6 g of the titled compound was collected as a red liquid in 86.3 % yield. HRFAB- MS (measured m/z: 238.0221 $[M+H]^+$; calculated m/z: 237.0153).

4.2.1.13 Synthesis of intermediate ethyl (E)-3-(2,3,3-trimethyl-3H-indol-5-yl)acrylate [8]

After sightly modification in the procedure as reported by [27] compound [8] was synthesized. Added 5-Bromo-2,3,3-trimethyl-3H-indole [7] 2 g (8.4 mmol) in High pressure reaction tube with silicon gasket, to it 102 mg (0.33 mmol) of $P(O\text{-}tol)_3$ and $Pd(OAc)_2$ 18 mg (0.084 mmol) were added, followed by 6 ml trimethylamine, ethyl acrylate 1.34 ml (12.6 mmol) and 20 ml DMF. The reaction was heated at 130 ^{0}C for 10-12 hrs. After the reaction mixture cool to room temperature, Reaction monitoring was done by TLC. Thereafter Ethyl acetate was used to extract the product. After evaporating the solvent, column chromatography was performed by using ethyl acetate-hexane as mobile phase. 1.2 g of the titled compound was collected as a solid in 52.1 % yield. HRFAB- MS (measured m/z: 258.1489 $[M+H]^+$; calculated m/z: 257.1416).

4.2.1.14 Synthesis of intermediate (E)-5-(3-ethoxy-3-oxoprop-1-en-1-yl)-1-ethyl-2,3,3-trimethyl-3H-indol-1-ium [9]

To a round bottom flask fitted with a reflux condenser, 1.2 gm (4.66 mmol) of ethyl (E)-3-(2,3,3-trimethyl-3H-indol-5-yl) acrylate [8] and 1.12 ml (14.0 mmol) of 1-Iodoethane was dissolved in 20 ml Acetonitrile and the mixture was refluxed under nitrogen for 24 hrs. After the complete consumption of the starting material, confirmed by TLC. Solvent and the excess of 1-Iodoethane were removed by evaporation under vacuum. The residue was precipitated out in diethylether.0.900 mg of desired compound was obtained as red solid in 69.2% Yield. HRFAB-MS (measured m/z: 286.1809 $[M+H]^+$; calculated m/z: 286.1802).

4.2.1.15 Synthesis of intermediate (E)-4-((3-dodecyl-1,1-dimethyl-1H-benzo[e]indol-3-ium-2-yl)methylene)-2-(((E)-5-((E)-3-ethoxy-3-oxoprop-1-en-1-yl)-1-ethyl-3,3-dimethylindolin-2-ylidene)methyl)-3-oxocyclobut-1-en-1-olate [10]

To a round bottom flask fitted with condenser, 900 mg (3.1 mmol) of tert-butyl (E)-5-(3-ethoxy-3-oxoprop-1-en-1-yl)-1-ethyl-2,3,3-trimethyl-3H-indol-1-ium [9] and 1.48 g (3.1 mmol) of (E)-4-((3-dodecyl-1,1-dimethyl-1H-benzo[e]indol-3-ium-2-yl)methylene)-2-hydroxy-3-oxocyclobut-1-en-1-olate intermediate [4] was dissolved in 30 mL of 1:1 toluene/n-butanol. The reaction mixture was then refluxed for 6-8 hrs. Reaction progress was monitored by TLC, Thereafter the solvent was evaporated and the crude was purified with column chromatography using chloroform methanol solvent as eluent. 1.2 g of the desired compound was collected as a blue solid in 52.1 % yield. HR-FAB-MS (measured m/z: 741.4626$[M]^+$; calculated m/z: 740.4553).

4.2.1.16 Synthesis of Unsymmetrical Squarine dye SQ-139

1.2 g (1.6 mmol) of (E)-4-((3-dodecyl-1,1-dimethyl-1H-benzo[e]indol-3-ium-2-yl) methylene)-2-(((E)-5-((E)-3-ethoxy-3-oxoprop-1-en-1-yl)-1-ethyl-3,3-dimethylindolin-2-ylidene) methyl)-3-oxocyclobut-1-en-1-olate [10] was dissolved in 20 mL ethanol in a 50 mL round bottom flask. To this solution 5 equivalent 4 N NaOH was added and refluxed for 2 h. Reaction progress was monitored by TLC, the reaction mixture was cooled to room temperature and the solvent was evaporated under vacuum. After complete evaporation, the reaction mixture was acidified by

diluted HCl and rection mass was then extracted in chloroform and chloroform layer was washed with brine. 400 mg of the desired compound was collected as a blue solid in 34.7 % yield. HR-FAB-MS (measured m/z: 713.4318[M] $^{+}$; calculated m/z: 712.4240). ^{1}H NMR (500 MHz, CDCl3): δ/ppm = 8.22(s,H-4); 7.89(d,H-7); 7.79(d,H-8); 7.61(d,H-44); 7.60(d,H-9); 7.49(t,H-6); 7.48(d,H-43); 7.45(s,H-41); 7.34(t,H-5); 6.96(d,H-45); 6.94(d,H-48); 6.46(s,H-28); 6.43(s,H-33); 4.1(q,H-46); 4.03(d,H-16); 1.86(s, H-39 and H-40); 1.41(s,H-14-15), 1.39(m,H-17-26); 1.27(t,H-47),0.88 (t,H-27).

4.2.1.17 Synthesis of intermediate 2,3,3-trimethyl-3H-indole-5-carbonitrile [12]

The compound was synthesized by the slightly modified procedure as reported [28] and reported by Pham et al [29]. To a round bottom flask fitted with a reflux condenser, 2 gm (11.79 mmol) of 4-hydrazineylbenzonitrile hydrochloride [11] and 3.81 ml (35.3 mmol) of 3-methyl-2-butanone was dissolved in ethanol and the mixture was refluxed under nitrogen for 2 h. After the complete consumption of 4-cyano hydrazine hydrochloride, confirmed by TLC. Dry the reaction mass under vacuum. The residue was dissolved in 100 mL glacial acetic acid and refluxed for 12 h. After the completion of the reaction acetic acid was removed under vacuum and column chromatography was performed by using ethyl acetate and hexane as eluent.1.6 g of titled compound was obtained as red solid in 73.7% Yield. HRFAB- MS (measured m/z: 185.1083 [M+H] $^{+}$; calculated m/z: 184.1000).

4.2.1.18 Synthesis of intermediate 5-cyano-1-ethyl-2,3,3-trimethyl-3H-indol-1-ium iodide [13]

After slight modification in the procedure as reported by [28]. To a round bottom flask fitted with a reflux condenser, 1.6 gm (8.69 mmol) of 2,3,3-trimethyl-3H-indole-5-carbonitrile [12] and 2.09 ml (26.08 mmol) of 1-Iodoethane was dissolved in Acetonitrile and the mixture was refluxed under nitrogen for 24 hrs. Reaction progress was monitored by TLC. Solvent and the excess of 1-Iodoethane were removed by evaporation under vacuum. The residue was precipitated out in diethylether.1.55 g of titled compound was obtained as red solid in 86.1% Yield. HRFAB- MS (measured m/z: 341.0508 [M+H] $^{+}$; calculated m/z: 340.0436).

4.2.1.19 Synthesis of intermediate tert-butyl (E)-2-cyano-3-(1-ethyl-3,3-dimethyl-2-ethyleneindolin-5-yl)acrylate [16]

After hydrolyzing 1.5 g (4.4 mmol) of 5-cyano-1-ethyl-2,3,3-trimethyl-3H-indol-1-ium iodide salt [13], using 16 ml of 2 N NaOH and toluene to its methylene base, the resulting base was isolated by extracting in toluene, drying, and evaporating to obtained 800 mg solid as 1-ethyl-3,3-dimethyl-2-methyleneindoline-5-carbonitrile [14]. To a solution of methylene base [14] in 15 mL dichloromethane at 0 ^{0}C, was added slowly 4.4 mL (4.40 mmol, 1 M solution in THF) of DIBAL-H. After stirring for 12 hrs under nitrogen atmosphere, the reaction mixture was quenched by dilute HCl (2 ml) and the reaction mass was refluxed for 30 min. The crude product was extracted into chloroform, washed with water, and dried over Na_2SO_4. After evaporating the solvent under vacuum, 700 mg (3.2 mmol, 86.3%) of 1-ethyl-3,3-dimethyl-2-methyleneindoline-5-carbaldehyde [15] thus obtained was dissolved in 15 mL of acetonitrile. To this solution was added 0.9 mL (6.5 mmol) of tert-butyl-cyan acetate and 0.48 ml (4.8 mmol) of Piperidine. After refluxing the reaction mixture for 7-8 hrs, the solvent was evaporated and performed column chromatography by using hexane: ethyl acetate (6:1) as eluting solvent to obtain colored liquid desired compound in Yield 850 mg (77.2%). HRFAB- MS (measured m/z: 339.2078 $[M+H]^{+}$; calculated m/z: 338.1994).

4.2.1.20 Synthesis of intermediate (E)-2-(((E)-5-((E)-3-(tert-butoxy)-2-cyano-3-oxoprop-1-en-1-yl)-1-ethyl-3,3-dimethylindolin-2-ylidene) methyl)-4-((3-dodecyl-1,1-dimethyl-1H-benzo[e]indol-3-ium-2-yl) methylene)-3-oxocyclobut-1-en-1-olate [17]

To a round bottom flask, 500 mg (1.47 mmol) of tert-butyl (E)-2-cyano-3-(1-ethyl-3,3-dimethyl-2-methyleneindolin-5-yl) acrylate [12] and 699 mg (1.47 mmol) of (E)-4-((3-dodecyl-1,1-dimethyl-1H-benzo[e]indol-3-ium-2-yl) methylene)-2-hydroxy-3-oxocyclobut-1-en-1-olate intermediate [4] was dissolved in 30 mL of 1:1 toluene/n-butanol. The reaction mixture was then refluxed for 6-8 hrs. Thereafter the solvent was evaporated and product purification was done by column chromatography using chloroform methanol solvent as mobile phase. 650 mg of the titled compound was collected as a greenish solid in 55.5 % yield. HR-FAB-MS (measured m/z: 794.4894 $[M]^{+}$; calculated m/z: 793.4819).

4.2.1.21 Synthesis of Unsymmetrical Squarine dye SQ-140

600 mg (0.75 mmol) *(E)-2-(((E)-5-((E)-3-(tert-butoxy)-2-cyano-3-oxoprop-1-en-1-yl)-1-ethyl-3,3-dimethylindolin-2-ylidene) methyl)-4-((3-dodecyl-1,1-dimethyl-1H-benzo[e]indol-3-ium-2-yl)*

methylene)-3-oxocyclobut-1-en-1-olate dye [17] was dissolved in 3 mL of trifluoroacetic acid (TFA) and stirred for 6-8 hrs at room temperature. Reaction progress was monitored by TLC, TFA was evaporated and performed column chromatography by using methanol: chloroform (1:9) solvent system as eluent to give 420 mg of targeted compound SQ-140 as greenish solid 75.4% yield. HRFAB- MS (measured m/z: 738.4273 $[M+H]^+$; calculated m/z: 737.4193).^{1}H NMR (500 MHz, CDCl3): δ/ppm = 8.28(s,H-43); 8.24(d,H-4); 8.06(d,H-7); 7.99(d,H-8); 7.94(d,H-9); 7.63(d,H-44); 7.51(t,H-5); 7.46(t,H-6); 7.05(s,H-41); 6.99(d,H-45); 6.20(s,H-28); 6.05(s,H-33); 4.28(q,H-46); 4.06(t,H-16); 2.97(s,H-39 and H-40); 2.83(s, H-14 and H-15); 1.88(t,H-47), 1.46(m,H-17-26); 0.97(d,H-27).

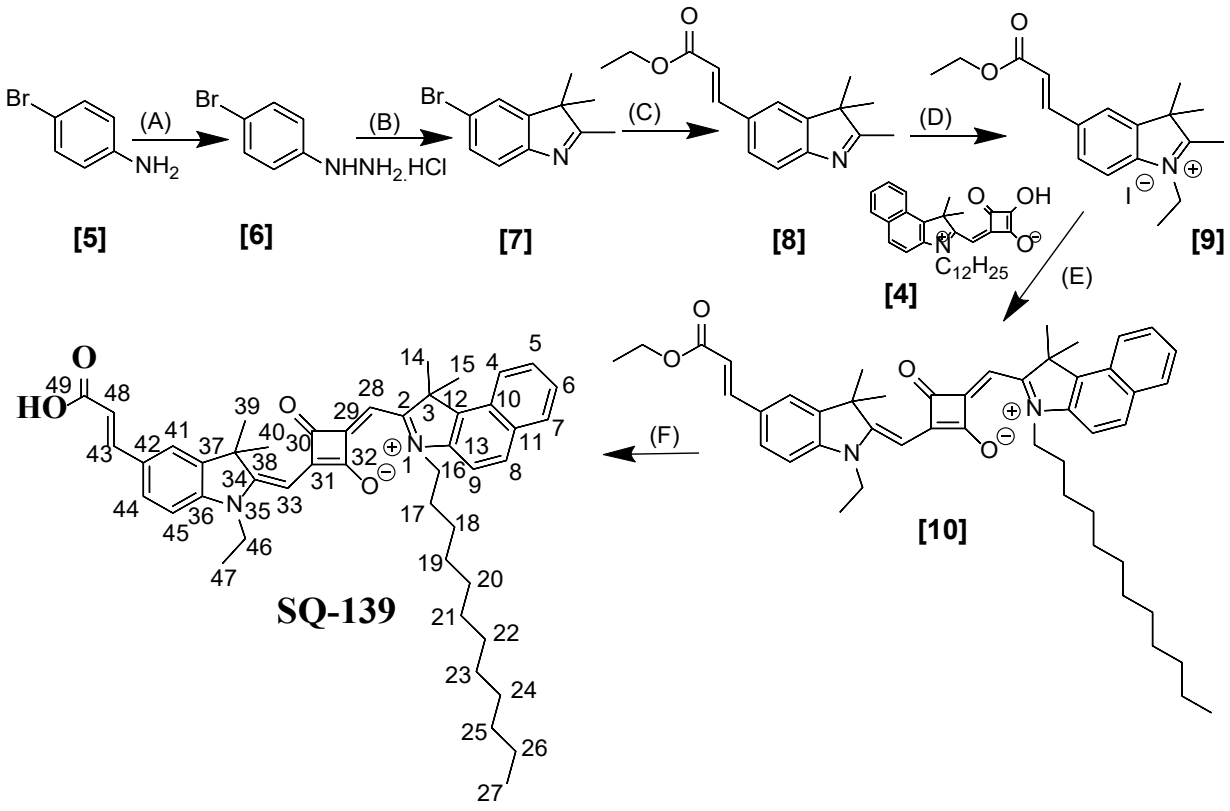

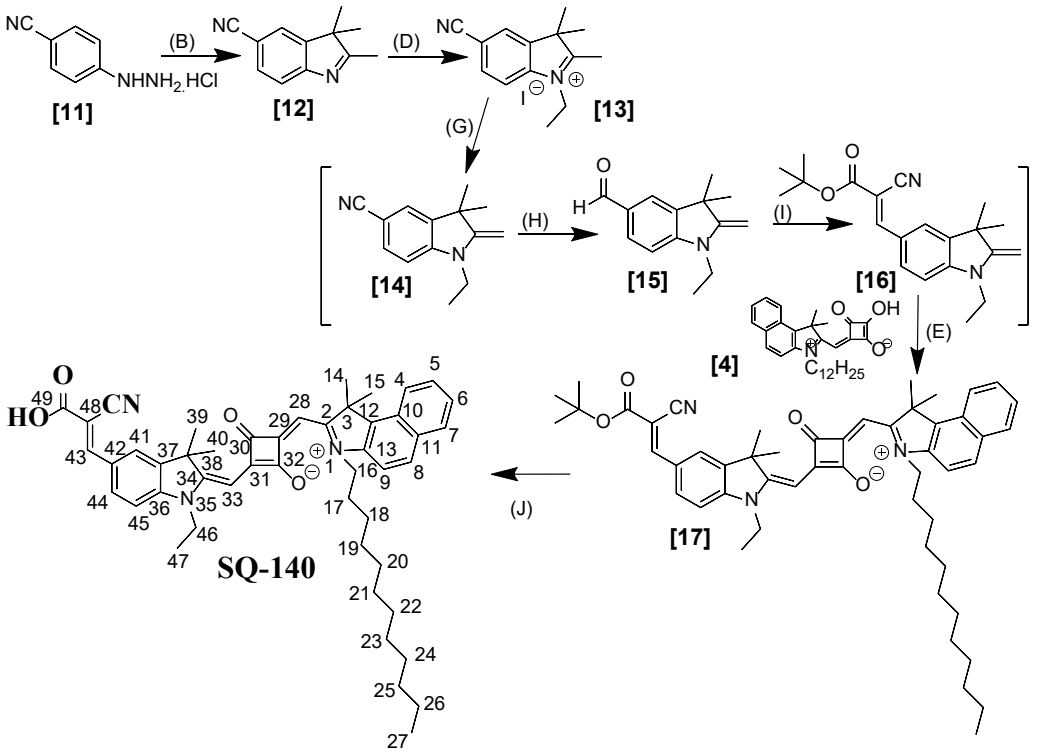

Scheme-2 Synthetic scheme for the preparation of SQ-139 and SQ-140 unsymmetrical squaraine dyes bearing different anchoring groups. (A) $NaNO_2$, $SnCl_2$, Conc. HCl, 0^0C, 12 hrs (B) 3-Methyl-2-butanone, Acetic acid, Reflux, 12 hrs (C) Ethyl acrylate, $Pd(OAc)_2$, $P(O\text{-}tol)_3$, TEA, DMF, High Pressures reaction tube, 130^0C, 10-12hrs (D) 1-Iodoethane, Acetonitrile, Reflux, 24hrs (E) n-butanol, Toluene, Reflux, 6-8hrs (F) 4N NaOH, Ethanol, Reflux, 1hr (G) 2N NaOH, Toluene, RT, 2 hrs (H) DIBAL, DCM, RT, 12 hrs (I) Tert. Butyl cyanoacetate, Piperidine, Acetonitrile, Reflux, 7-8 hrs (J) TFA, RT, 6-8 hrs

4.2.2 Structural elucidation

Structure elucidation of the dye is the process of determining the chemical structure of a compound from the identification and characterization of the intermediates and the finished products. Nuclear magnetic resonance (NMR) spectroscopy is a very sensitive method for characterizing the stereo- chemical structure. Structure elucidation of the synthesized products has been done by nuclear magnetic resonance (NMR) spectroscopy and mass spectrometry. In this work structural elucidation was performed, and the final dyes were analyzed in the deuterated chloroform ($CDCl_3$) by NMR spectrometer (JEOL, 500 MHz) and the intermediates were confirmed by Matrix-Assisted Laser Desorption and Ionization (MALDI)-Time-of-Flight (TOF)-mass or Fast Ion Bombardment (FAB)-mass spectrometry in the positive ion-monitoring mode.

4.2.3 Dye Adsorption behavior

Dye adsorption behavior of the synthesized dyes was investigated using 4 μm thick PST-30NRD transparent TiO_2 paste (1 cm^2 area) coated on the non-conducting glass substrate. TiO_2 coated glass substrate was then dipped in 0.1 mM ethanolic solution of the respective dyes and extent of dye adsorption was observed till saturation with respect to the time as shown in the figure-3 was monitored spectrophotometrically by measuring the absorbance of dyes at their absorption maximum (λmax).

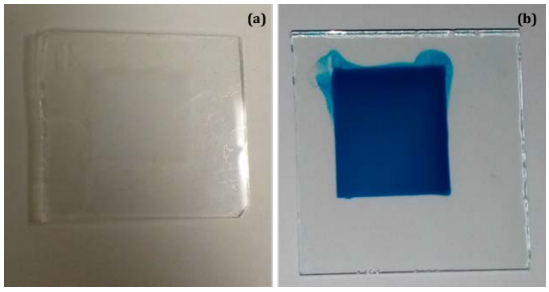

Figure-3. 4 μm thick and 1 cm^2 area PST-30NRD TiO_2 for the dye adsorption behavior (a) before dye adsorption and (b) after complete dye adsorption.

4.2.4 Electrochemical characterization

The electrochemical stability of the sensitizing dyes is an important criterion for the functioning of the solar cell. Upon light irradiation electrons of the molecule excites from their Highest Occupied Molecular Orbital (HOMO) to the Lower Unoccupied Molecular Orbital (LUMO). For the best energy matching, LUMO should be higher than the conduction band of the semiconductor TiO_2 and HOMO should be lower than the electrode potential of the redox electrolyte.

HOMO was estimated from the first oxidation peak of the dye concerning the Ferrocene reference by the cyclic voltammetry method. Cyclic voltammetry (CV) technique is one of the widely used technique in DSSC research for electrochemical characterization and HOMO estimation. The estimation of the HOMO from this method is more reliable and all HOMO values are nearly similar to the theoretical HOMO values which were calculated by TD-DFT using 6-311 G/B3PW91. Cyclic voltammetry of unsymmetrical squaraine dyes (0.2 mM concentration) was recorded in Dimethylformamide (DMF) solution along with ferrocene (0.2 mM concentration) reference standard using a similar electrode, tetrabutylammonium

hexafluorophosphate (0.1M) as the supporting electrolyte and scan rate, which is shown in the Figure-4. All the squaraine dyes bearing different functional group and introduction of electron-withdrawing groups like −COOH (SQ-138), Acrylic acid (SQ-139), Cyano acrylic acid (SQ-140), $–SO_3H$ (SQ-142), and $-PO_3H_2$ (SQ-143) shifts the oxidation peak towards higher potential as compared to that of electron-donating −OH group (SQ-141) containing squaraine dye. This could be attributed to the stabilization of molecular orbitals upon the introduction of functional groups with an electron-withdrawing nature. In this work, 1st oxidation potential of the corresponding dyes has been used to estimate the HOMO energy level of dyes. A shift in oxidation potential of the dyes concerning the oxidation potential of Fc/Fc^+ redox couple was used to calibrate the HOMO energy level of dyes concerning the vacuum level. To conduct the CV, 0.2 mM concentration dye were dissolved in Dimethylformamide (DMF) with 0.1 mM tetrabutylammonium hexafluorophosphate as the supporting electrolyte. The HOMO value of the dyes was calculated from the shift in the oxidation peak concerning the Fc/Fc^+, whose value was taken as -5.01 eV as per the published by Su and Girault [30]. In the end, energy band diagram was constructed by calculating the HOMO value.

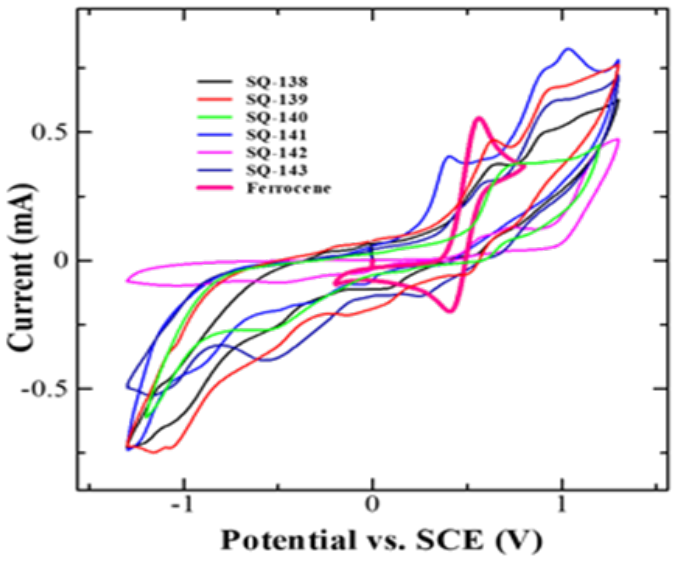

Figure-4 Cyclic Voltammetry of the unsymmetrical squaraine dyes and ferrocene as a reference standard in DMF recorded using Pt working/counter electrode and saturated calomel electrode (SCE) as a reference electrode.

4.2.5 Dye adsorption stability

The stability behavior of the dyes on the mesoporous TiO_2 was estimated by UV spectrometry. 0.2 mM respective dye and 20 mM of disaggregating agent CDCA were dissolved in dehydrated Ethanol. Dye was completely adsorbed on the glass substrate coated with mesoporous TiO_2 paste D/SP (Solaronix) having a ~15 μm thickness and 6.25 cm^2 area as shown in figure-5. The relative stability behavior of the dyes was estimated by putting the dye adsorbed TiO_2 in Acetonitrile: water (1:1) ratio at room temperature and the extent of dyes desorbed from substrate in to the solution was record spectrophotometrically. Quantitation of the desorbed dyes after a defined time of dye desorption was carried estimated by spectrophotometry using standard calibration curves of the respective dyes. 40 mM NaOH solution in t-Butanol: Acetonitrile: Water: Ethanol solution taken in an equal ratio for the removal of the remaining dyes from the mesoporous TiO_2 has been used.

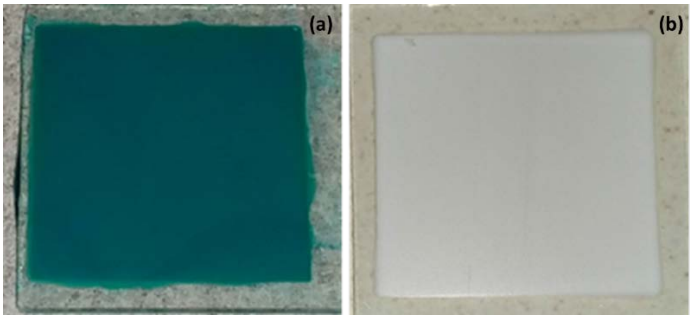

Figure-5. Mesoporous TiO_2 for the dye adsorption stability (a) after complete dye adsorption and (b) after complete dye desorption.

4.2.6 Device fabrication and characterization

Photo anode (Working electrode) was constructed by Fluorine doped Tin oxide (FTO) glass substrate coated with D/SP mesoporous *opaque 15-20* particles *size* TiO_2 paste. D/SP was printed on a glass substrate by screen printing method followed by sintering at 500 ^{0}C for 1 hr. to obtain the optimum thickness (10-12 μm) as shown in the figure-6 double layer of D/SP was screen printed and baked at the same temperature. The substrate was then dipped into the solution of 0.2 mM of the respective dyes and 20 mM de-aggregating agent chenodeoxycholic acid (CDCA) in dehydrated ethanol till complete adsorption.

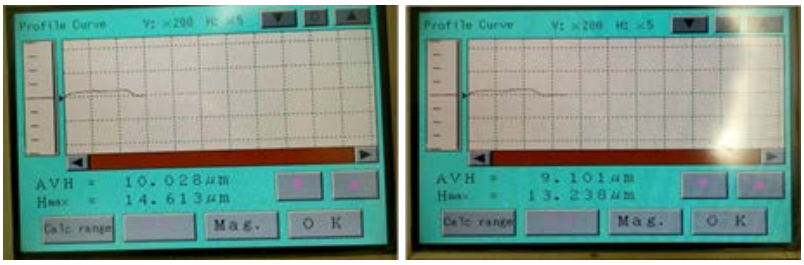

Figure-6. Thickness of the theTiO_2 paste working electrode

A catalytic Pt sputtered or spin coated 50 µl Hexachloroplatinate (Plastisol T) on FTO glass was employed as the counter electrode. Iodine based redox couple electrolyte (I_3^-/I^-) containing composition LiI (0.5 M), iodine (0.05 M), t-butyl pyridine (0.5 M), 1, 2-dimethyl-3-propylimidazolium iodide (0.6 M) in acetonitrile was used for solar cell fabrication and filled through the diagonal or the hole between the working electrode and counter electrode. The device was finally sealed by using a 25 µm hot melt spacer and epoxy resin by exposing UV light. Photoconversion efficiency of the solar cells was evaluated using a solar simulator (CEP-2000 Bunko Keiki Co. Ltd, Japan) equipped with a xenon lamp (Bunko Keiki BSO-X150LC) used as a source of simulated solar irradiation at 100 mW/cm^2, AM 1.5 G.)

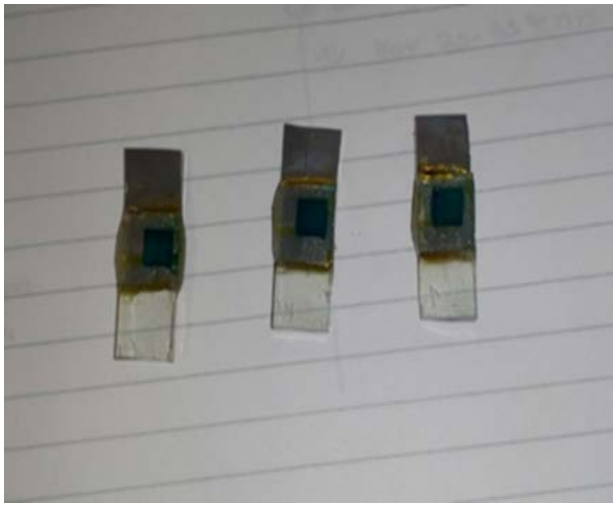

Figure-7. A dye-sensitized solar cell made in the lab.

4.3 Results and discussion

4.3.1 Optical characterizations

4.3.1.1 Electronic absorption spectra

Electronic absorption spectra of the synthesized unsymmetrical squaraine dyes were performed in 5μM ethanolic solution as shown in Figure-9. It can be seen from this figure that these dyes exhibit very sharp, intense, and narrow light absorption mainly in the far-red (550 nm–700 nm) wavelength window of the solar spectrum. At the same time, these dyes show very high molar extinction coefficients (ε) in the range $1-3\times10^5$ $dm^3. mol^{-1}. cm^{-1}$ and ε values of these dyes are about 10 times higher than the typical ruthenium complex-based dyes like N3 [31]. The reason of the appreciably high molar extinction coefficient might be due to the intramolecular charge transfer along with the extended π-electron donor network, π-π* electronic transition, and also due to the presence of central squaric acid moiety having a strong electron-withdrawing nature [32]. It can also be seen from this figure that dyes SQ- 138, SQ-139, and SQ-140 bearing carboxylic acid, acrylic acid, and cyano acrylic acid functional groups, respectively, exhibit relatively red-shifted absorption maximum (λmax) at SQ-138 (654nm), SQ-139 (664 nm) and SQ-140 (670 nm), which could be defend due to the extended π-conjugation of the anchoring group carboxylic acid to acrylic acid to cyano acrylic acid respectively, contributed from the S and P atoms of the anchoring groups.

Figure-8. Solutions of the different dyes for Electronic absorption spectra and Fluorescence emission spectra

4.3.1.2 Fluorescence emission spectra

Squaraine dyes exhibits strong fluorescence intensity. Fluorescence emission spectra of these dyes were also recorded in the 5 µm ethanol solution and shown in Figure-9 along with the summarization of optical parameters in Table 1. It can also be seen from the figure that emission spectra of the dyes are mirror images of their absorption spectra with narrow spectral width and emission maxima shifted to the longer wavelength region with the offset above 700 nm. The wavelength difference between absorption maximum and emission maximum (Stokes shift) was also calculated and shown in Table 1. A perusal of the Figure-9 and Table 1 reveals that small stokes shift of 12−17 nm depicts the conformational rigidity of the molecules in the excited state [33]. SQ-142 with sulphonic acid anchoring group possess the minimal stokes shift of only 12 nm signifying the highest conformational stability.

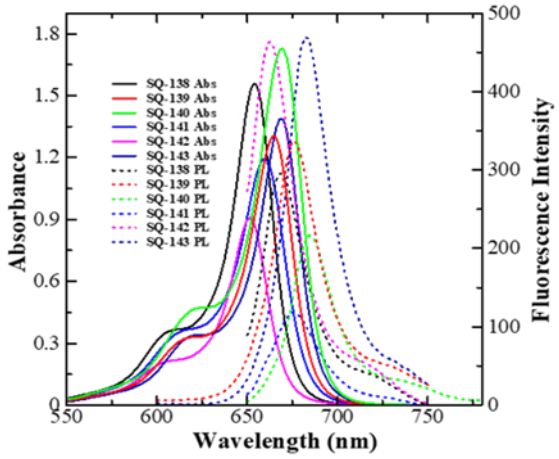

Figure-9. Electronic absorption (solid line) and fluorescence emission (dotted line) spectra of unsymmetrical squaraine dyes in ethanol solution.

Table-1. Optical parameters for unsymmetrical squaraine dyes in ethanol solution and on a thin film with dye adsorbed on TiO_2.

Sensitizing dyes	Ɛ (dm3. Mol−1. cm-1)	Absorption (solution) λmax (nm)	Emission (solution) λmax (nm)	Stokes Shift (nm)	Absorption (TiO_2) λmax (nm)	Optical absorption edge (eV)
SQ-138	3.1×10^5	654	668	14	654	710 nm (1.75 eV)
SQ-139	$4..8\times10^5$	652	664	12	656	710 nm (1.75 eV)
SQ-140	3.4×10^5	670	684	14	678	740 nm (1.67 eV)
SQ-141	2.4×10^5	660	674	14	670	725 nm (1.71 eV)
SQ-142	1.8×10^5	652	660	8	652	700 nm (1.77 eV)
SQ-143	4.8×10^5	652	664	12	656	710 nm (1.75 eV)

4.3.2 Theoretical molecular orbital calculations

The recent past has witnessed that MO calculations is one of the best tool in the field of DSSC research aiming towards the design and development of novel sensitizers by prior prediction of their energetics and electronic absorption spectra. Due to reliable prediction of energies and electronic absorption spectra of functional molecules, Time Dependent DFT theory has been widely used [34]. Different basis set and hybrid functional like 6-311G B3PW91 respectively in combination with polarization continuum model PCM model as implemented Gaussian 09 based for the geometry of the squaraine dyes as per our earlier publications [35-36]. The optimized geometric structure along with the distribution of electron density in the HOMO and LUMO of unsymmetrical dyes is shown in Figure-10. It can be seen that electron clouds in HOMO for these dyes are mainly concentrated at the central squaric acid core and slightly extended to the π-framework attached near to the core of the dye molecules. However, in the LUMO it exhibits relative reduction near the squaric acid core and dominance of electron density towards anchoring group bearing indole unit indicating the possibility of intramolecular charge transfer (ICT) upon photoexcitation. This is desirable for the sensitizer of DSSC ensuring sufficient electronic coupling between the excited dye molecule and vacant d-orbitals of the wide-bandgap semiconductor (TiO_2 in present work). This also ensures the facile electron injection if the LUMO energy level of the dye is above the CB energy level of electron-accepting TiO_2. Electron density distribution in HOMO of all four newly designed sensitizers is almost the same. On the other hand, electron density distribution in the LUMO of dyes bearing different anchoring groups varies, which is shown in Figure-10. It can be seen from the Figure-10 that electron density distribution in the LUMO unsymmetrical squaraine dyes SQ-138, SQ-139, SQ-140, and SQ-142 bearing -COOH, acrylic acid, cyano acrylic acid, and -SO_3H anchoring groups respectively not only exhibits ICT but also diversion of sufficient electron density at the anchoring group. This suggests their suitability as sensitizers of DSSC since both of them possess a sufficient driving force for electron injection in the TiO_2 as shown in Figure-10. since these sensitizer dyes possess a sufficient driving force for electron injection in the CB of TiO_2. On the other hand, the other two dyes SQ-141 and SQ-143 bearing −OH and –PO_3H_2 anchoring groups not only lack prominent ICT but also appear to face hindrance in the electron injection is due to the low electron density on LUMO despite sufficient driving force for the electron injection. This also explains the reason

behind the relatively lower photovoltaic performance of dyes bearing -PO_3H_2 anchoring groups as compared to that of their –COOH, acrylic acid, and cyano acrylic acid anchoring group counterparts [37, 38]. As discussed earlier, the energetics of the photo functional molecules play a dominant role in their utilization as sensitizers in the DSSCs, therefore, their prior accurate prediction is expected to accelerate the development of novel sensitizers.

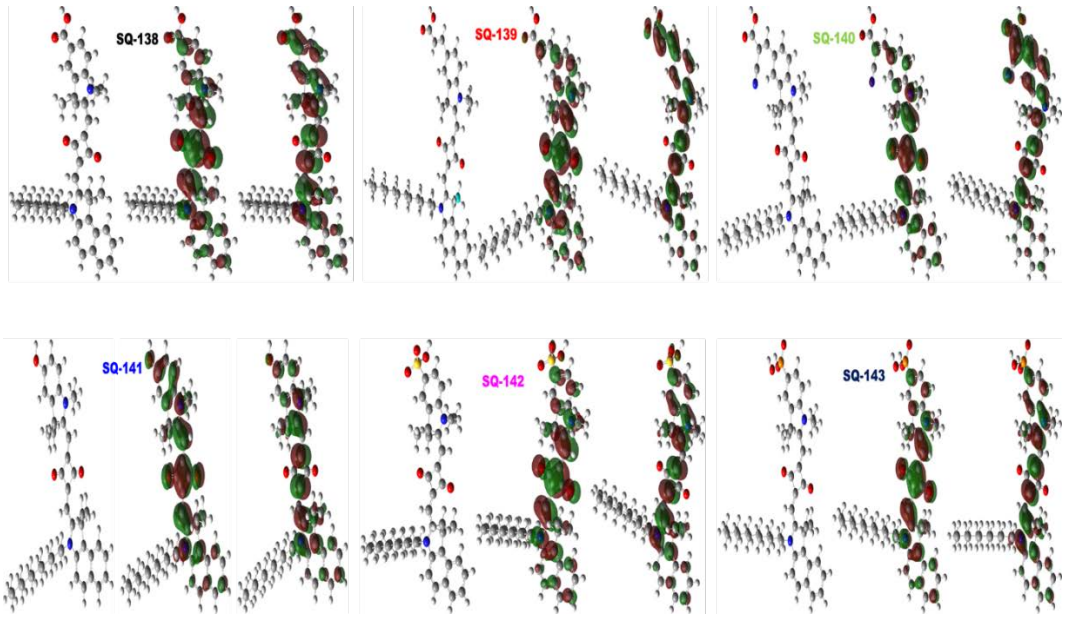

Figure-10. Theoretically calculated optimized structure, electron density distribution in the HOMO and LUMO respectively for the unsymmetrical squaraine dyes bearing different anchoring groups.

4.3.3 Dye Adsorption behavior

Sensitizing dyes are adsorbed onto the surface of wide bandgap semiconductors TiO_2 via suitable chemical linkage and the nature of binding not only controls the electron injection but also affect stability behavior to the DSSCs. Therefore, optimal adsorption of sensitizing dyes on the mesoporous TiO_2 is one of the most major steps for the fabrication of photo anode of DSSCs. Complete adsorption of the monolayer of sensitizing dyes on the TiO_2 nanoparticle is sufficient for the optimal performance of the photo anode. In-sufficient dye adsorption not only leads to hampered photon harvesting but also results in back electron transfer from electrons injected in TiO_2 and oxidized dye and electrolyte [39]. An excess amount of the adsorbed dye leads to

unwanted dye aggregation resulting in poor electron injection [40]. Structure of the dye, nature of the of the dye molecule, and the interaction of the dye molecule with TiO_2 defines the adsorption behavior and binding strength of the sensitizer dye molecule with TiO_2.

In this work, an effort was also directed to investigate the adsorption behavior of NIR dyes bearing different types of functional groups involved for anchoring on the TiO_2 nanoparticles.

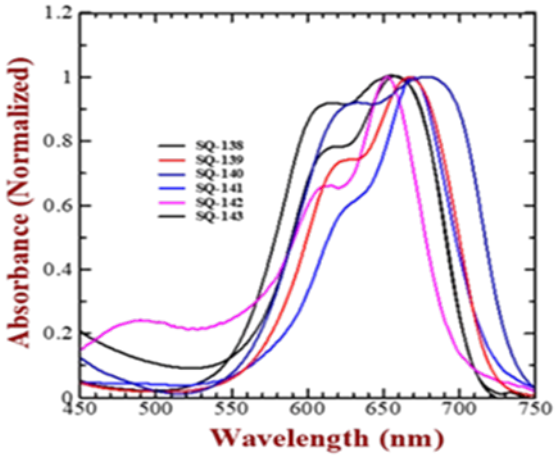

Figure-11. Normalized solid-state absorption spectra of squaraine dyes adsorbed on mesoporous TiO_2.

Figure 11 depicts the adsorption behavior of unsymmetrical squaraine dyes with different types of anchoring groups on TiO_2. Adsorption of the squaraine dyes was conducted using 4 mm thick mesoporous TiO_2 (PST-30NRD, Solaronix) from the 0.1 mM ethanolic solution of the respective dyes at room temperature. It can be seen that the nature of the anchoring group highly affects the dye aggregation behavior, SQ-140 bearing cyano acrylic acid and SQ-138 having carboxylic acid as an anchoring group are highly prone to the H-aggregation (92.02%) and (91.81%) respectively as shown in the figure-12 and table-2 as compare to the other sensitizers. This could be attributed to the enhanced dye aggregation due to H-aggregate formation associated with promoted hydrogen bonding interactions. Kim et al. have also emphasized that some squaraine surfactants easily form blue-shifted H-aggregates on TiO_2 surfaces absorbing around 500 nm wavelength region [41].

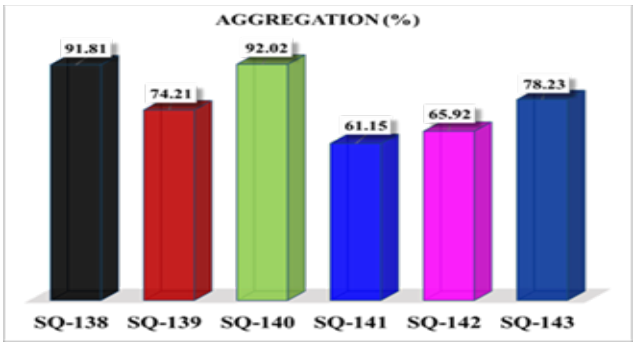

Figure-12. The extent of dye aggregation of squaraine dyes on mesoporous TiO_2.

Table-2. The extent of dye aggregation of unsymmetrical squaraine dyes on thin-film mesoporous TiO_2.

Sensitizing dye	Aggregation (%)
SQ-138	91.81
SQ-139	74.21
SQ-140	92.02
SQ-141	61.15
SQ-142	65.92
SQ-143	78.23

This also can be explained because contrary to the –COOH groups of both the dyes SQ-138 and SQ-140 lies in the same plane of the dye framework, additionally in the case of SQ-140 cyano group will also take the part in the H-bond formation resulting in high aggregation behavior. From the figure-12 and table-2, It is highly worth mentioning here that in-spite of sufficient electron density in the LUMO, the planner structure of the –COOH in the SQ-139 which bearing acrylic acid as an anchoring group exhibit less aggregation (74.21%) as compare to SQ-138 and SQ-140. On the other hand, SQ-143 containing Phosphonic acid as an anchoring group does not have good electron density in its LUMO but this dye shows less aggregation behavior (78.23) which might be good for its binding strength with Mesoporous TiO_2. At the same, time SQ-142 bearing sulfonic acid anchoring group not only exhibit clear vibronic peak but also additional absorption shoulder peak in the 450 nm–550 nm, which is not present in the other dyes. Planarity of the sulphonic acid, highly prone to aggregation and presence of S=O bond, amongst all the dyes SQ-143 tends to highly dye aggregation.

The rate of dye adsorption was estimated by monitoring the change in the peak absorbance of the respective dyes after different time intervals. Kinetics of dye adsorption was monitored by the absorbance at the λ_{max} of respective dyes for different time intervals which have been shown in Figure 13. A perusal from this figure corroborates that squaraine dyes bearing acrylic acid (SQ-139) adsorb more swiftly as compared to carboxylic (SQ-138), cyano acrylic acid (SQ-140) and phosphonic acid (SQ-143), adsorb more swiftly as compared to that bearing sulfonic acid (SQ-142) and hydroxyl groups (SQ-141). And rate of dye adsorption follows the order Acrylic acid > carboxylic acid > cyano acrylic acid > phosphonic acid > hydroxyl > sulphonic acid. Adsorption of sensitizing dyes starts with activation of the OH groups on the TiO_2 surface by functional group present on the dye via protonation followed by chemical bonding.

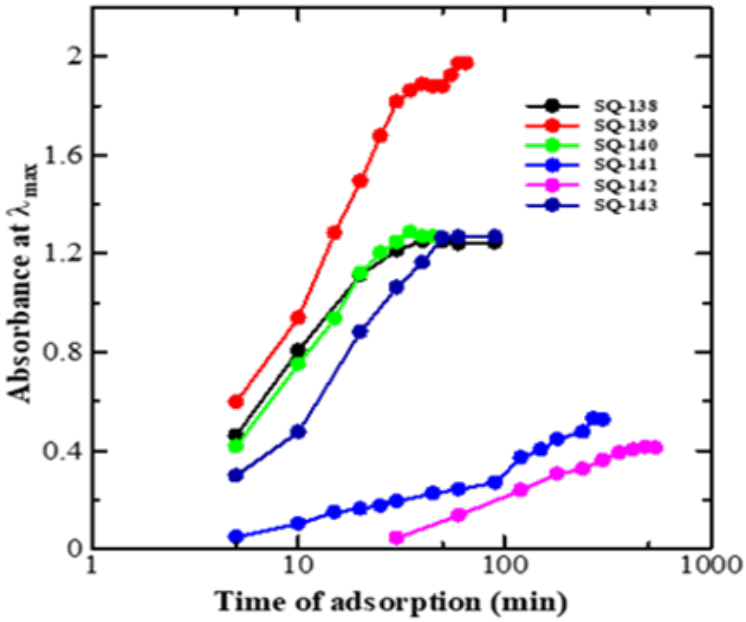

Figure-13. Kinetics of dye adsorption by monitoring the absorbance at the λ_{max} of respective dyes for different time intervals.

As an industrial prospect, strong binding of the dye molecule and swift adsorption of the dye on the mesoporous TiO_2 is highly desired. The implication of the nature of anchoring groups on their adsorption behavior on the thin films of mesoporous TiO_2 was conducted by monitoring the extent of adsorbed dyes as a function of time spectrophotometrically as shown in figure-14.

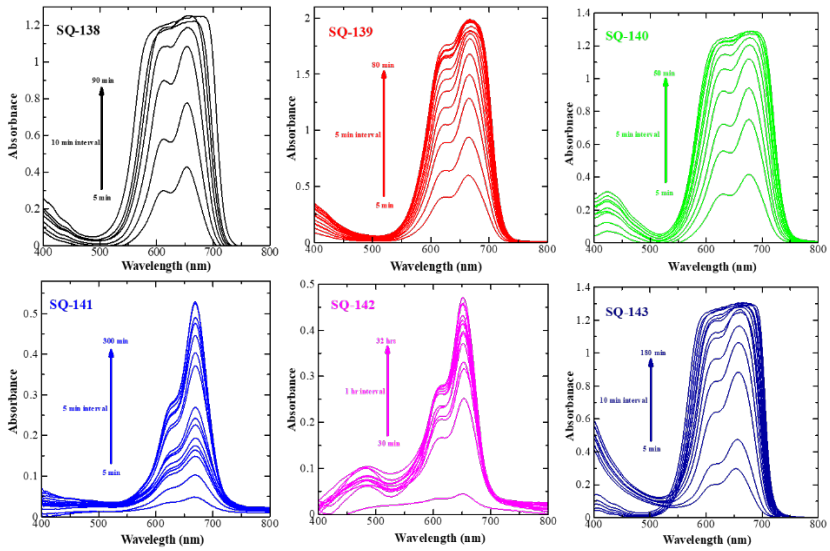

Figure-14. Time-dependent dye adsorption of unsymmetrical Squaraine dyes.

4.3.4 Dye Adsorption stability

To evaluate the rate of dye adsorption of unsymmetrical dyes on mesoporous TiO_2 was conducted on 4 µm thick and 1 cm^2 are of TiO_2 was dipped in the 0.1 mM dye solution and measured the absorbance with time spectrophotometrically. After the calculation of the slope with a maximum co-relation factor rate of dye adsorption evaluated as shown in figure-15.

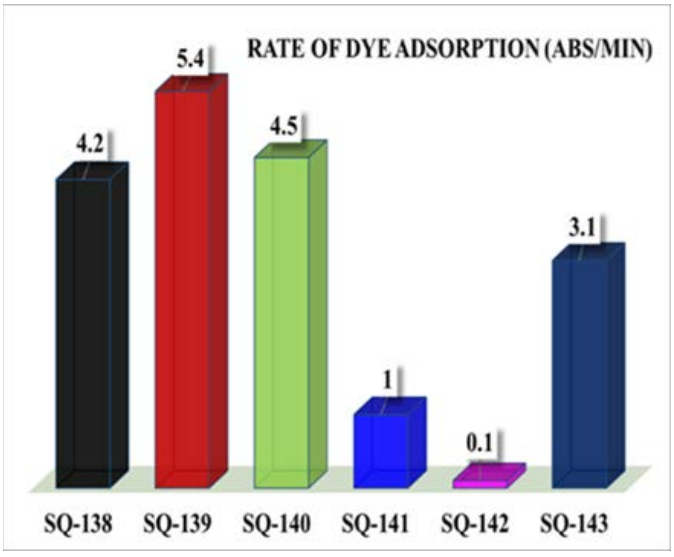

Figure-15. Rate of dye adsorption of squaraine dyes on mesoporous TiO_2.

To evaluate the stability behavior of unsymmetrical squaraine dyes on the mesoporous TiO_2, a dye desorption experiment was conducted. To estimate, total dye loading, 6.25 cm^2 area, and a defined thickness of mesoporous TiO_2 were dipped into the 0.2 mM dye and 20 mM CDCA in ethanol complete adsorption. After complete dye adsorption, the dye was completely desorbed from the surface using 40 mM sodium hydroxide in a solvent mixture of ethanol, acetonitrile, tert. Butanol and water in equal ratio. For relative dye stability studies, dye adsorbed TiO_2 substrate of respective dye, was put in 1:1 (V/V) mixture of acetonitrile and water at room temperature and amount of dye desorbed after a defined time in each case was estimated spectrophotometrically. Results of dye desorption for the photoanodes fabricated using dyes bearing different anchoring groups are summarized in the figure-16 and table-3. A perusal of Table-3 corroborates that under identical conditions of dye desorption on TiO_2 sensitizing dyes exhibit differential binding strength on the mesoporous TiO_2 as estimated by the percentage removal dyes upon putting them into the acetonitrile-water mixture after a defined time. It is worth mentioning here that the weakest binding was exhibited by SQ-140 bearing cyano acrylic acid as an anchoring group (99.7 % removal) and SQ-142 (99.3 %) while SQ-143 bearing phosphonic acid anchoring group, exhibited the strongest binding (1.1 % removal). This suggested that SQ-143, which is containing the PO_3H_2 functional group exhibited the highest stability on the mesoporous TiO_2 as compared to dyes bearing other functional groups. It is very important to notice here that SQ-139 bearing acrylic acid exhibits the second strongest binding strength (42.34 %) after SQ-143. SQ-143 exhibited the highest dye loading (14.29 nmol/µm.cm^2) as shown in figure-17 and table -3.

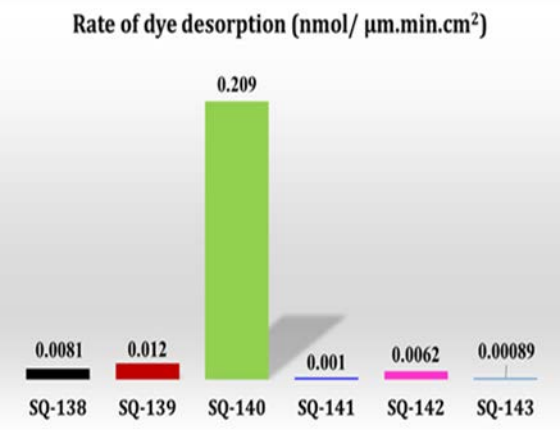

Figure-16. Binding strength of squaraine dyes on mesoporous TiO_2

Which is significantly higher than that of SQ-138 (1.90 nmol/µm.cm^2) bearing the most commonly utilized −COOH functional group, SQ-140 (6.29 nmol/µm.cm^2), bearing cyano acrylic acid and SQ-139 (4.89 nmol/µm.cm^2) bearing acrylic acid which might be attributed to the presence of two −OH functionality of the phosphonic acid anchoring group. Based on dye desorption studies conducted under identical experimental conditions, relative binding strength from the figure-16 and table-3 on the mesoporous TiO_2 follow the order Cyano acrylic acid < – SO_3H <−COOH<−OH< Acrylic acid <-PO_3H_2. (SQ-140 < SQ-142 < SQ-138 < SQ-141 < SQ-139 < SQ-143).

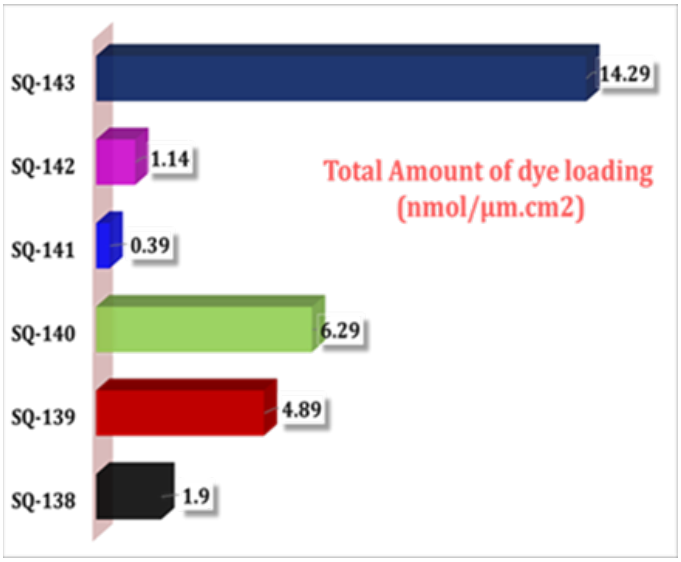

Figure-17. Amount of Dye loading on mesoporous TiO_2

Table-3. Dye adsorption, desorption behavior, and anchoring stability of unsymmetrical squaraine dyes on the mesoporous TiO_2.

Sensitizing Dye	Slope Value	Co-relation factor (%)	Rate of dye adsorption (Abs/min)	Total Amount of dye loading (nmol/µm.cm^2)	Rate of dye desorption (nmol/µm.min.cm^2)	% Removal
SQ-138	0.042	97.40	4.2×10^{-2}	1.90	0.0081	76.7
SQ-139	0.054	98.96	5.4×10^{-2}	4.89	0.012	42.34
SQ-140	0.045	98.74	4.5×10^{-2}	6.29	0.209	99.73
SQ-141	0.010	99.88	1.0×10^{-2}	0.39	0.001	47.5
SQ-142	0.001	98.10	0.1×10^{-2}	1.14	0.0062	99.3
SQ-143	0.031	98.58	3.1×10^{-2}	14.29	0.00089	1.1

SQ-138	
Partial Desorption	Complete desorption
Slope= 0.486	
➢ Abs at λ_{max} = 2.37 ➢ Volume Used = 30 ml ➢ Time = 180 min ➢ 0.486 =1 µM = 2.37/0.486 = 4.87 µM = 4.87 µM/lit = 4.87 nmol/ml = 4.87 nmol/ml × 30 ml **Partial Desorption = 146.1 nmol**	➢ Abs at λ_{max} = 0.720 ➢ Volume Used = 30 ml ➢ 0.486 =1 µM = 0.720/0.486 = 1.48 µM = 1.48 µM/lit = 1.48 nmol/ml = 1.48 nmol/ml × 30 ml **Complete desorption = 44.44 nmol**
➢ Total Amount of dye = Partial Desorption + Complete desorption = 146.1 nmol + 44.44 nmol **= 190.54 nmol** Area of the device= 6.25 cm^2 Total Amount of dye = **30.48 nmol/cm^2** Thickness of the device = 16.0 µm Total Amount of dye = **1.90 nmol/µm.cm^2** ➢ Rate of dye Desorption Partial desorption=146.1 nmol Time= 180 min Rate of dye Desorption = **0.81 nmol/min** Area of the device= 6.25 cm^2 Rate of dye Desorption = **0.129 nmol/min. cm^2** Thickness of the device = 16.0 µm Rate of dye Desorption = **0.0081 nmol/µm. min. cm^2** % Removal = Partial Desorption / Total amount of dye *100 =146.1 nmol/190.54 nmol × 100 **= 76.7 %**	

SQ-139	
Partial Desorption	Complete desorption
Slope= 0.185	
➢ Abs at λ_{max} = 1.208 ➢ Volume Used = 20 ml ➢ Time = 180 min ➢ 0.185 =1 µM = 1.208/0.185 = 6.53 µM = 6.53 µM/lit = 6.53 nmol/ml = 6.53 nmol/ml × 20 ml **Partial Desorption = 130.67 nmol**	➢ Abs at λ_{max} = 1.65 ➢ Volume Used = 20 ml ➢ 0.185 =1 µM = 1.65/0.185 = 8.89 µM = 8.89 µM/lit = 8.89 nmol/ml = 8.89 nmol/ml × 20 ml **Complete desorption = 177.94 nmol**
➢ Total Amount of dye = Partial Desorption + Complete desorption = 130.67 nmol + 177.94 nmol **= 308.61 nmol** Area of the device= 6.25 cm^2 Total Amount of dye = **49.38 nmol/cm^2** Thickness of the device = 10.09 µm Total Amount of dye = **4.89 nmol/µm.cm^2** ➢ Rate of dye Desorption Partial desorption=130.67 nmol Time= 180 min Rate of dye Desorption = **0.73 nmol/min** Area of the device= 6.25 cm^2 Rate of dye Desorption = **0.116 nmol/min. cm^2** Thickness of the device = 10.09 µm Rate of dye Desorption = **0.012 nmol/µm. min. cm^2** % Removal =Partial Desorption / Total amount of dye *100 =130.67 nmol/308.61 nmol × 100 **= 42.34 %**	

SQ-140

Partial Desorption	Complete desorption
Slope= 0.206	
➢ Abs at λ_{max}= 1.92 ➢ Volume Used= 80 ml ➢ Time= 30 min ➢ 0.206=1 µM = 1.92/0.206 = 9.32 µM = 9.32 µM/lit = 9.32 nmol/ml = 9.32 nmol/ml × 80 ml **Partial Desorption = 745.63 nmol**	➢ Abs at λ_{max}= 0.02 ➢ Volume Used= 20 ml ➢ 0.206= 1 µM = 0.02/0.206 = 0.097 µM = 0.097 µM/lit = 0.097 nmol/ml = 0.097 nmol/ml × 20 ml **Complete desorption = 1.94 nmol**

➢ Total Amount of dye = Partial Desorption + Complete desorption
= 745.63 nmol + 1.94 nmol
= 747.57 nmol
Area of the device= 6.25 cm^2
Total Amount of dye = **119.62 nmol/cm^2**
Thickness of the device = 19 µm
Total Amount of dye = **6.29 nmol/µm.cm^2**

➢ Rate of dye Desorption
Partial desorption=745.63 nmol
Time= 30 min
Rate of dye Desorption = **24.85 nmol/min**
Area of the device= 6.25 cm^2
Rate of dye Desorption = **3.97 nmol/min. cm^2**
Thickness of the device = 19 µm
Rate of dye Desorption = **0.209 nmol/µm. min. cm^2**

% Removal =745.63 nmol/747.57 nmol × 100
= 99.73 %

SQ-141

Partial Desorption	Complete desorption
Slope= 0.374	
➢ Abs at λ_{max} = 0.232 ➢ Volume Used = 30 ml ➢ Time = 180 min ➢ 0.374 =1 µM = 0.232/0.374 = 0.62 µM = 0.62 µM/lit = 0.62 nmol/ml = 0.62 nmol/ml × 30 ml **Partial Desorption = 18.6 nmol**	➢ Abs at λ_{max} = 0.256 ➢ Volume Used = 30 ml ➢ 0.374 = 1 µM = 0.256/0.374 = 0.68 µM = 0.68 µM/lit = 0.68 nmol/ml = 0.68 nmol/ml × 30 ml **Complete desorption = 20.53 nmol**

➢ Total Amount of dye = Partial Desorption + Complete desorption
= 18.6 nmol + 20.53 nmol
= 39.13 nmol
Area of the device= 6.25 cm^2
Total Amount of dye = **6.26 nmol/cm^2**
Thickness of the device = 16.0 µm
Total Amount of dye = **0.39 nmol/µm.cm^2**

➢ Rate of dye Desorption
Partial desorption = 18.6 nmol
Time = 180 min
Rate of dye Desorption = **0.10 nmol/min**
Area of the device= 6.25 cm^2
Rate of dye Desorption = **0.016 nmol/min. cm^2**
Thickness of the device = 16.0 µm
Rate of dye Desorption = **0.001 nmol/µm. min. cm^2**

% Removal = Partial Desorption / Total amount of dye *100
= 18.6 nmol/ 39.13 nmol × 100
= 47.5 %

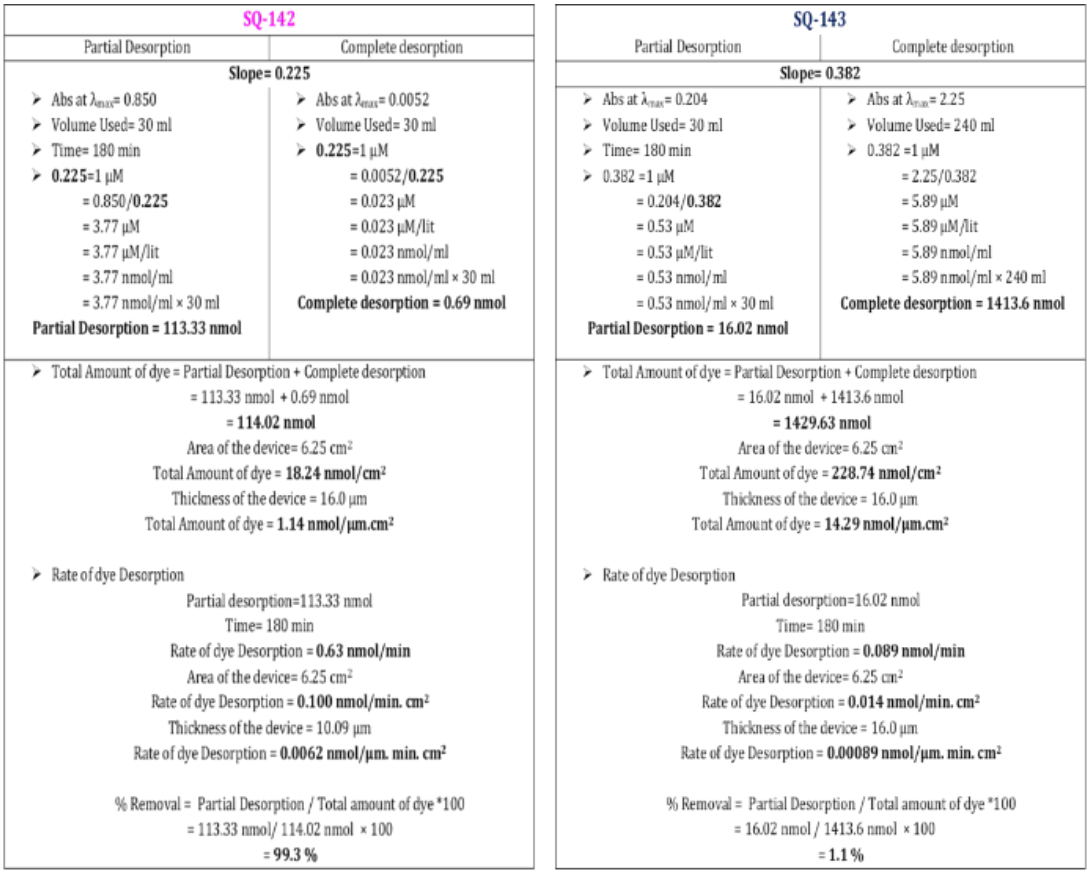

Figure-18. Detailed calculation of the dye adsorption, dye desorption, and amount of dye loading

4.3.5 Energy band diagram

There should be an energy cascade between the HOMO and LUMO of the dye concerning the conduction band of TiO_2 and electrode potential of the redox couple electrolyte for the function of the solar cell. As mentioned earlier, the HOMO energy level of the dyes was estimated from the CV, while the energy of the LUMO was estimated by the equation, LUMO=HOMO+Eg, where Eg is the optical band gap estimated from the optical absorption edge of electronic absorption spectra of dyes adsorbed on thin transparent films of TiO_2. A perusal of the energy band diagram is shown in the Figure. 18 corroborates that LUMO of the sensitizers always should be above then the CB of the semiconductor TiO_2 for the facile electron injection from its LUMO to CB of TiO_2, at the same time HOMO should be lower than the electrode potential of the Iodine

redox couple electrolyte. As we can see in this work all dyes except SQ-141 bearing hydroxyl group as an anchoring group, are energetically favorable for the solar cell performance. In this regard, we can see that the dye SQ-142 and SQ-140 bear the lowest HOMO energy level, which could be attributed to the relatively strong electron-withdrawing nature of $–SO_3H$ and cyano acrylic acid anchoring groups leading to stabilization of molecular orbitals and is by CV results. On the other hand, SQ-141 with the −OH anchoring group seems to be a non-optimal sensitizer owing to its shallow HOMO energy level leading to difficulty in the regeneration of oxidized dye. A relatively upward shift of HOMO energy of this dye could be attributed to the presence of the electron-donating nature of the hydroxyl group. To accomplish this, the CB energy level of TiO_2 and redox energy level of the electrolyte were taken to be -4.00 eV and -4.90 eV, respectively, as per the previous reports [42].

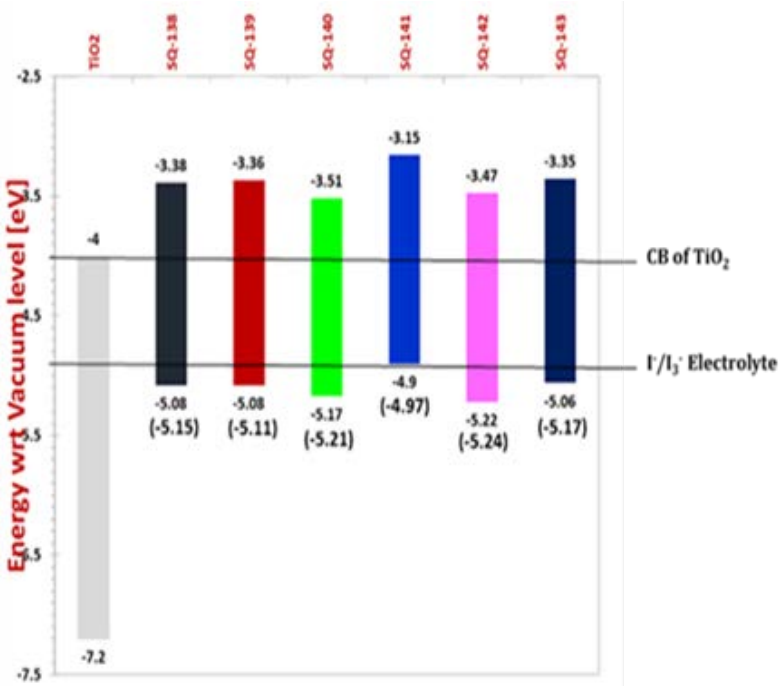

Figure-19. Energy band diagram for the unsymmetrical squaraine dyes under investigation. Values shown in the parentheses are theoretically calculated values by TD-DFT using 6-311 G/B3PW91.

4.3.6 Photovoltaic properties

Current-voltage (I–V) characteristics, and IPCE of DSSCs based on the same mother core but different anchoring groups unsymmetrical NIR squaraine dyes used in this work under standard global AM 1.5, 100 mW/cm^2 simulated solar irradiation have been shown in Figure-20 along with their photovoltaic parameters deduced from the I–V characteristics as shown in Table 4. A perusal of Figure- 20 and Table 4 indicates that all of the designed squaraine sensitizers are capable of harvesting photons and exhibit photovoltaic behavior. In each case, 20 mM of CDCA was used as a co-absorber to prevent the dye aggregation along with 0.2 mM of respective dyes in dehydrated ethanol. All the unsymmetrical squaraine dyes having exactly similar molecular framework and alkyl chain length exhibit superior photovoltaic performance. Within the same framework, only the anchoring groups are different and we can see from the table that SQ-138, SQ-139, and SQ-140 bearing similar kinds of anchoring groups but the only change in the π-conjugation of the anchoring groups affect the photovoltaic performances. SQ-138 bearing carboxylic avid as anchoring group showing photovoltaics behavior 12.49 mA/cm^2 JSC, 0.60 V VOC, 0.53 FF and 4.07 % PCE with 68.6 % IPCE while the only introduction of the vinyl group impacts the photovoltaics SQ-139 which is having acrylic acid as anchoring group showing 11.56 mA/cm^2 JSC, 0.65 V VOC, 0.59 and 4.49% PCE with 62.5 % IPCE on the other hand SQ-140 bearing cyano acrylic acid anchoring group shows the best photovoltaic performance with 5.95 PCE and 83.6 % IPCE along with 14.28 JSC, 0.64 VOC, and 0.65 FF, these results could be because of the extended π-conjugation in the anchoring groups. While the poorest performance (PCE = 0.63) was observed in the case of DSSC based on SQ-141 bearing −OH anchoring group. One of the possible causes for the poorest performance exhibited by SQ-141 could be attributed to the energetic mismatch of this dye concerning the redox energy level of iodine-based electrolyte as shown in Figure. 19. A very small driving force for the dye regeneration leads to pronounced back electron transfer after the photoexcitation leading to hampering in both of the JSC as well as Voc. It is interesting to note that SQ-143 with phosphonic acid anchoring group exhibited much hampered photovoltaic performance with PCE of 1.03 % as compared to that of DSSC based on SQ-138 bearing –COOH, SQ-139 bearing acrylic acid anchoring group, and SQ-140 bearing cyano acrylic acid as an anchoring group. Even though SQ-143 possesses several favorable conditions required for a sensitizer like high dye loading, binding strength (Table-3), and suitable energetic cascade for electron injection and dye regeneration Figure. 19. This could

be attributed to the tetrahedral nature of phosphonic acid as compared to that of planer carboxylic acid leading to a relatively small diversion of electron density at LUMO as shown in Figure- 10. This represents small ICT and hampered electronic coupling with the 3d orbitals of TiO_2 leading to hampered electron injection ultimately resulting in very poor photovoltaic performance.

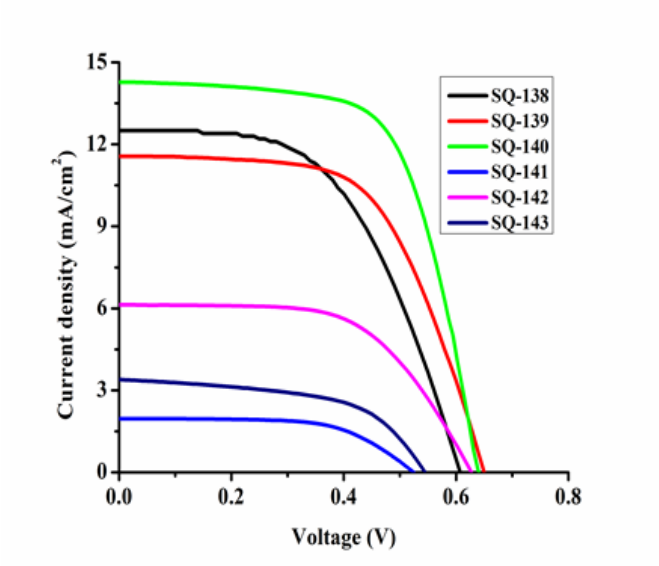

Figure-20. Photovoltaic characteristics of the DSSCs fabricated using unsymmetrical squaraine dyes bearing different anchoring groups.

Table-4. Short-circuit Photocurrent Density (Jsc), Open-circuit Voltage (Voc), Fill Factor (FF), Power conversion Efficiency (PCE, η), and Maximum Incident-to-Current Conversion Efficiency ($IPCE_{max}$) for the fabricated DSSCs Employing I^-/I_3^- Redox couple electrolyte.

Sensitizing dye	Anchoring groups	JSC (mA/cm^2)	VOC (V)	FF	PCE (η, %)	IPCE at λ_{max} (%)	Wavelength at $IPCE_{max}$ (nm)
SQ-138	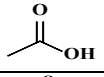	12.49	0.60	0.53	4.07	68.6	660
SQ-139		11.56	0.65	0.59	4.49	62.5	662
SQ-140	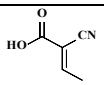	14.28	0.64	0.65	5.95	83.6	685
SQ-141	—OH	1.96	0.52	0.61	0.63	-	-
SQ-142	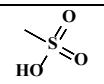	6.13	0.62	0.59	2.28	50.0	660
SQ-143	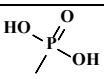	3.39	0.54	0.55	1.02	25.6	560

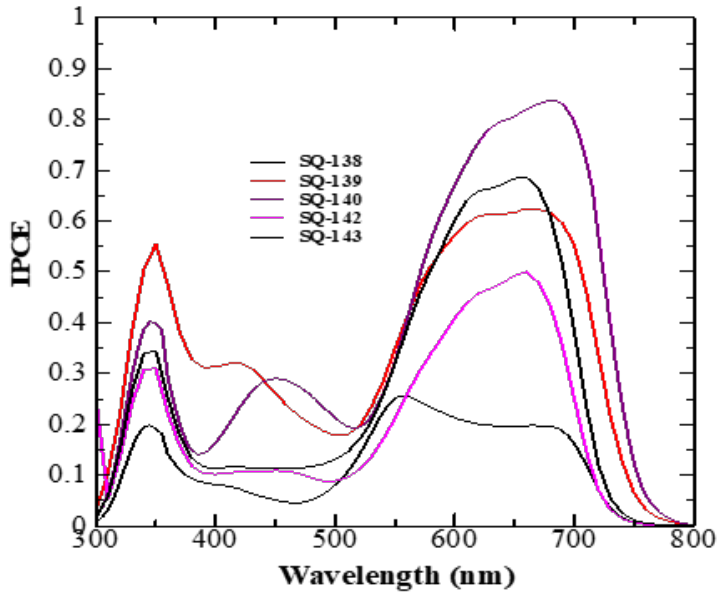

Figure-21. Photocurrent action spectra of the DSSCs based on different squaraine dyes after monochromatic light illumination.

Looking for the results shown in the Table-3 for the dye adsorption behavior and Table-4 for photovoltaic parameters, one can argue that there was a differential dye adsorption depending on the nature of the anchoring group and the amount of the dyes present on the photoanode have also good impact on controlling the overall PCE. Stability of the respective dyes SQ-138, SQ-141, SQ-142, SQ-143 can be seen form the Figure. 22. This data has been recorded for very short period of only 3 hr. and we found that there was a drastic decrease in the PCE of SQ-138 bearing −COOH, while there are many reports of sensitizers bearing −COOH group with fairly good stability. This is can be due to the fast evaporation of the volatile acetonitrile solvent under continuous 1 Sun solar irradiation resulting heating of the DSSCs. This the reason why, either electrolytes using high boiling solvents like Propionitrile, ionic liquids, or quasi-solid gel electrolytes have quite frequently used for long-term stability studies. Thus the observed trend of DSSC stability was the same as that of the anchoring stability of dyes on the mesoporous TiO_2. Therefore, the trend of anchoring stability of the dyes on the mesoporous TiO_2 gets directly translated into overall device stability.

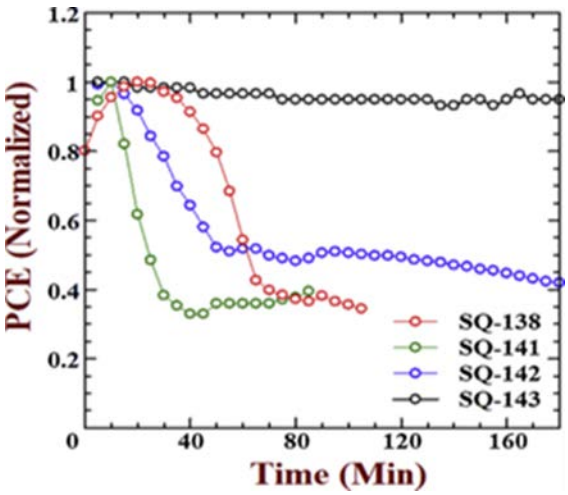

Figure-22. Photovoltaic stability of the DSSCs under continuous 1 Sunlight (100 mW/cm^2) irradiation fabricated using unsymmetrical squaraine dyes bearing different anchoring groups.

4.4 Conclusion

Finally, it can be concluded that we have designed and synthesized six novel unsymmetrical NIR squaraine dyes keeping the same main molecular mother core but bearing different anchoring groups such as carboxylic acid, acrylic acid, cyano acrylic acid, hydroxyl, sulfonic acid, and phosphonic acid along with excellent solubility in the majority of common organic solvent. After successful synthesis, characterization, and structural elucidation they have been subjected to photophysical investigation utilizing, electronic absorption spectroscopy, fluorescence emission spectroscopy, cyclic voltammetry, construction of energy band diagram, and theoretical MO calculation using Gaussian G09. Investigation of adsorption behavior of these dyes on mesoporous TiO_2 revealed the rate of dye adsorption following the order SQ-139 > SQ-140 > SQ-138 > SQ-143 > SQ-141 > SQ-142, while desorption studies indicated that binding strength on the mesoporous TiO_2 follows the order SQ-143 > SQ-141 > SQ-139 > SQ-142 > SQ-138 > SQ-140. Squaraine dye with phosphonic acid anchoring group exhibited the strongest binding strength as compared to other sensitizers. Theoretically predicted value of HOMO energy for all of the sensitizers is in very well agreement with the corresponding experimental values obtained by cyclic voltammetry. Theoretical MO calculation about the electron density distribution in HOMO and LUMO indicated good ICT and the possibility of strong electronic coupling with TiO_2 for the dyes bearing −COOH (SQ-138) and –SO_3H (SQ-142) functional groups, which is also supported by their relatively improved photovoltaic performance as compared to other

anchoring groups. The energy band diagram has indicated that except SQ-141 bearing hydroxyl anchoring group form energetic cascade concerning CB of TiO_2 and redox energy level of I_3^-/I^-, which is responsible for its poorest photovoltaic performance. Despite very good dye loading, very high binding strength, and favorable energetic cascade, SQ-143 exhibited highly hampered photovoltaic performance as compared to that of SQ-138, SQ-139, and SQ-140, which was attributed to poor ICT and electronic coupling with TiO_2 as indicated by theoretical MO calculations. SQ-140 is the champion sensitizer in the case of photoconversion efficiency but this dye is highly unstable on the mesoporous TiO_2. From the above all results we can conclude SQ-139 is the best sensitizer in the case of PCE and the term of stability. It is highly worth mentioning here that from the figure-21, SQ-143 exhibits the highest stability so if can tune and design some sensitizers which are more stable and efficient in the case of PCE there will be remarkable work for the future aspect. So keeping this ideology in our mind, we design some NIR dyes which are stable and efficient, discussed in the next chapter.

References

1. S. Mekhilef, R. Saidur, A. Safari: "A review on solar energy use in industries", Renewable and Sustainable Energy Reviews, 15, 1777-1790 (2011).
2. M. Grätzel: "Photoelectrochemical Cells", Nature, 414, 338– 344 (2001).
3. C-Y Chen, M Wang, J-Y Li, N Pootrakulchote, L Alibabaei, C-h Ngoc-le, J-D Decoppet, J-H Tsai, C Grätzel, C-G Wu, S M. Zakeeruddin and M Grätzel: "Highly Efficient Light-Harvesting Ruthenium Sensitizer for Thin-Film Dye-Sensitized Solar Cells" ACS Nano 3 (10), 3103–3109 (2009).
4. S Mathew, A Yella, P Gao, R Humphry-Baker, BF Curchod, N Ashari-Astani, I Tavernelli, U Rothlisberger, MK Nazeeruddin, M Grätzel: "Dye-Sensitized Solar Cells with 13% Efficiency Achieved Through the Molecular Engineering of Porphyrin Sensitizers", Nature Chemistry, 6(3), 242-7 (2014).
5. A Yella, H-W Lee, H N Tsao, C Yi, AK Chandiran, MK Nazeeruddin, E W-G Diau, C-Y Yeh, SM Zakeeruddin, M Grätzel: "Porphyrin-Sensitized Solar Cells with Cobalt (II/III)–Based Redox Electrolyte Exceed 12 Percent Efficiency", Science, 334, 629-634 (2011).

6. K Kakiage, Y Aoyama, T Yano, K Oya, J-i Fujisawa, and M Hanaya: "Highly-efficient dye-sensitized solar cells with collaborative sensitization by silyl-anchor and carboxy-anchor dyes", Chemical Communications, 51, 15894-15897 (2015).

7. C Stanley, A Mojiri, G Rosengarten: "Spectral light management for solar energy conversion systems", Nanophotonics, 5 (1), 161–179 (2016).

8. M. Grätzel: "Photoelectrochemical Cells", Nature, 414, 338– 344 (2001).

9. C. Anselmi, E. Mosconi, M. Pastore, E. Ronca, F. De Angelis, Adsorption of organic dyes on TiO_2 surfaces in dye-sensitized solar cells: an interplay of theory and experiment, Phys. Chem. Chem. Phys. 14 (2012) 15963–15974.

10. C-Y Chen, M Wang, J-Y Li, N Pootrakulchote, L Alibabaei, C-h Ngoc-le, J-D Decoppet, J-H Tsai, C Grätzel, C-G Wu, S M. Zakeeruddin and M Grätzel: "Highly Efficient Light-Harvesting Ruthenium Sensitizer for Thin-Film Dye-Sensitized Solar Cells" ACS Nano 3 (10), 3103–3109 (2009).

11. S Mathew, A Yella, P Gao, R Humphry-Baker, BF Curchod, N Ashari-Astani, I Tavernelli, U Rothlisberger, MK Nazeeruddin, M Grätzel: "Dye-Sensitized Solar Cells with 13% Efficiency Achieved Through the Molecular Engineering of Porphyrin Sensitizers", Nature Chemistry, 6(3), 242-7 (2014).

12. A Yella, H-W Lee, H N Tsao, C Yi, AK Chandiran, MK Nazeeruddin, E W-G Diau, C-Y Yeh, SM Zakeeruddin, M Grätzel: "Porphyrin-Sensitized Solar Cells with Cobalt (II/III)–Based Redox Electrolyte Exceed 12 Percent Efficiency", Science, 334, 629-634 (2011).

13. S. Ko, H. Choi, M.-S. Kang, H. Hwang, H. Ji, J. Kim, J. Ko, Y. Kang, Silole-spaced triarylamine derivatives as highly efficient organic sensitizers in dye-sensitized solar cells (DSSCs), J. Mater. Chem. 20 (2010) 2391–2399.

14. Z. Ning, Q. Zhang, W. Wu, H. Pei, B. Liu, H. Tian, Starburst triarylamine based dyes for efficient dye-sensitized solar cells, J. Org. Chem. 73 (2008) 3791–3797.

15. N. Koumura, Z.S. Wang, M. Miyashita, Y. Uemura, H. Sekiguchi, Y. Cui, A. Mori, S. Mori, K. Hara, Substituted carbazole dyes for efficient molecular photovoltaics: long electron lifetime and high open-circuit voltage performance, J. Mater. Chem. 19 (2009) 4829–4836.

16. K. Hara, Z.S. Wang, Y. Cui, A. Furube, N. Koumura, Long-term stability of organic–dye-sensitized solar cells based on an alkyl-functionalized carbazole dye, Energy Environ. Sci. 2 (2009) 1109–1114.

17. Yum J, Walter P, Huber S, Rentsch D, Geiger T, Nu F. Efficient far-red sensitization of Nanocrystalline TiO_2 films by an unsymmetrical squaraine dye. J Chem Am Soc 2007; 129:10320–1.

18. Maeda T, Arikawa S, Nakao H, Yagi S, Nakazumi H. Linearly π-extended squaraine dyes enable the spectral response of dye-sensitized solar cells in the NIR region over 800 nm. New J Chem 2013; 37:701–8. https://doi.org/10.1039/c2nj40991g.

19. Kuster S, Sauvage F, Nazeeruddin MK, Grätzel M, Nüesch F, Geiger T. Unsymmetrical squaraine dimer with an extended π-electron framework: an approach in harvesting near infra-red photons for energy conversion. Dye Pigment 2010; 87:30–8. https://doi.org/10.1016/j.dyepig.2010.01.019.

20.] Kim S, Han S. High-performance aquarium dyes for high-tech use. Color Technol 2001; 117:61–7.

21. A. Pradhan, T. Morimoto, M. Saikiran, G. Kapil, S. Hayase, S.S. Pandey, Investigation of the minimum driving force for the dye regeneration utilizing model squaraine dyes for dye-sensitized solar cells, J. Mater. Chem. A 5 (2017) 22672–22682.

22. M. Saikiran, D. Sato, S.S. Pandey, T. Ohta, S. Hayase, T. Kato, Photophysical characterization and BSA interaction of the direct ring carboxy functionalized unsymmetrical NIR cyanine dyes, Dye. Pigment. 140 (2017) 6–13.

23. J.W. Park, Y.S. Kim, K.J. Lee, D.J. Kim, Novel cyanine dyes with vinylsulfone group for labeling biomolecules, Bioconjugate Chem. 23 (2012) 350–362.

24. S.A. Archer, T. Keane, M. Delor, E. Bevon, A.J. Auty, D. Chekulaev, I.V. Sazanovich, M. Towrie, A.J.H.M. Meijer, J.A. Weinstein, Directly coupled versus spectator linkers on diimine PtII acetylides—change the structure, keep the function? Chem. Eur. J. 23 (2017) 8239–18251.

25. Carbazole dye with phosphonic acid anchoring groups for long-term heat stability of dye-sensitized solar cells Takurou N. Murakami ∗, Eri Yoshida, Nagatoshi Koumura∗ T.N. Murakami et al. / Electrochimica Acta 131 (2014) 174–183

26. A. Pradhan, T. Morimoto, M. Saikiran, G. Kapil, S. Hayase and Shyam S. Pandey, *J. Mater. Chem. A*, 2017, 5, 22672-22682

27. Li, C.Y. Chen, W.C. Ho, S.H. Chen, and C.G. Wu. ORGANIC LETTERS 2012 Vol. 14, No. 21 5420–5423.

28. G.M. Shivashimpi, S.S. Pandey, R. Watanabe, N. Fujikawa, Y. Ogomi, Y. Yamaguchi, S. Hayase, Journal of Photochemistry and Photobiology A: Chemistry *273 (2014) 1– 7*

29. W. Pham, W.-F. Lai, R. Weissleder and C.-H. Tung, *Bio conjugate Chem*., 2003, 14, 1048-1051

30. B. Su, H.H. Girault, Absolute standard redox potential of monolayer-protected gold nanoclusters, J. Phys. Chem. B 109 (2005) 11427–11431.

31. A. Anthonysamy, Y. Lee, B. Karunagaran, V. Ganapathy, S.W. Rhee, S. Karthikeyan, K.S. Kim, M.J. Ko, N.-G. Park, M.-J. Ju, J.K. Kim, Molecular design and synthesis of ruthenium (II) sensitizers for highly efficient dye-sensitized solar cells, J. Mater. Chem. 21 (2011) 12389–12397.

32. S. Sreejith, P. Carol, P. Chithraa, A. Ajayaghosh, Squaraine dyes: a mine of molecular materials, J. Mater. Chem. 18 (2008) 264–274.

33. J.M. Lim, Z.S. Yoon, J.Y. Shin, K.S. Kim, M.C. Yoon, D. Kim, The Photophysical properties of expanded porphyrins: relationships between aromaticity, molecular geometry, and non-linear optical properties, Chem. Commun. (Camb.) 3 (2009) 261–273.

34. MK Nazeeruddin, FD Angelis, S Fantacci, A Selloni, G Viscardi, P Liska, S Ito, B Takeru, and M Grätzel: "Combined experimental and DFT-TDDFT computational study of photoelectrochemical cell ruthenium sensitizers", J Am Chem Soc. , 127(48), 16835-16847 (2005).

35. SS Pandey, T Morimoto, N Fujikawa, S Hayase: "Combined theoretical and experimental approaches for the development of squaraine dyes with small energy barrier for electron injection", Solar Energy Materials and Solar Cells, 159, 625-632 (2017).

36. A. Pradhan, T. Morimoto, M. Saikiran, G. Kapil, S. Hayase, and S.S. Pandey: Pradhan: "Investigation of the minimum driving force for dye regeneration utilizing model squaraine dyes for dye-sensitized solar cells", Journal of Materials Chemistry A, 5, 22672-22682 (2017).

37. A. Baktash, B. Khoshnevisan, A. Sasani, K. Mirabbaszadeh, Effects of carboxylic acid and phosphonic acid anchoring groups on the efficiency of dye-sensitized solar cells: a computational study, Org. Electron. 33 (2016) 207–212.

38. T.N. Murakami, E. Yoshida, N. Koumura, Carbazole dye with phosphonic acid anchoring groups for long-term heat stability of dye-sensitized solar cells, Electrochim. Acta 131 (2014) 174–183.

39. V. Johansson, L. E. Gibbings, T. Clarke, M. Gorlov, G.G. Andersson and L. Kloo: "On the correlation between dye coverage and photoelectrochemical performance in dye-sensitized solar cells", Physical Chemistry Chemical Physics, 16,711-718 (2014).

40. A. C. Khazraji, S. Hotchandani, S. Das, and P. V. Kamat: "Controlling Dye (Merocyanine-540) Aggregation on Nanostructured TiO_2Films. An Organized Assembly Approach for Enhancing the Efficiency of Photosensitization", J. Phys. Chem., 103 (22), 4693-4700 (1999)

41. Y. S. Kim, K. Liang, K. Y. Law, and D. G. Whitten: "An investigation of photocurrent generation by squaraine aggregates in monolayer-modified tin oxide (SnO2) electrodes", J. Phys. Chem., 98 (3), 984-988 (1994

42. Y. Ogomi, T. Kato, S. Hayase, Dye-sensitized solar cells consisting of ionic liquid and solidification, J. Photopolym. Sci. Technol. 19 (2006) 403–408.

Chapter-5

Fine-tuning of dyes with phosphonate anchoring group for improved stability and efficiency

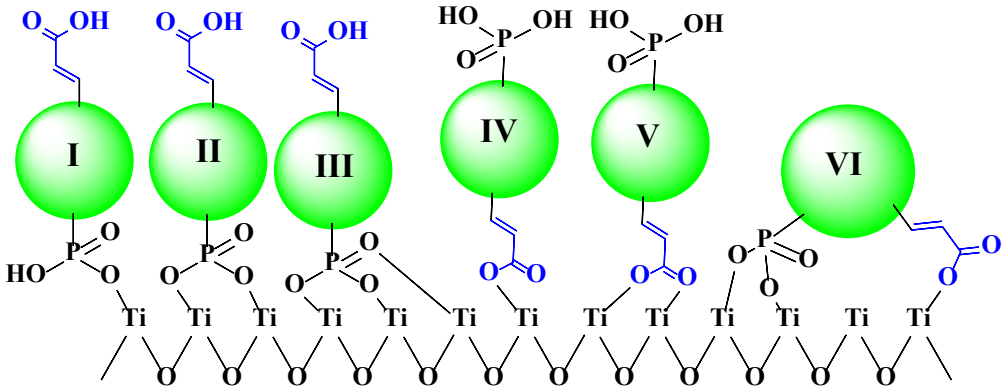

Contents (some of the part) of this chapter have been published in Photochemistry and Photobiology-A, A. K. Vats, A. Pradhan, S. Hayase, SS. Pandey, *Journal of Photochemistry & Photobiology A: Chemistry,* 2020, 394,112467. The material of the chapter has been reproduced with the permission of the *Journal of Photochemistry & Photobiology A: Chemistry*

5.1 Introduction

The fast depletion of precious non-renewable energy resources owing to the speedy industrialization encompassing from developed nations to developing countries has brought us to the brink of global warming owing to the enhanced greenhouse gas emissions [1]. This has compelled us towards the utilization of renewable energy resources, amongst them solar energy is one of the plausible due to its huge availability as a gift from Mother nature [2]. In this context, the utilization of solar cells to tap this immensely available solar energy is going to be a key player to circumvent the issues about the huge energy demands of the future. Even though solar energy is huge but it has to be implemented over a large area to provide sufficient usable energy imposes an obvious need for cost reduction to compete with the energy production cost of fossil fuels [3]. Owing to the utilization of cheap raw materials in combination with low-cost fabrication processes next-generation solar cells such as dye-sensitized solar cells, organic polymer solar cells and recently came in the limelight perovskite solar cells have got considerable attention. Amongst the next-generation solar cells, dye-sensitized solar cells (DSSCs) have attracted a good deal of attention of the material science community owing to the ease of fabrication, aesthetic variable colour, transparency, and very high indoor light-harvesting capability [4].

Since its inception in 1991 by Grätzel and O-Reagan [5] 1991 demonstrating photo conversion efficiency (PCE) of 7.8 % ignited the field of DSSC research which is proliferating to date. Since then several optimization and improvisation in DSSC and their components like mesoporous TiO_2 [6], redox electrolytes [7], counter electrodes [8], and last but not least sensitizing dyes [9] leading to the proposal of state-of-art DSSCs achieving the PCE of 10-13%, surpassing amorphous silicon solar cells [10-13]. The importance and the critical role of sensitizing dyes in the DSSC working cycle and controlling the PCE are undoubtedly un-questionable and a perusal of state-of-art DSSCs utilizing potential dyes have demonstrated the PCE of >13% despite the photon harvesting only in the visible reason (mainly 400-700 nm) with nearly quantitative photon harvesting [14]. This demonstrates that all of the components of such state-of-art DSSCs are functioning optimally. At the same time, this provides hope for further enhancement in the PCE by design and development of the near infra-red (NIR) sensitizers absorbing beyond

700 nm. Therefore, the logical design of efficient NIR sensitizers and their implementation with several already available efficient visible sensitizers for panchromatic photon harvesting utilizing hybrid and tandem device architecture are expected to further boost the achievable PCE [15-17].

Amongst the principal requirements for an optimal sensitizer of DSSCs such as energetic matching and high molar extinction coefficient, the presence of suitable anchoring is inevitable. Anchoring groups are involved in the fixation of the dye-molecules on the mesoporous wide bandgap semiconductor like TiO_2, ZnO, etc. The nature of the anchoring group affects the PCE by controlling the electron injection from excited dye molecules to the conduction band of TiO_2 depending on the effectiveness of electronic coupling between the excited dye molecules and vacant d-orbitals of the TiO_2 [18]. At the same time, they also control the stability of DSSCs by controlling the strength of binding with the mesoporous wide bandgap semiconductors [19]. Therefore, anchoring groups are highly responsible for controlling the PCE as well the stability of the DSSCs, which currently intriguing issues for the commercialization of the DSSCs. A perusal of the nature of anchoring groups of the dyes reported so far imparting appreciably good PCE, carboxylic and cyanoacrylic acid have shown their dominance and are preferred anchoring groups utilized extensively [20]. Contrary to this, in terms of the stability of DSSCs and their binding strength on the mesoporous TiO_2, they are far-behind the anchoring groups like silyl ester, silatrane, and phosphonic acids [21-22]. The extremely high binding strength of dyes bearing silyl ester anchoring group over the most commonly used carboxylic as well as cyano acrylic acid functional group of sensitizers has been demonstrated by Kakiage et al and Higashino et al [23-24]. Utilizing squaraine class NIR dyes, we have also recently shown that Phosphonic acid anchoring exhibited about 70 times higher binding strength as compared to -COOH on the mesoporous TiO_2, which was also translated into higher stability of DSSCs utilizing dye [25]. At the same time, PCE of DSSCs using phosphonic acid anchored dye was highly hampered owing to poor electron injection owing to their out-of-plane tetrahedral geometry [26].

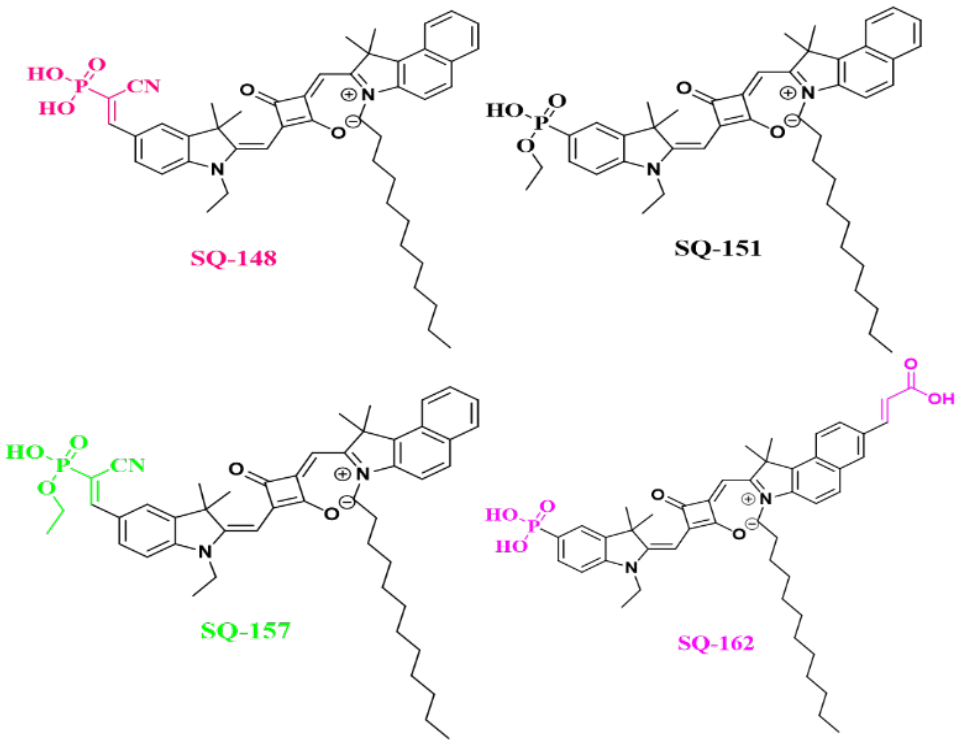

Figure-1. Chemical structure of the unsymmetrical squaraine dyes with varying anchoring groups used in the present investigation.

5.2 Experimental

Tunable Photophysical properties and applications of the Squarine dyes make the research interesting of the squaraine chemistry and mainly of the unsymmetrical Squarine dyes. Difficult and complicated synthesis of squaraine dyes make them challenging dyes to synthesize [27].

5.2.1 Synthesis of unsymmetrical squaraine dyes

Keeping the same π-conjugated mother core and varying different Anchoring groups, all the intermediates and final unsymmetrical squaraine dyes were synthesized as per the route of synthesis as shown in scheme-1. Starting compound 1, 1, 2-trimethylbenzo (e) indole [1] was purchased from Sigma-Aldrich and 4-hydrazineylbenzonitrile hydrochloride [6] and 6-bromonaphthalen-2-ol [13] were purchased from Tokyo Chemical Industry and used without further purification.

5.2.1.1 Synthesis of 3-dodecyl-1,1,2-trimethyl-1H-benzo[e]indol-3-umiodide [2]

In a 100 ml round bottom flask, 6 g (28.7 mmol) of 1, 1, 2-trimethyl-2, 3-dihydro-1H-benzo[e]indole [1] was taken and added Propionitrile (40 mL). Then 12 g (43 mmol) of 1-Iodododecane (1.5 equivalent) was added to it. The mixture was reflux at 110 °C for 26 h. Reaction progress was monitored by TLC in a 15 % ethyl acetate: Hexane solvent system. After the completion of the reaction, evaporated the solvent under vacuum and precipitated out the product by adding diethyl ether. Washed compound by diethyl ether. The residue was collected as a light pink solid to give the desired compound in 78 % yield (11.2 g). FAB mass (measured m/z: 378.3164 [M] +; calculated m/z: 378.3161).

5.2.1.2 Synthesis of (E)-4-((3-dodecyl-1,1-dimethyl-1H-3l4-benzo[e]indol-2-yl) methylene)-2-ethoxy-3-oxocyclobut-1-en-1-olate [3]

1 equivalent of compound [2], (5 g, 9.9 mmol) and 1 equivalent of 3, 4-Diethoxy-3-cyclobutene-1, 2-dione 1.6 g (9.9 mmol) were added 25 mL ethanol in followed by 5 equivalents of triethylamine was added in to the 50 ml round bottom flask. The reaction mass was reflux for 6 h, which soon turned to yellow color. Cooled the reaction mass and the solvent was evaporated under a vacuum. Crude product was extracted with ethyl acetate followed by thorough washing with distilled water and brine. Combined ethyl acetate layer was evaporated under vacuum and performed column chromatography by using 10 % Ethyl acetate: Hexane. The solvent was removed to get the titled compound as a yellow powder in 77 % yield (3.8 g). FAB-mass (measured m/z: 502.0 $[M+H]^+$; calculated m/z: 501.3).

5.2.1.3 Synthesis of (E)-4-((3-dodecyl-1,1-dimethyl-1H-benzo[e]indol-3-ium-2-yl)methylene)-2-hydroxy-3-oxocyclobut-1-en-1-olate [4]

In a 50 mL round bottom flask, 3 g (6.0 mmol) of compound [3] was dissolved in 15 mL ethanol followed by 5 equivalent 4 N NaOH was added and refluxed for 2 h. The reaction mixture was cooled and the solvent was evaporated under a vacuum. After complete evaporation of the solvent, the reaction mixture was acidified by diluted HCl and acidified crude was then extracted in chloroform and subjected to thorough washing by brine. The final hydrolyzed product was obtained as a red solid in 88 % yield (2.5 g).

5.2.1.4 Synthesis of 5-(diethoxyphosphoryl)-1-ethyl-2,3,3-trimethyl-3Hindol-1-ium iodide (i)

After the slight modification in a procedure as reported by Archer et al. [28]. To a solution of 4-Iodoindole (1 g, 3.5 mmol) in toluene was added Tetrakis (triphenylphosphine) palladium (0) (0.18 mmol), and trimethylamine (12.4 mmol) followed by the addition of Diethylphosphite (0.31 mmol), and the reaction mixture was refluxed for 12 h. Upon completion of the reaction as monitored by TLC, the solvent was evaporated. The product was extracted with ethyl acetate and washed with water and brine. Finally, product purification was done by column chromatography giving desired compound diethyl (2, 3, 3-trimethyl-3H-indol-5-yl) phosphonate as a colorless liquid. To a solution of this compound in acetonitrile was added ethyl iodide flowed by reflux for 12 h. Upon completion of the reaction, the solvent was evaporated followed by precipitation using diethyl ether. It was then filtered, washed with diethyl ether, and dried under vacuum to obtain the titled compound 5-(diethoxyphosphoryl)-1-ethyl-2, 3, 3-trimethyl-3H-indol-1-ium iodide (i).

5.2.1.5 Synthesis of SQ-151

In a round bottom flask, 315 mg of 5-(diethoxyphosphoryl)-1-ethyl-2, 3, 3-trimethyl-3Hindol- 1-ium iodide (i) and 302 mg of semi squaraine dye intermediate [4] was dissolved in 1:1 toluene/n-butanol. The reaction mixture was then refluxed for 18 h. The solvent was evaporated and the crude was purified by column chromatography using chloroform methanol as the eluting system. After the evaporation of the collected pure fraction, 220 mg of ester compound was obtained as a blue solid in 54.3 % yield. Obtained ester was hydrolyzed by using TMS-Br as per the report [29] in DCM at room temperature for 6−8 hrs. Reaction progress was monitored TLC using Methanol chloroform as mobile phase. Purification was done by column chromatography by using Methanol chloroform as mobile phase. After the evaporation of the collected pure fraction, 250 mg of the titled compound was collected as a blue solid in 65 % yield. HRFAB- MS (measured m/z: 751.4224 $[M+H]^+$; calculated m/z: 750.4162). ^{1}H NMR (500 MHz, CDCl3): δ/ppm = 8.17(d,H-4); 8.16(d,H-7); 7.94(d,H-8); 7.89(d,H-9); 7.87(s,H-41); 7.83(t,H-5); 7.56(t,H-6); 7.81(d,H-44); 7.52(d,H-45); 7.20(s,H-28); 6.01(s,H-33); 4.12(q,H-48); 3.96(q,H-46); 3.82(t,H-16); 2.17(s,H-39 and H-40); 1.83(s, H-14 and H-15); 1.41(t,H-47), 1.38(t,H-49); 1.17(m,H-17-26); 0.96(t,H-27).

5.2.1.6 Synthesis of intermediate 2,3,3-trimethyl-3H-indole-5-carbonitrile [7]

Upon slight modification in the procedure as reported [30] and the method reported by Pham et al [31]. 2 gm (11.79 mmol) and 3.81 ml (35.3 mmol) of 3-methyl-2-butanone were dissolved in ethanol and the mixture was refluxed under nitrogen for 2 h in a round bottom flask fitted with a reflux condenser. After the complete consumption of 4-cyano hydrazine hydrochloride, confirmed by TLC. Solvent and the excess of 3-methyl-2-butanone were evaporated under vacuum. The residue was dissolved in 100 mL glacial acetic acid and refluxed for 12 h. After the completion of the reaction acetic acid was removed under vacuum and the crude product was purified by column chromatography using ethyl acetate and hexane as eluent.1.6 g of titled compound was obtained as red solid in 73.7% Yield. HRFAB- MS (measured m/z: 185.1083 $[M+H]^+$; calculated m/z: 184.1000).

5.2.1.7 Synthesis of intermediate 5-cyano-1-ethyl-2,3,3-trimethyl-3H-indol-1-ium iodide [8]

After slight modification in the procedure as reported by [30]. 1.6 gm (8.69 mmol) of 2,3,3-trimethyl-3H-indole-5-carbonitrile [7] and 2.09 ml (26.08 mmol) of 1-Iodoethane was dissolved in Acetonitrile in a 50 ml round bottom flask fitted with a reflux condenser and the mixture mass was refluxed under nitrogen for 24 hrs. reaction progress was confirmed by TLC. Solvent and the excess of 1-Iodoethane were removed by evaporation under vacuum. The residue was precipitated out in diethylether.1.55 g of titled compound was obtained as red solid in 86.1% Yield. HRFAB-MS (measured m/z: 341.0508 $[M+H]^+$; calculated m/z: 340.0436).

5.2.1.8 Synthesis of intermediate diethyl (E)-(1-cyano-2-(1-ethyl-3,3-dimethyl-2-methyleneindolin-5-yl)vinyl)phosphonate [11]

After hydrolyzing 1.5 g (4.4 mmol) of 5-cyano-1-ethyl-2,3,3-trimethyl-3H-indol-1-ium iodide salt [8], using 16 ml of 2 N NaOH and toluene to its methylene base, the resulting methylene base was isolated in toluene, dried the reaction mass under vacuum and obtained 800 mg solid as 1-ethyl-3,3-dimethyl-2-methyleneindoline-5-carbonitrile [9]. To a solution of methylene base [9] in 15 mL dichloromethane at 0 ^{0}C, was added slowly 4.4 mL (4.40 mmol, 1 M solution in THF) of DIBAL-H. After stirring for 12 hrs under a nitrogen atmosphere, the reaction mixture was quenched with 2 mL of dilute HCl, and the reaction mass was refluxed for 30 min. The crude product was extracted into chloroform, washed with water, and dried over Na_2SO_4. After

evaporating the solvent under vacuum, 700 mg (3.2 mmol, 86.3%) of 1-ethyl-3, 3-dimethyl-2-methyleneindoline-5-carbaldehyde [10] thus obtained was dissolved in 15 mL of acetonitrile. To this solution was added 1.05 mL (6.5 mmol) of Diethylcyanomethylphosphonate and 0.48 ml (4.8 mmol) of Piperidine. After refluxing the reaction mixture for 7-8 hrs, completion of the reaction as monitored by TLC, Solvent was evaporated and the crude product was passed through a small silica gel column using hexane: ethyl acetate (6:1) as eluting solvent to obtain colored liquid titled compound [11] in Yield 770 mg (64.2%).

5.2.1.9 Synthesis of intermediate (E)-2-(((E)-5-((E)-2-cyano-2-(diethoxyphosphoryl)vinyl)-1-ethyl-3,3-dimethylindolin-2-ylidene)methyl)-4-((3-dodecyl-1,1-dimethyl-1H-benzo[e]indol-3-ium-2-yl)methylene)-3-oxocyclobut-1-en-1-olate [12]

770 mg (2.05 mmol) of diethyl (E)-(1-cyano-2-(1-ethyl-3,3-dimethyl-2-methyleneindolin-5-yl) vinyl) phosphonate [11] and 973 mg (2.05 mmol) of (E)-4-((3-dodecyl-1,1-dimethyl-1H-benzo[e]indol-3-ium-2-yl) methylene)-2-hydroxy-3-oxocyclobut-1-en-1-olate intermediate [4] was dissolved in 30 mL of 1:1 toluene/n-butanol in a round bottom flask fitted with condenser. Refluxed the reaction mass for 6-8 hrs. Reaction progress was monitored by TLC, after completion, solvent was evaporated and the crude product was purified with column chromatography using chloroform-methanol solvent as eluent. 700 mg of the desired compound was collected as a blue solid 41.7 % yield.

5.2.1.10 Synthesis of Unsymmetrical Squarine dye SQ-157

After slight modification in the procedure as reported [29]. To a round bottom flask, 350 mg (0.42 mmol) of (E)-2-(((E)-5-((E)-2-cyano-2-(diethoxyphosphoryl)vinyl)-1-ethyl-3,3-dimethylindolin-2-ylidene)methyl)-4-((3-dodecyl-1,1-dimethyl-1H-benzo[e]indol-3-ium-2-yl)methylene)-3-oxocyclobut-1-en-1-olate [12] and 0.027 ml (0.21 mmol) of Bromotrimethylsilane (TMS-Br) was dissolved in 10 mL of Dichloromethane (DCM). The reaction mixture was stirred at Room Temperature (RT) for 36 hrs. Reaction progress was monitored by TLC using 5% MeOH: chloroform as mobile phase. Quenched the reaction mass by MeOH and solvent was evaporated and the crude was purified with column chromatography using chloroform methanol solvent system. 205 mg of the titled compound was collected as a blue solid in 60.6 % yield. HRFAB-MS (measured m/z: 802.4361 $[M+H]^+$; calculated m/z: 801.4271). ^{1}H NMR (500 MHz, CDCl3):

δ/ppm = 8.17(d,H-4); 7.90(d,H-7); 7.58(d,H-8); 7.46(d,H-44); 7.40(d,H-9); 7.09(t,H-6); 7.04(s,H-43); 7.02(s,H-41); 7.01(t,H-5); 6.99(d,H-45); 6.64(s,H-28); 6.21(s,H-33); 6.09 (s, H-49); 5.93 (q, H-50); 4.36(q,H-46); 3.34(s,H-39 and H-40); 1.77(s,H-14 and 15); 1.46(t,H-47); 1.20 (t,H-51); 1.17(m, H16 to H-26); 0.96(d,H-27).

5.2.1.11 Synthesis of Unsymmetrical Squaraine dye SQ-148

After slightly modification in the procedure as reported by [29]. To a round bottom flask, 350 mg (0.42 mmol) of *(E)-2-(((E)-5-((E)-2-cyano-2-(diethoxyphosphoryl)vinyl)-1-ethyl-3,3-dimethylindolin-2-ylidene)methyl)-4-((3-dodecyl-1,1-dimethyl-1H-benzo[e]indol-3-ium-2-yl)methylene)-3-oxocyclobut-1-en-1-olate* [12] and 0.054 ml (0.42 mmol) of Bromotrimethylsilane (TMS-Br) was dissolved in 10 mL of Dichloromethane (DCM). The reaction mixture was stirred at Room Temperature (RT) for 12 hrs. Reaction monitoring was done by TLC using 5% MeOH: chloroform as mobile phase. Thereafter the reaction was quenched by MeOH and solvent was evaporated and performed column chromatography using chloroform methanol mobile phase. 220 mg of the titled compound was collected as a blue solid in 67.4 % yield. HRFAB- MS (measured m/z: 774.4027 $[M+H]^+$; calculated m/z: 773.3958). ^{1}H NMR (500 MHz, CDCl3): δ/ppm = 8.17(d,H-4); 7.90(d,H-7); 7.58(d,H-8); 7.46(d,H-44); 7.40(d,H-9); 7.09(t,H-6); 7.04(s,H-43); 7.02(s,H-41); 7.01(t,H-5); 6.99(d,H-45); 6.64(s,H-28); 6.21(s,H-33); 5.41(s, H-49 and H-50); 4.36(q,H-46); 3.34(s,H-39 and H-40); 1.77(s,H-14 and 15); 1.46(t,H-47); 1.17(m, H16 to H-26); 0.96(d,H-27).

5.2.1.12 Synthesis of intermediate 6-bromonaphthalen-2-amine [14]

The compound was synthesized by the slightly modified procedure as reported by [32]. Added 6-bromonaphthalen-2-ol [13] 3 g (13.4 mmol) in a High-pressure reaction tube with a silicon gasket, to it 6.99 g (67.2 mmol) of Sodium bisulfite and 70 ml of 28% Ammonia solution were added. The reaction was heated at 150 ^{0}C for 24 hrs. After the reaction mixture cool to room temperature, Reaction monitoring was done by TLC. Thereafter Ethyl acetate was used to extract the product. After evaporating the solvent the crude product was used for the next step. 2.2 g of the titled compound was collected as a solid in 73.8 % yield. HRFAB- MS (measured m/z: 221.9918 $[M+H]^+$; and 223.9894 $[M+3H]^+$; calculated m/z: 220.9840).

5.2.1.13 Synthesis of intermediate (6-bromonaphthalen-2-yl)hydrazine hydrochloride [15]

To a round bottom flask, 2 g (9.0 mmol) 6-bromonaphthalen-2-amine [14] was dissolved in 30 ml conc. HCl 25 ml. after cooling the reaction mass at 0^0C, Sodium nitrite 0.749 mg (10.8 mmol) was dissolved in 2 V of water and added to the reaction mass slowly. Stirred the reaction mass at the same temperature for 30 min and then dissolved Tin chloride 4.26 g (22.5 mmol) in 3 V of water and added slowly. After complete addition, allow the reaction mass to room temperature and stirred overnight at the same temperature. Reaction monitoring was done by TLC. Thereafter filtered the reaction mass and dried it under vacuum and proceed to the next step. 1.9 g of the titled solid compound was collected as solid in 79.1 % yield.

5.2.1.14 Synthesis of intermediate 7-bromo-1,1,2-trimethyl-1H-benzo[e]indole [16]

The compound was synthesized by the slightly modified procedure as reported by [30] (6-bromonaphthalen-2-yl)hydrazine hydrochloride [15] 1.9 g (6.9 mmol) and 3-Methyl-2-Butanone 1.85 ml (17.2 mmol) was dissolved in 20 ml acetic acid and reflux the reaction mass for 12 hrs. Reaction monitoring was done by TLC. Thereafter solvent was evaporated and the crude was purified with column chromatography using ethyl acetate-hexane as a solvent system. 1.4 g of the titled compound was collected as a Solid in 70.0 % yield. HRFAB- MS (measured m/z: 288.0391 $[M+H]^+$; calculated m/z: 287.0310).

5.2.1.15 Synthesis of intermediate ethyl (E)-3-(1,1,2-trimethyl-1H-benzo[e]indol-7-yl)acrylate [17]

The compound was synthesized by the slightly modified procedure as reported by [33].Added 7-bromo-1,1,2-trimethyl-1H-benzo[e]indole [16] 1.4 g (4.8 mmol) in High pressure reaction tube with silicon gasket, to it 58 mg (0.192 mmol) of $P(O\text{-}tol)_3$ and $Pd(OAc)_2$ 10 mg (0.048 mmol) were added, followed by 4 ml trimethylamine, ethyl acrylate 0.84 ml (7.2 mmol) and 20 ml DMF. The reaction mass was heated at 130 ^{0}C for 10-12 hrs. under pressure. Cool the reaction mass to room temperature, Reaction progress was monitored by TLC. Thereafter Ethyl acetate was used to extract the product. After evaporating the solvent the crude product was purified by column chromatography with ethyl acetate-hexane. 900 mg of the titled compound was collected as a solid in 60.4 % yield. HRFAB- MS (measured m/z: 309.0507 $[M+H]^+$; calculated m/z: 307.1572).

5.2.1.16 Synthesis of intermediate (E)-3-dodecyl-7-(3-ethoxy-3-oxoprop-1-en-1-yl)-1,1,2-trimethyl-1H-benzo[e]indol-3-ium [18]

900 mg (2.93 mmol) of ethyl (E)-3-(1,1,2-trimethyl-1H-benzo[e]indol-7-yl) acrylate [17] and 1.0 ml (4.39 mmol) of 1-Iodododecane was dissolved in 20 ml Propionitrile and the mixture was refluxed under nitrogen for 48 hrs. in a round bottom flask fitted with a reflux condenser. After the complete consumption of the starting material, confirmed by TLC. Solvent and the excess of 1-Iodododecane were removed by evaporation under vacuum. Product was precipitated out in diethyl ether. 710 mg of titled compound was obtained as solid in 51.07 % Yield. HRFAB- MS (measured m/z: 477.3660 $[M+H]^+$; calculated m/z: 476.3523).

5.2.1.17 Synthesis of intermediate (Z)-4-((3-dodecyl-7-((E)-3-ethoxy-3-oxoprop-1-en-1-yl)-1,1-dimethyl-1H-benzo[e]indol-3-ium-2-yl)methylene)-2-ethoxy-3-oxocyclobut-1-en-1-olate [19]

710 mg (1.49 mmol) of (E)-3-dodecyl-7-(3-ethoxy-3-oxoprop-1-en-1-yl)-1,1,2-trimethyl-1H-benzo[e]indol-3-ium [18] and 1 equivalent of 3,4-Diethoxy-3-cyclobutene-1,2-dione 0.22 ml (1.49 mmol) was taken in 25 mL ethanol, followed by 5 equivalent of trimethylamine 1.04 ml (7.45 mmol) was added in a round bottom flask fitted with condenser. Reflux the reaction mass for 12 hrs., which soon turned to yellow color. Reaction monitoring was done by TLC. Evaporated the solvent under a vacuum. Extracted the crude product with ethyl acetate followed by thoroughly washing with distilled water and brine. Combined ethyl acetate layer was dried under vacuum and performed column chromatography with 20 % Ethyl acetate: Hexane. The solvent was removed to get the titled compound as a yellow powder in 76.1 % yield (680 mg). FAB-mass (measured m/z: 600.3679 $[M+H]^+$; calculated m/z: 599.3611).

5.2.1.18 Synthesis of intermediate (Z)-4-((7-((E)-2-carboxyvinyl)-3-dodecyl-1,1-dimethyl-1H-benzo[e]indol-3-ium-2-yl)methylene)-2-hydroxy-3-oxocyclobut-1-en-1-olate [20]

To a 50 ml round bottom flask, 680 mg (1.13 mmol) of (Z)-4-((3-dodecyl-7-((E)-3-ethoxy-3-oxoprop-1-en-1-yl)-1,1-dimethyl-1H-benzo[e]indol-3-ium-2-yl) methylene)-2-ethoxy-3-oxocyclobut-1-en-1-olate [19] was dissolved in 20 ml ethanol followed by 5 equivalent 4 N NaOH was added and refluxed for 1 h. Reaction progress was monitored was by TLC, the reaction mixture was cooled and the solvent was evaporated under vacuum. After complete evaporation

of the solvent, the reaction mixture was acidified by diluted HCl and crude product was extracted in chloroform and washed by brine. 500 mg of the desired compound was collected as a yellow solid in an 81.1 % yield.

5.2.1.19 Synthesis of Unsymmetrical Squarine dye SQ-162

500 mg (0.92 mmol) of (Z)-4-((7-((E)-2-carboxyvinyl)-3-dodecyl-1,1-dimethyl-1H-benzo[e]indol-3-ium-2-yl)methylene)-2-hydroxy-3-oxocyclobut-1-en-1-olate [20] and 298 mg (0.92 mmol) of 5-(diethoxyphosphoryl)-1-ethyl-2,3,3-trimethyl-3H-indol-1-ium (i) synthesized by our previous work [34] was dissolved in 30 mL of 1:1 toluene/n-butanol in a round bottom flask fitted with condenser,. Refluxed the reaction mass for 6-8 hrs. Reaction progress was monitored by TLC, evaporated the solvent and the crude product was purified with column Chromatography using chloroform methanol solvent as eluent. 250 mg of the desired compound [26] was collected as a blue solid in 31.7 % yield. HR-FAB-MS (measured m/z: 849.4593 $[M+H]^+$; calculated m/z: 848.4529). NMR (500 MHz, CDCl3): δ/ppm = 8.02(d,H-4); 7.89(s,H-7); 7.85(d,H-8); 7.81(d,H-5); 7.47(s,H-45); 7.45(d,H-47); 7.39(d,H-9); 7.28(d,H-15); 7.23(d,H-48); 7.16(d,H-14); 7.15(s,H-32); 6.90(s,H-37); 6.40(q,H-52 and H-54); 4.08(q,H-49); 3.88(t,H-20); 3.67(s, H-43 and H-44); 3.65(s,H-18 and H-19), 2.29(t,H-50); 1.54(m,H-21 to H-30),1.19 (t,H-53 and H-55), 0.79 (t,H-31).

After the hydrolysis of, 250 mg (0.29 mmol) of intermediate (Z)-4-((7-((E)-2-carboxyvinyl)-3-dodecyl-1,1-dimethyl-1H-benzo[e]indol-3-ium-2-yl)methylene)-2-(((Z)-5-(diethoxyphosphoryl)-1-ethyl-3,3-dimethylindolin-2-ylidene)methyl)-3-oxocyclobut-1-en-1-olate [21] by using 0.038 ml (0.29 mmol) of Bromotrimethylsilane (TMS-Br) in 10 mL of Dichloromethane (DCM) in round bottom flask. The reaction mixture was stirred at room temperature (RT) for 12 hrs. Reaction progress was monitored by TLC using 10% MeOH: chloroform as a mobile phase. Thereafter the reaction was quenched by MeOH and solvent was evaporated and the crude product was purified with column chromatography using a chloroform-methanol solvent system. 80 mg of the titled compound was collected as a blue solid in 34.3 % yield.

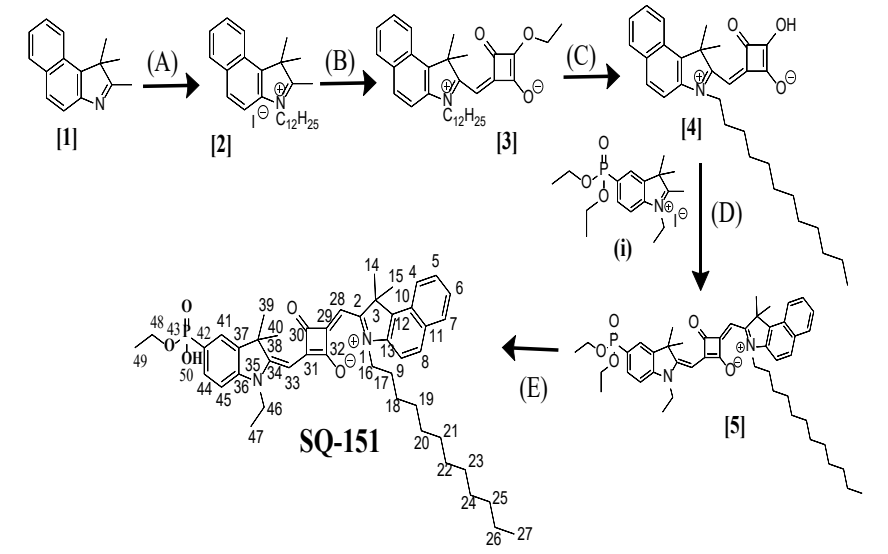
(A)
(B)
(C)
(D)
(E)
[1]
[2]
[3]
[4]
[5]
(i)
SQ-151

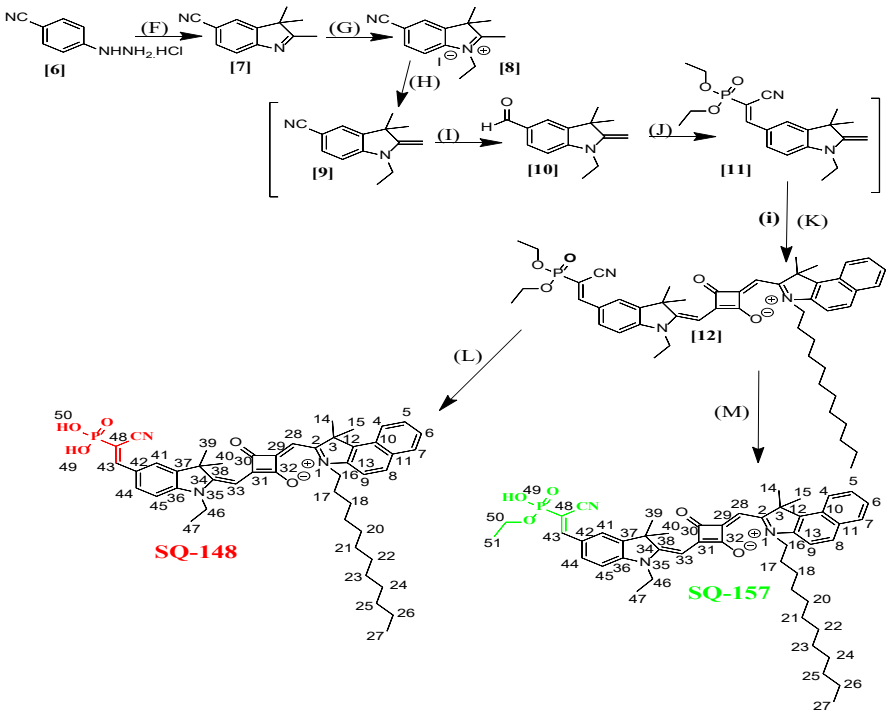
(F)
(G)
(H)
(I)
(J)
(K)
(L)
(M)
(i)
[6]
[7]
[8]
[9]
[10]
[11]
[12]
SQ-148
SQ-157

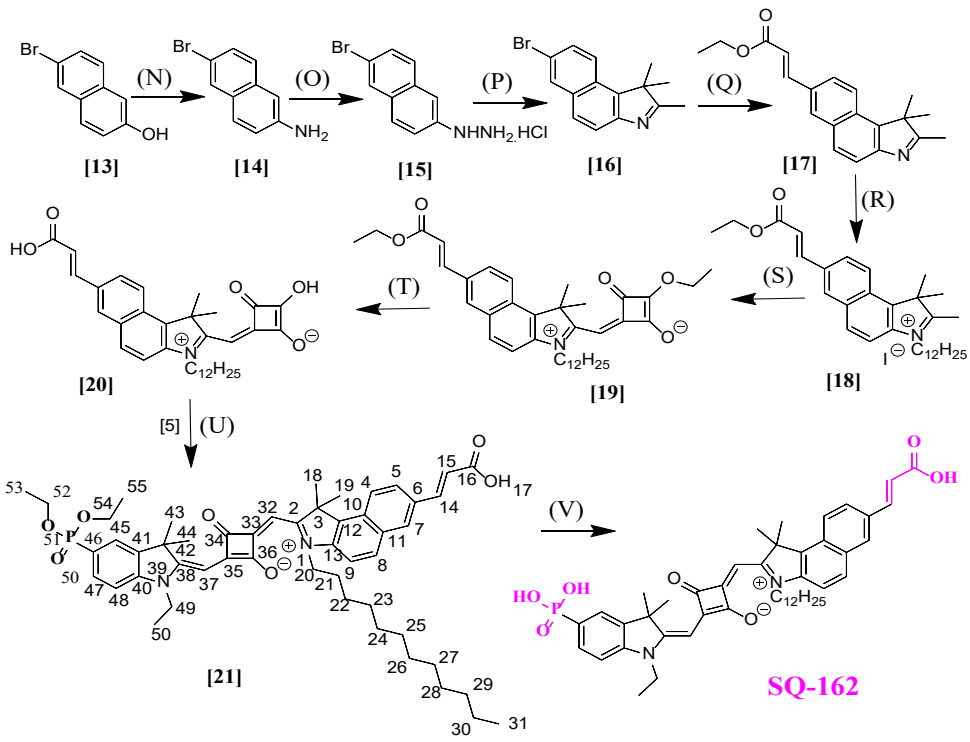

Scheme-1. Synthetic scheme for the preparation of unsymmetrical squaraine dyes bearing different anchoring groups. (A) 1-Iodododecane, Propionitrile, Reflux/ 26 h. (B) 3, 4-Diethoxy-3-cyclobutene-1, 2-dione, Triethylamine, Ethanol, Reflux/15 h. (C) 4 N NaOH, Ethanol, Reflux/2 h. (D) n-Butanol: Toluene (1:1). (E) TMS-Br, DCM, RT 36 hrs. (F) 3-Methyl-2-butanone, Ethanol, Acetic acid, Reflux, 12 hrs (G) 1-Iodoethane, Acetonitrile, Reflux, 24 hrs (H) 2N NaOH, Toluene, RT, 2 hrs (I) DIBAL, DCM, RT, 12 hrs (J) Diethylcyanomethylphosphonate, Piperidine, Acetonitrile, Reflux, 7-8 hrs (K) n-Butanol: Toluene (1:1). (L) Bromotrimethylsilane (1 eq.), DCM, RT, 36 hrs (M) Bromotrimethylsilane (0.5 eq.), DCM, RT, 36 hrs (N) NaHSO3, Liq. Ammonia, High pressure reaction tube, 150 ^{0}C, 24 hrs (O) $NaNO_2$, $SnCl_2$, Conc. HCl, 0^{0}C, 12 hrs (P) 3-Methyl-2-butanone, Acetic acid, Reflux, 12 hrs (Q) Ethyl acrylate, Pd(OAc)2, P(O-tol)3, TEA, DMF, High Pressures reaction tube, 130^{0}C, 10-12 hrs (R) 1-Iodododecane, Propionitrile, Reflux, 48 hrs (S) Diethylsquarate, TEA, Ethanol, Reflux, 12 hrs (T) 4N NaOH, Ethanol, Reflux, 1hr (U) n-butanol, Toluene, Reflux, 6-8hrs (V) Bromotrimethylsilane, DCM, RT, 12 hrs.

5.2.2 Structural elucidation

Structure elucidation of the dye is the process of determining the chemical structure of a compound from the identification and characterization of the intermediates and the finished products. Nuclear magnetic resonance (NMR) spectroscopy is a very sensitive method for characterizing the stereo- chemical structure. Structure elucidation of the squaraine dyes used in this work has been done by nuclear magnetic resonance (NMR) spectroscopy and mass spectrometry.

In this work structural elucidation was performed, and the final dyes were analyzed in the deuterated chloroform ($CDCl_3$) by NMR spectrometer (JEOL, 500 MHz) and the intermediates were confirmed by Matrix-Assisted Laser Desorption and Ionization (MALDI)-Time-of-Flight (TOF)-mass or Fast Ion Bombardment (FAB)-mass spectrometry in the positive ion-monitoring.

5.2.3 Dye Adsorption behavior

4 μm thick PST-30NRD transparent TiO_2 paste (1 cm^2 area) was coated on the glass substrate for investigating the dye adsorption behavior. TiO_2 coated glass substrate was then dipped in 0.1 mM ethanolic solution of the respective dyes and extent of dye adsorption as a function of time (until saturation) as shown in the figure-2 was monitored spectrophotometrically by measuring the absorbance of dyes at their absorption maximum (λ_{max}).

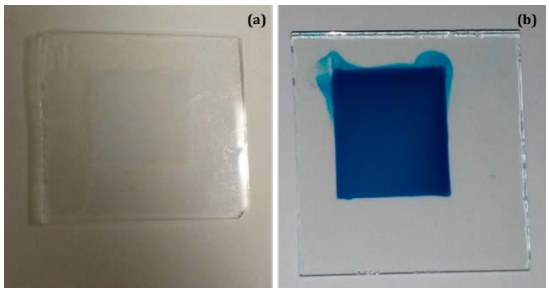

Figure-2. 4 μm thick and 1 cm^2 area PST-30NRD TiO_2 for the dye adsorption behavior (a) before dye adsorption and (b) after complete dye adsorption.

5.2.4 Electrochemical characterization

The electrochemical stability of the sensitizing dyes is an important criterion for the functioning of the solar cell. Upon light irradiation electrons of the molecule excites from their Highest Occupied Molecular Orbital (HOMO) to the Lower Unoccupied Molecular Orbital (LUMO). For the best energy matching, LUMO should be higher than the conduction band of the semiconductor TiO_2 and HOMO should be lower than the electrode potential of the redox electrolyte.

HOMO was estimated from the first oxidation peak of the dye concerning the Ferrocene reference by the cyclic voltammetry method. Cyclic voltammetry (CV) has been widely used in DSSC research for electrochemical characterization and HOMO estimation. The estimation of the HOMO from this method is more reliable and all HOMO values are nearly similar to the

theoretical HOMO values which were calculated by TD-DFT using 6-311 G/B3PW91. In this work, CV of unsymmetrical squaraine dyes (0.2 mM concentration) was recorded in Dimethylformamide (DMF) solution along with ferrocene (0.2 mM concentration) reference standard using a similar electrode, tetrabutylammonium hexafluorophosphate (0.1M) as the supporting electrolyte and scan rate, which is shown in the Figure-3. This could be attributed to the stabilization of molecular orbitals upon the introduction of functional groups with electron-withdrawing nature. In this work, a potential corresponding to 1st oxidation wave of the dyes has been used to estimate the HOMO energy level of dyes. The shift in oxidation potential of the dyes concerning the oxidation potential of Fc/Fc^+ redox couple was used to calibrate the HOMO energy level of dyes concerning the vacuum level. To conduct the CV, the respective dyes (0.2 mM) were dissolved in dimethylformamide (DMF) with tetrabutylammonium hexafluorophosphate (0.1M) as the supporting electrolyte. The HOMO value of the dyes was calculated from the shift in the oxidation peak concerning the Fc/Fc^+, whose value was taken as -5.01 eV as per the report by Su and Girault [35]. HOMO energy level of the dyes thus calculated was used to construct the energy band diagram of dyes.

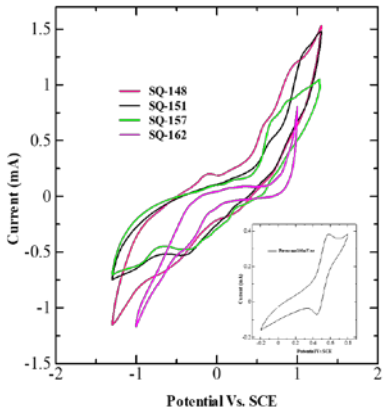

Figure-3. Cyclic Voltammetry of the unsymmetrical squaraine dyes and ferrocene as a reference standard in DMF recorded using Pt working/counter electrode and saturated calomel electrode (SCE) as a reference electrode.

5.2.5 Dye adsorption stability

4 µm thick transparent TiO_2 paste (PST-30 NRD) of 1 cm^2 area was coated on the glass substrate by screen printing followed by sintering at 500°C for the investigating the dye adsorption behaviour on mesoporous TiO_2. TiO_2 coated glass substrate was then dipped in 0.1 mM solution of the respective dyes and the extent of dye adsorption as a function of

time (until saturation) was monitored spectrophotometrically by measuring the absorbance of dyes at their absorption maximum (λ_{max}). Stability behaviour and amount of adsorbed dyes were investigated using glass substrate coated with mesoporous TiO_2 paste (D/SP, Solaronix) having an area of 6.25 cm^2 and thickness of ~10 μm by screen printing followed by sintering at 500^0C. TiO_2 coated glass substrates were dipped in 0.2 mM ethanolic solution of the respective dyes until complete dye adsorption. The relative stability of these dyes on the TiO_2 was studied by putting the adsorbed dye TiO_2 substrate in the solvent mixture of acetonitrile and water (1:1) at room temperature and monitoring the extent of dyes desorbed from substrate to the solution after a definite time interval. Quantitation of the desorbed dyes was carried out spectrophotometrically using standard calibration curves of the respective dyes. The remaining dyes on the mesoporous TiO_2 were then completely desorbed and quantitated using 40 mM NaOH solution in t-butanol, acetonitrile, Water, and ethanol solution were taken in the 1:1:1:1 volume ratio.

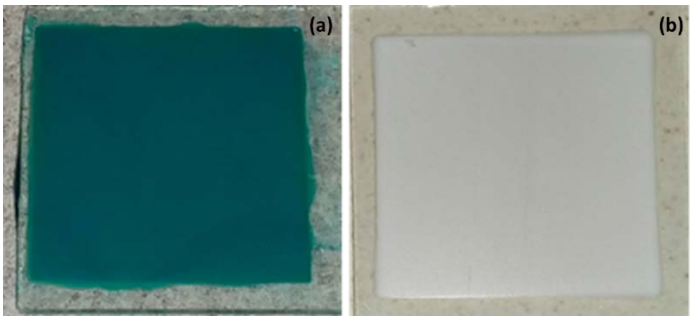

Figure-4. Mesoporous TiO_2 for the dye adsorption stability (a) after complete dye adsorption and (b) after complete dye desorption.

5.2.6 Device fabrication and characterization

Photo anode was prepared using Fluorine doped Tin oxide (FTO) coated glass as a transparent conducting substrate. FTO was coated with Anatase Titania nanoparticle (15-20 nm, D/SP paste, Solaronix) by screen-printing followed by sintering at 500^0C for 1 hr and this process was repeated to attain the thickness of the mesoporous TiO_2 ~10 μm. After sintering the substrate was then dipped into the solution of 0.2 mM of the respective dyes

along with 20 mM of the de-aggregating agent chenodeoxycholic acid (CDCA) in dehydrated ethanol to preventing dye aggregation. Surface treatment of FTO and mesoporous TiO_2 was conducted using 40 mM of Titanium chloride in water at 70°C for 1 hour followed by sintering at 500^0C for 30 min. A catalytic Pt sputtered FTO glass was used as the counter electrode. Iodine based redox electrolyte consisted of Lithium iodide (0.1 M), iodine (0.05 M), t-butyl pyridine (0.5 M), 1,2-dimethyl-3-propylimidazolium iodide (0.6 M) in dehydrated acetonitrile was used for the regeneration of the oxidized dye. Redox Electrolyte was injected through a diagonal hole between the photoanode and counter electrode, which was finally sealed using 20 μm hot melt spacer (Solaronix Meltonix 1170-25) and UV curing resin 3017 exposed under UV light. Photovoltaic Performance of the solar cells was evaluated using a solar simulator (CEP-2000 Bunko Keiki Co. Ltd, Japan) equipped with a xenon lamp (Bunko Keiki BSO-X150LC) used as a source of simulated solar irradiation at 100 mW/cm^2, AM 1.5G. The light intensity of the solar simulator was calibrated with an amorphous silicon photodetector (Bunko Keiki BS-520 S/N353). During the photovoltaic measurement, the 0.25 cm^2 active area was precisely controlled using a black metal mask.

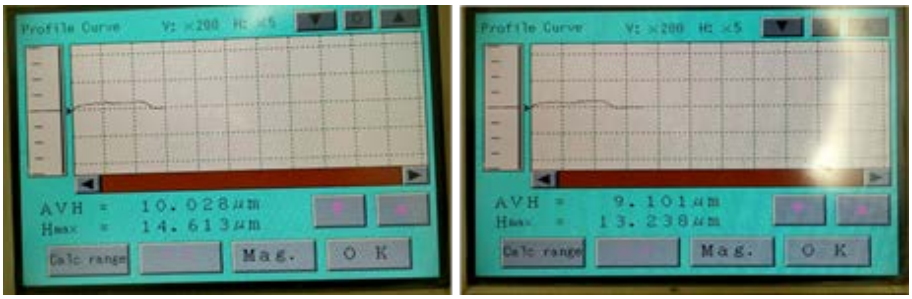

Figure-5. Thickness of the theTiO_2 paste working electrode

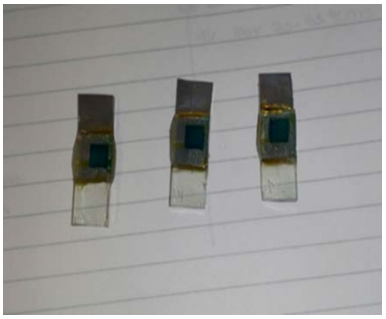

Figure-6. Dye-sensitized solar cells made in the lab.

5.3 Results and discussion

5.3.1 Optical characterizations

Electronic absorption spectra of unsymmetrical squaraine dyes in the ethanol solution have been shown in Figure-7 along with the summarization of the optical parameters after absorption and emission spectral investigations in table 1. It can be seen from this figure that they exhibit intense and narrow light absorption with a high molar extinction coefficient ($\varepsilon>10^5$ dm^3 mol^{-1} cm^{-1}). This is associated with the π-π* electronic transition appearing in the wavelength window of 500 nm-700 nm with vibronic shoulders between 600 nm-630 nm, exhibiting typical characteristics of the squaraine dyes. Normalized absorption spectra of dyes in ethanol solution as shown in the inset reveals that expect SQ-151 bearing ethyl phosphonate anchoring group, all of the other dyes exhibited red-shifted absorption maximum (λ_{max}). This is attributed to the extension of π-conjugation of dye molecules facilitated by the anchoring groups since the main dye molecular framework was the same in all the cases as can be seen from the molecular structure of the dyes shown in Figure- 1. Owing to the largest extent of π-conjugation dye SQ-148 bearing cyanoacrylate and SQ-157 anchoring group exhibited the largest bathochromic shift with λ_{max} at 670 nm.

It worth mentioning here about intriguing absorption spectral feature of dye SQ-162 bearing phosphonic and acrylic acid double anchoring groups, where not only vibronic shoulder has been pronounced but also evolved as a clear peak indicating highly enhanced intermolecular interactions similar to that of typical dye aggregation observed after their adsorption on mesoporous TiO_2 in the solid-state. The ratio of this shoulder versus the main peak associated with monomeric dye has been widely utilized to represent the extent of dye aggregation (aggregation index). This ratio has been found to increase upon their adsorption on the TiO_2 and utilization of dye de-aggregating agent CDCA has been reported to suppress this ratio [36-37]. Apart from the electronic absorption spectral measurements, Fluorescence emission spectra of the dyes in the same ethanolic solution were also measured, which has been shown in Figure-7 as respective dotted lines along with the summarization of deduced parameters in table 1.

5.3.2 Fluorescence emission spectra

Square dyes are also known to strong fluorescence intensity. Fluorescence emission spectra of these dyes were also recorded in the ethanol solution and shown in Figure-7 along with the summarization of optical parameters in Table 1. A perusal of the emission spectra of the investigated dyes is not only the mirror images of their respective absorption spectra but also a very small Stokes Shift of only 3 nm-14 nm (305 cm^{-1} to 930 cm^{-1}). Such a small Stokes Shift is also a typical characteristic of the squaraine dyes bearing a rigid molecular framework and represents their conformational stability in the excited state. This is further supported by the fact that introducing flexible moieties in the rigid molecular framework led to enhancement in the Stokes shift for a variety of organic dyes [38].

Sensitizing Dye	ε ($dm^3.Mol^{-1}.cm^{-1}$)[a]	Abs^{orb} (nm)	Em_{max}[c] (nm)	Stokes shift[ed] (nm)	Abs_{max}[e] (nm) (On TiO_2)	E_{opt}[f] (eV)
SQ-151	1.36×10^5	652 nm	662 nm	10 nm	650 nm	687 nm (1.80 eV)
SQ-148	1.68×10^5	668 nm	676 nm	8 nm	680 nm	734 nm (1.68 eV)
SQ-157	2.02×10^5	668 nm	680 nm	12 nm	669 nm	705 nm (1.75 eV)
SQ-162	1.18×10^5	665 nm	668 nm	3 nm	664 nm	741 nm (1.67 eV)

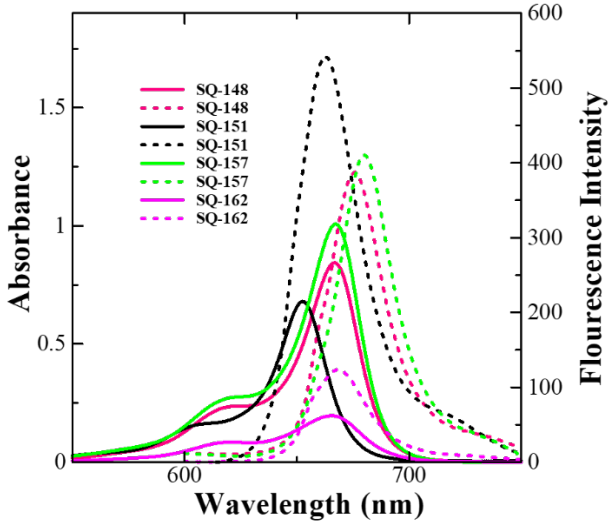

Figure-7. Electronic absorption (solid line) and fluorescence emission (dotted line) spectra of unsymmetrical squaraine dyes in ethanol solution.

Table-1. Optical parameters for unsymmetrical squaraine dyes in ethanol solution and on a thin film with dye adsorbed on TiO_2. [a] Molar extinction coefficient of dyes in ethanol solution. [b] electronic absorption maxima of dyes in the ethanol solution. [c] Fluorescence emission maxima of dyes in the ethanol solution. [d] Stokes shift was estimated from the separation between the absorption maximum and emission maximum. [e]Absorption maximum of dyes adsorbed on a thin film (4 μm) of mesoporous TiO_2. [f] Optical absorption edge (E_{opt}) was estimated from the onset wavelength of the solid-state electronic absorption spectrum of the respective dyes adsorbed on a thin layer of mesoporous TiO_2.

5.3.3 Theoretical molecular orbital calculations

The recent past has witnessed the widespread utilization of density functional theory (DFT) under quantum chemical calculation for the development of novel sensitizing dye molecules of DSSCs aiming towards the prior prediction of the energetics and electronic absorption spectra [39]. The beauty of the DFT calculations lies in the fact that it considers the lone pair electronic correlation similar to the ab-initio method at relatively much computational cost like Hartree-Fock. The introduction of the Time-dependent (TD) as an improvisation of DFT has been reported to provide very reliable results of the electronic absorption spectra in the presence of standard correlation functional under the Gaussian program [40]. In this work, the first structural optimization of the unsymmetrical squaraine dyes under investigation was carried out using 6-311G basis set, DFT, and B3PW91 functional by Gaussian G09 program. We have already demonstrated that utilization and B3PW91 and LSDA functional in a combination of polarization continuum model (PCM) [41] provided a very good correlation between the theoretically calculated and experimental values about not only the HOMO energy level but also the λ_{max} of the electronic absorption spectra [42-43].

It can be also clearly seen that theoretically calculated values of HOMO energy level shown in Figure-8 exhibit an excellent correlation with the experimentally determined valued utilizing CV further validating the reliability of the theoretical MO calculation. Electron density distribution in the HOMOs and LUMOs of the unsymmetrical squaraine after TD-DFT calculation are shown in the Figure. A perusal of this figure corroborates that electron density in the HOMO in all of the cases is mainly present on the squaraine core. On the other hand, in the corresponding Lumos, there is a clear shift of

electron density distribution from the central squaraine core to the outer indole ring bearing the different anchoring groups with the highest diversion of the electronic density especially in the case of dye SQ-148 bearing cyanophosponic acid and SQ-157 cyanophosphonate anchoring group. Such a shift in the electron density from the HOMO to LUMO of a molecule is an indicator of the intramolecular charge transfer (ICT) and sufficient diversion of the electron density at the anchoring group ensures the good electronic coupling between the excited dye molecules and the 3d-orbital of the TiO_2 ensuring facile injection of electrons from the excited dye molecule to CB of TiO_2. The strong electron-withdrawing nature of cyanophosponic as compared to that of Phosphonic acid favours the relatively enhanced ICT in the case of dye SQ-148 and SQ-157 as compared to that of SQ-151 indicating facile electron injection and better photon harvesting as a sensitizer of the DSSC. Similarly, SQ-162 bearing Phosphonic acid on one side and acrylic acid anchoring group on another side are expected to work as relatively better sensitizers as compared to that SQ-148 and SQ-157 bearing acrylic acid anchoring group owing to the enhanced ICT.

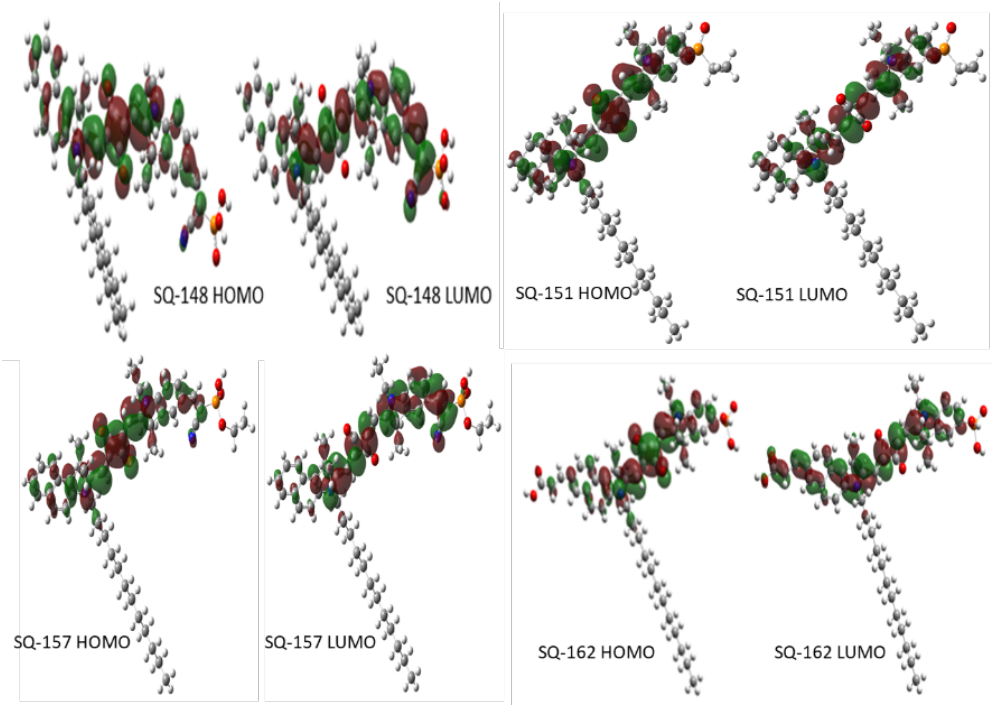

Figure-8. Electron density distribution in the calculated HOMO (bottom) and LUMO (top) orbitals of the unsymmetrical squaraine dyes after structural optimization using B3PW91 functional under the TD-DFT and 6-311G basis set.

5.3.4 Dye Adsorption behavior

4 μm thick transparent TiO_2 paste (PST-30 NRD) of 1 cm^2 area was coated on the glass substrate by screen printing followed by sintering at 500^0C for the investigating dye adsorption behavior on mesoporous TiO_2. TiO_2 coated glass substrate was then dipped in 0.1 mM ethanolic solution of the respective dyes and the extent of dye adsorption as a function of time (until saturation) was monitored spectrophotometrically by measuring the absorbance of dyes at their absorption maximum (λ_{max}). Sensitizing dyes are adsorbed onto the surface of wide bandgap semiconductors via suitable chemical linkage and the nature of this not only controls the electron injection but also imparts stability to the DSSCs. Therefore, optimal adsorption of sensitizing dyes on the mesoporous TiO_2 is one of the most important steps for the fabrication of photoanode of DSSCs. Complete coverage of monolayer of sensitizing dyes on the TiO_2 nanoparticle is sufficient for the optimal performance of the photoanode. In-sufficient dye adsorption not only leads to hampered photon harvesting but also results in back electron transfer from electrons injected in TiO_2 and oxidized dye and electrolyte [44]. An excess amount of the adsorbed dye leads to unwanted dye aggregation resulting in poor electron injection [45]. Structure of the dye molecules, nature of the anchoring group, and their interaction with the TiO_2 defines the adsorption behavior and binding strength of the sensitizer dye on mesoporous TiO_2.

In this work, the effort was also directed to investigate the adsorption behavior of NIR dyes bearing different types of functional groups involved for anchoring on the TiO_2 nanoparticles. The extent of the dye molecules and their interaction with TiO_2 in the solid-state is responsible for the optimal functioning of the photoanodes of DSSCs. Normalized electronic absorption spectra of unsymmetrical squaraine dyes bearing different anchoring groups and adsorbed onto the thin film of the mesoporous TiO_2 have been shown in the Figure-9 along with the summarization deduced optical parameters in table 1. It can be seen from this figure that upon adsorption to the TiO2, dyes exhibit not only a slight bathochromically shifted λ_{max} but also the spectral broadening associated with the enhanced intermolecular interactions aggregation of dye molecules on to the surface depending on the nature of anchoring groups. Extended broadening especially towards the lower wavelength region in combination with a higher ratio indicates a higher extent of dye aggregation [46]. In line with solution-based absorption spectra, dyes like SQ-148 exhibited red-shifted absorption owing to the overall extended π-conjugation. At the same

dyes SQ-148 bearing cyanophosponic groups, respectively, exhibited the highest dye aggregation with an aggregation index of about 0.91. The incorporation of alkyl substituent suppresses the dye aggregation, which has been reflected by the dye SQ-157, where the aggregation index was found to be decreased to 0.61 as compared to its non-alkyl substituted dye counterpart SQ-148 (0.91). Interestingly, it is worth mention here that dye SQ-162 bearing double anchoring groups (acrylic and phosphonic acids) has not only exhibited narrow spectral broadening but also a highly diminished aggregation index of only 0.51. This could be attributed to the dual binding mode on the TiO_2 via both of the anchoring groups simultaneously restricts the inter-dye interactions amongst themselves leading to hampered dye aggregation on the TiO_2 surface.

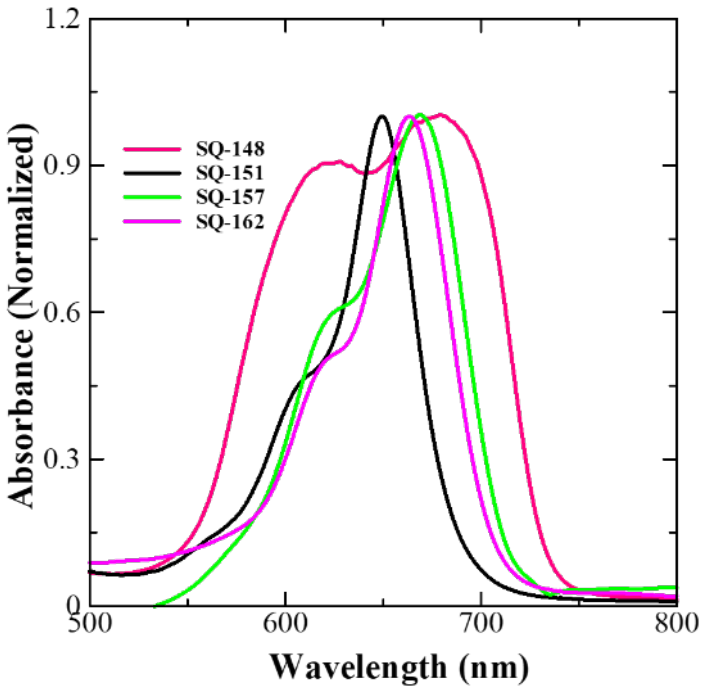

Figure-9. Normalized solid-state absorption spectra of squaraine dyes adsorbed on mesoporous TiO_2.

Figure-9 depicts the adsorption behavior of unsymmetrical squaraine dyes with a different type of anchoring groups on TiO_2. Adsorption of the squaraine dyes was conducted using 4 mm thick mesoporous TiO_2 (PST-30NRD, Solaronix) from the 0.1 mM ethanolic solution of the respective dyes at room temperature. It can be seen that the nature of the anchoring group highly affects the dye aggregation behavior, SQ-148 bearing cyano phosphonic acid and SQ-157 bearing

ethylcyano phosphonate as an anchoring group are highly prone to the H-aggregation (90.84%) and (61.08%) respectively as shown in the figure-10 and table-2 as compare to the other sensitizers. This could be attributed to the enhanced dye aggregation due to H-aggregate formation associated with promoted hydrogen bonding interactions. Kim et al. have also emphasized that some squaraine surfactants easily form blue-shifted H-aggregates on TiO_2 surfaces absorbing around 500 nm wavelength region [47].

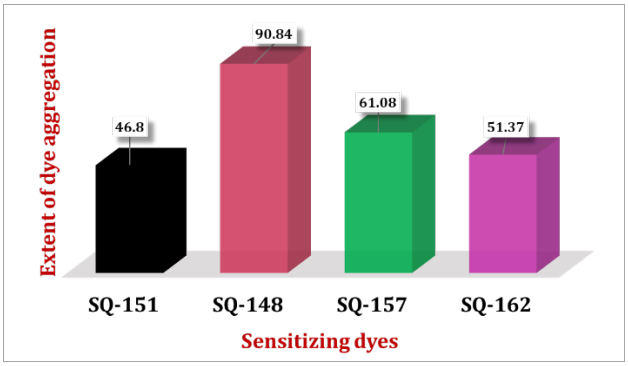

Figure-10. The extent of dye aggregation of squaraine dyes on mesoporous TiO_2.

Table-2. The extent of dye aggregation of unsymmetrical squaraine dyes on thin-film mesoporous TiO_2.

Sensitizing dye	Aggregation (%)
SQ-148	90.84
SQ-151	46.8
SQ-157	61.08
SQ-162	51.37

This also can be explained because contrary to the cyano phosphonic acid groups of the dyes SQ-148 and its corresponding ethyl ester analog sensitizer SQ-157 are highly prone to H-aggregation. From figure-10 and table-2. It is highly worth mentioning here that in-spite of sufficient electron density in the LUMO, SQ-162 which bearing acrylic acid and phosphonic acid dual anchoring group exhibit less aggregation (51.37 %) as compared to other sensitizers. On the other hand, in the previous chapter as we noticed, SQ-143 containing Phosphonic acid as an anchoring group does not have good electron density in its LUMO and the extent of dye aggregation in this dye was 78.23% whereas its corresponding analog sensitizer SQ-151 containing one –OH group exhibit less extent of dye aggregation.

Change in the absorbance peak of the respective dyes after different time intervals of the dye adsorption considered as the rate of dye adsorption. Kinetics of dye adsorption by monitoring the absorbance at the λ_{max} of respective dyes for different time intervals which have been shown in Figure 11. A perusal from this figure corroborates that squaraine dyes bearing Cyano phosphonic acid (SQ-148) adsorb more swiftly as compared to ethylcyanophosphonate (SQ-157), ethyl phosphonate (SQ-151), and dual anchored sensitizer phosphonic acid and acrylic acid (SQ-162). And the rate of dye adsorption follows the order Cyano phosphonic acid > ethylcyanophosphonate > ethyl phosphonate > dual anchored sensitizer phosphonic acid and acrylic acid. Adsorption of sensitizing dyes starts with activation of the OH groups on the TiO_2 surface by functional group present on the dye via protonation followed by chemical bonding.

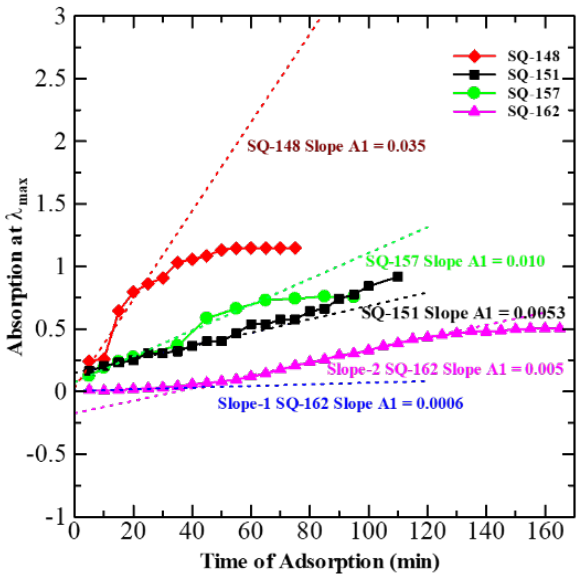

Figure-11. Kinetics of dye adsorption by monitoring the absorbance at the λ_{max} of respective dyes for different time intervals.

As an industrial prospects of DSSC, Swift adsorption of dye molecules on mesoporous wide bandgap semiconductor and strong binding is highly desired. The implication of the nature of anchoring groups on their adsorption behavior on the thin films of mesoporous TiO_2 was conducted by monitoring the extent of adsorbed dyes as a function of time spectrophotometrically as shown in figure-12.

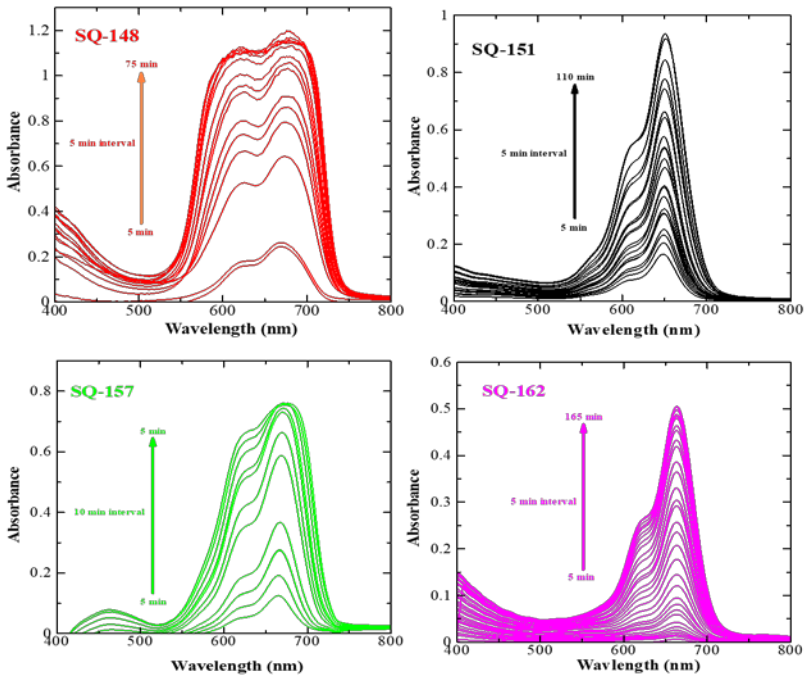

Figure-12. Time-dependent dye adsorption of unsymmetrical Squaraine dyes.

5.3.5 Dye Adsorption stability

Glass substrate was coated with mesoporous TiO_2 paste (D/SP, Solaronix) having an area of 6.25 cm^2 and thickness of ~15 µm by screen printing followed by sintering at 500^0C for investigating the stability behaviour and amount of adsorbed dyes. TiO_2 coated glass substrates were dipped in 0.2 mM ethanolic solution until complete dye adsorption. The relative stability of these dyes on the TiO_2 was studied by putting the dye adsorbed TiO_2 substrate in the solvent mixture of acetonitrile and water (1:1) at room temperature for define time. Quantitation of the desorbed dyes was carried out spectrophotometrically using standard calibration curves of the respective dyes. The remaining dyes on the mesoporous TiO_2 were then completely desorbed and quantitated using 40 mM NaOH solution in t-butanol, acetonitrile, Water, and ethanol solution were taken in the 1:1:1:1 volume ratio. To evaluate the rate of dye adsorption of unsymmetrical dyes on mesoporous TiO_2 was conducted on 4 µm thick and 1 cm^2 are of TiO_2 was dipped in the 0.1 mM dye solution and measured the absorbance with time spectrophotometrically. After the

calculation of the slope with a maximum co-relation factor rate of dye adsorption evaluated as shown in figure-11.

Results of dye desorption for the photo anodes fabricated using dyes bearing different anchoring groups are summarized in the table-3. A perusal of Table-3 corroborates that under identical conditions of dye desorption on TiO_2 sensitizing dyes exhibit differential binding strength on the mesoporous TiO_2 as estimated by the percentage removal dyes upon putting them into the acetonitrile-water mixture after a defined time. It is worth mentioning here that the weakest binding was exhibited by SQ-157 bearing ethylcyanophosphonate as an anchoring group (44.25 % removal) and SQ-151 (43.46 %) while SQ-162 bearing dual anchoring group phosphonic acid and acrylic acid, exhibited the strongest binding (0.182 % removal). This suggested that SQ-162, which is containing phosphonic acid and acrylic acid functional group exhibited the highest stability on the mesoporous TiO_2 as compared to dyes bearing other functional groups. It is very important to notice here that SQ-162 bearing acrylic acid and phosphonic acid dual anchoring group exhibits strongest binding strength as compare to SQ-148, SQ-151, and SQ-157 figure-15 and table -3.

Based on dye desorption studies conducted under identical experimental conditions, relative binding strength from the table-3 on the mesoporous TiO_2 follows the order SQ-162 < SQ-148 <SQ-157< SQ-151.

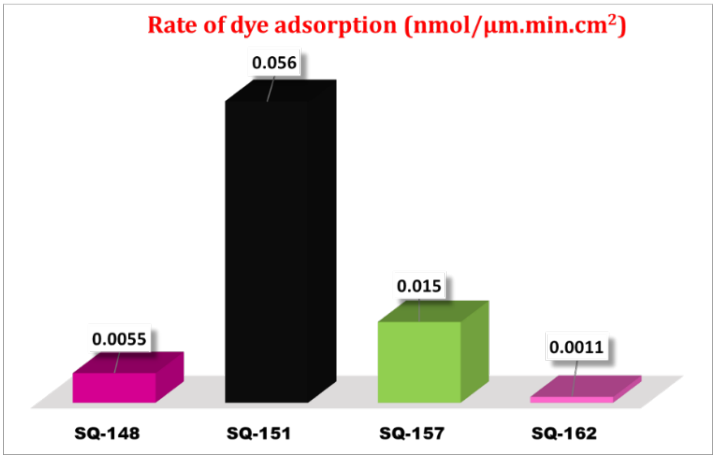

Figure-14. The binding strength of squaraine dyes on mesoporous TiO_2.

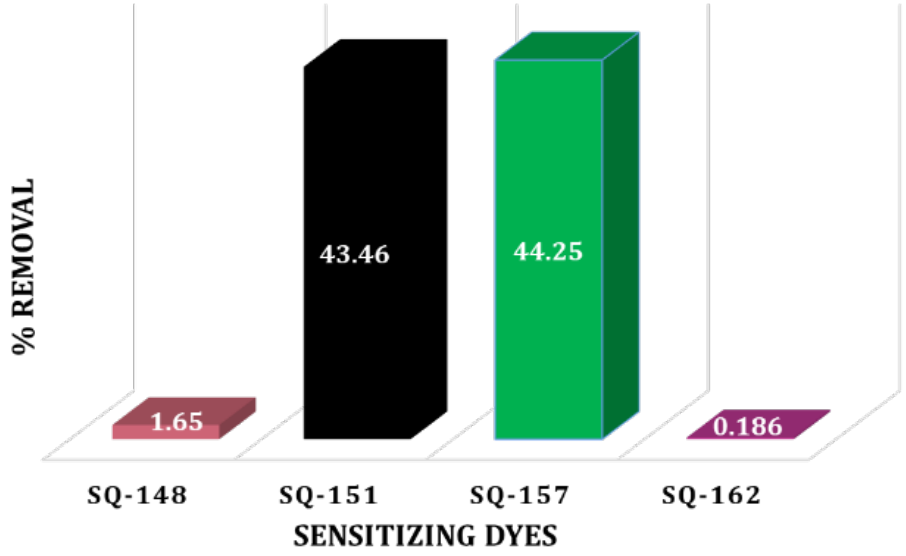

Figure-15. Amount of Dye loading on mesoporous TiO_2.

Table-3. Dye adsorption, desorption behavior, and anchoring stability of unsymmetrical squaraine dyes on the mesoporous TiO_2.

Dye	Rate of dye adsorption (Abs/min)	Rate of dye desorption (nmol/µm.min.cm^2)	Total dye loading (nmol/µm.cm^2)	Amount removed in 30 min (nmol/cm^2) (@ 10 µm Thickness)	Total dye loading (nmol/cm^2) (@ 10 µm Thickness)	% Removal
SQ-148	3.5×10^{-2}	0.0055	10.04	1.66	100.4	1.65
SQ-151	0.53×10^{-2}	0.056	3.92	17.04	39.2	43.46
SQ-157	1.0×10^{-2}	0.015	1.01	4.47	10.1	44.25
SQ-162	Slope-10.06×10^{-2} Slope-20.5×10^{-2}	0.0011	19.27	0.352	192.7	0.182

SQ-148

Partial Desorption	Complete desorption
Slope= 0.119	
➢ Abs at λ_{max}= 0.907 ➢ Volume Used= 20 ml ➢ Time= 180 min ➢ 0.119=1 µM = 0.907/0.119 =7.62 µM = 7.62 µM/lit = 7.62 nmol/ml = 7.62 nmol/ml × 20 ml **Partial Desorption = 152.43 nmol**	➢ Abs at λ_{max}= 1.643 ➢ Volume Used= 100 ml ➢ 0.119=1 µM = 1.643/0.119 = 13.80 µM = 13.80 µM/lit = 13.80 nmol/ml = 13.80 nmol/ml × 100 ml **Complete desorption = 1380.67 nmol**

➢ Total Amount of dye = Partial Desorption + Complete desorption
= 152.43 nmol + 1380.67 nmol
= 1533.10 nmol
Area of the device= 6.25 cm^2
Total Amount of dye = **245.29 nmol/cm^2**
Thickness of the device = 24.43 µm
Total Amount of dye = **10.04 nmol/µm.cm^2**

➢ Rate of dye Desorption
Partial desorption=152.43 nmol
Time= 180 min
Rate of dye Desorption = **0.85 nmol/min**
Area of the device= 6.25 cm^2
Rate of dye Desorption = **0.135 nmol/ min. cm^2**
Thickness of the device = 24.43 µm
Rate of dye Desorption = **0.0055 nmol/ µm. min. cm^2**

% Removal =152.43 nmol/1533.10 nmol × 100
= **9.94 %**

SQ-151

Partial Desorption	Complete desorption
Slope= 0.153	
➢ Abs at λ_{max}= 1.48 ➢ Volume Used= 30 ml ➢ Time= 60 min ➢ 0.153=1 µM = 1.48/0.153 =9.67 µM = 9.67 µM/lit = 9.67 nmol/ml = 9.67 nmol/ml × 30 ml **Partial Desorption = 290 nmol**	➢ Abs at λ_{max}= 0.337 ➢ Volume Used= 20 ml ➢ 0.153=1 µM = 0.337/0.153 =2.20 µM = 2.20 µM/lit = 9.67 nmol/ml = 9.67 nmol/ml × 20 ml **Complete desorption = 44.05 nmol**

➢ Total Amount of dye = Partial Desorption + Complete desorption
290 + 44.05 nmol
= 334.05 nmol
Area of the device= 6.25 cm^2
Total Amount of dye = **53.44 nmol/cm^2**
Thickness of the device = 13.61 µm
Total Amount of dye = **3.92 nmol/µm.cm^2**

➢ Rate of dye Desorption
Partial desorption=290 nmol
Time= 60 min
Rate of dye Desorption = **4.83 nmol/ min**
Area of the device= 6.25 cm^2
Rate of dye Desorption = **0.77 nmol/ min. cm^2**
Thickness of the device = 13.61 µm
Rate of dye Desorption = **0.056 nmol/ µm. min. cm^2**

% Removal =290 nmol/334.05 × 100
= **86.81 %**

SQ-157

Partial Desorption	Complete desorption
Slope= 0.218	
➢ Abs at λ_{max}= 1.193 ➢ Volume Used= 30 ml ➢ Time= 60 min ➢ 0.218=1 µM = 1.193/0.218 = 5.47 µM = 5.47 µM/lit = 5.47 nmol/ml = 5.47 nmol/ml × 30 ml **Partial Desorption = 164.17 nmol**	➢ Abs at λ_{max}= 0.237 ➢ Volume Used= 20 ml ➢ 0.218=1 µM = 0.237/0.218 = 1.087 µM = 1.087 µM/lit = 1.087 nmol/ml = 1.087 nmol/ml × 20 ml **Complete desorption = 21.74 nmol**

➢ Total Amount of dye = Partial Desorption + Complete desorption
= 164.17 nmol + 21.74 nmol
= 185.91 nmol
Area of the device= 6.25 cm^2
Total Amount of dye = **29.74 nmol/cm^2**
Thickness of the device = 29.36 µm
Total Amount of dye = **1.01 nmol/µm.cm^2**

➢ Rate of dye Desorption
Partial desorption=164.17 nmol
Time= 60 min
Rate of dye Desorption = **2.73 nmol/min**
Area of the device= 6.25 cm^2
Rate of dye Desorption = **0.437 nmol/ min. cm^2**
Thickness of the device = 29.36 µm
Rate of dye Desorption = **0.015 nmol/µm. min. cm^2**

% Removal =164.17 nmol/185.91 nmol × 100
= **88.30 %**

SQ-162

Partial Desorption	Complete desorption
Slope= 0.0354	
➢ Abs at λ_{max}= 0.0368 ➢ Volume Used= 20 ml ➢ Time = 180 min 0.0354 =1 µM = 0.0368/0.0354 = 1.04 µM = 1.04 µM/lit = 1.04 nmol/ml = 1.04 nmol/ml × 20 ml **Partial Desorption = 20.79 nmol**	➢ Abs at λ_{max}= 1.326 ➢ Volume Used= 50 ml 0.0354 = 1 µM = 1.326/0.0354 = 37.46 µM = 37.46 µM/lit = 37.46 nmol/ml = 37.46 nmol/ml × 50 ml **Complete desorption = 1872.88 nmol**

➢ Total Amount of dye = Partial Desorption + Complete desorption
= 20.79 nmol + 1872.88 nmol
= 1893.67 nmol
Area of the device= 6.25 cm^2
Total Amount of dye = **302.98 nmol/cm^2**
Thickness of the device = 15.72 µm
Total Amount of dye = **19.27 nmol/µm.cm^2**

➢ Rate of dye Desorption
Partial desorption=20.79 nmol
Time= 180 min
Rate of dye Desorption = **0.12 nmol/min**
Area of the device= 6.25 cm^2
Rate of dye Desorption = **0.0184 nmol/min. cm^2**
Thickness of the device = 15.72 µm
Rate of dye Desorption = **0.0011 nmol/µm. min. cm^2**

% Removal =20.79 nmol/1893.67 nmol × 100
= **1.09 %**

Figure-18. Detailed calculation of the dye adsorption, dye desorption, and amount of dye loading.

5.3.6 Energy band diagram

Energetics cascade amongst the wide bandgap semiconductor, redox electrolyte, and sensitizer is one the important requirements for the DSSC working cycle. Energy band diagram for the DSSC utilizing mesoporous TiO_2 as wide bandgap semiconductor, unsymmetrical squaraine dyes under investigation and most commonly used iodine-based electrolyte (I^-/I_3^-) has been shown in the Figure-16. To construct this band diagram, the energy of conduction band (CB) of the TiO_2 and energy level of (I^-/I_3^-) redox electrolyte was considered as -4.00 eV and -4.90 eV, respectively as the values reported in the literature [48-49]. HOMO energy level of squaraine dyes was estimated from the shift in 1st oxidation potential of the dyes concerning the ferrocene redox couple. It can be seen from this figure that all of the unsymmetrical squaraine dyes used in work possess favorable energetics about the CB of TiO_2 and redox energy level of the I^-/I_3^- electrolyte indicating thermodynamically favorable conditions for electron injection of the photoexcited dyes along with the regeneration of the oxidized dye molecules by the redox electrolyte. A very good correlation of the theoretically calculated values of HOMO energy by TD-DFT calculations with that of experimentally observed values of HOMO energy estimated from cyclic voltammetry validates reliability theoretical calculations discussed in detail in the next section.

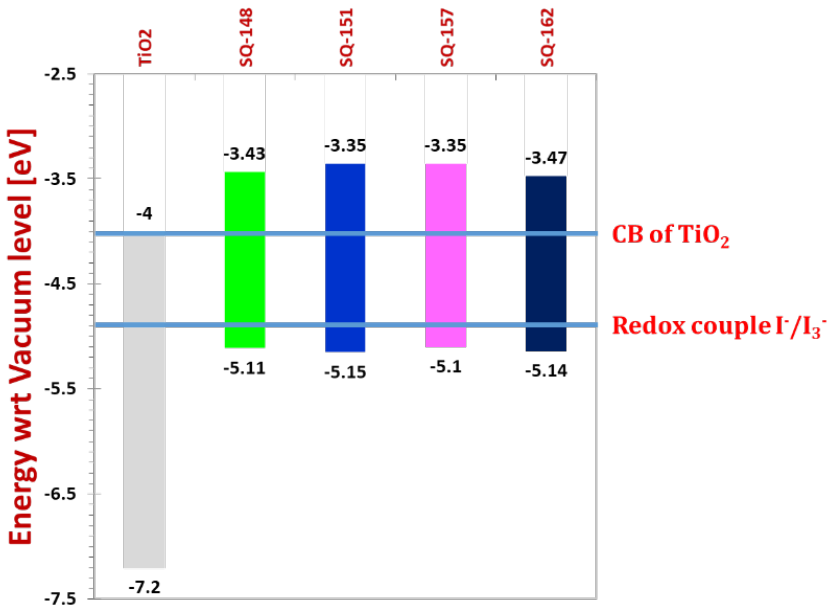

Figure-16. Energy band diagram for the unsymmetrical squaraine dyes under investigation.

5.3.7 Photovoltaic properties

The presence of the anchoring group, the high extinction coefficient of dyes, and their suitable energetic cascade with the CB of TiO_2 and I^-/I_3^- redox electrolyte justified their suitability as sensitizers for the DSSC. To investigate the influence of the nature of anchoring on photovoltaic behaviour, they were used as sensitizers to fabricate the photoanode after their adsorption onto the mesoporous TiO_2. Photoanodes were fabricated using unsymmetrical squaraine dyes under investigation keeping other variables such as dye concentration, the concentration of the CDCA, dye adsorption time, and redox electrolyte. Photovoltaic characteristics of DSSCs based unsymmetrical squaraine dyes after simulated solar irradiation of 100 mW/cm^2 has been shown in Fig. 17(A) along with the summarization of the photovoltaic parameters such as short-circuit current density (Jsc), open-circuit voltage (Voc), fill factor (ff) and PCE in table 3.

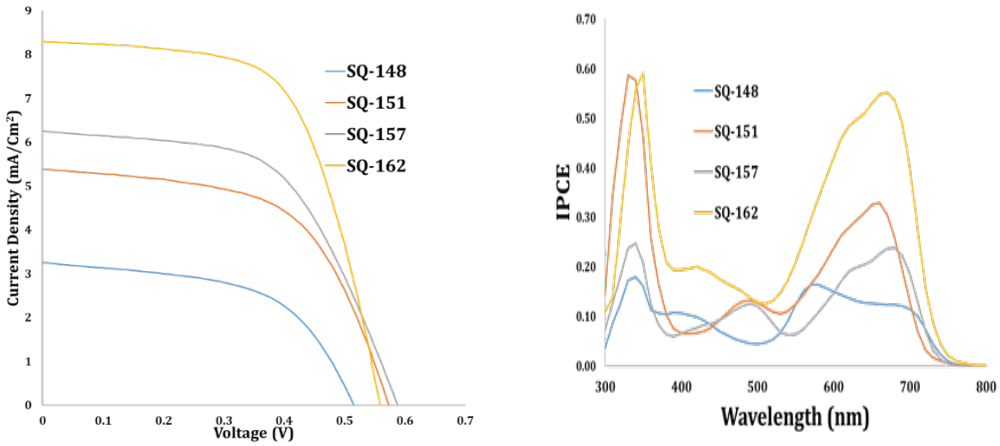

Figure 17. Photovoltaic characteristics of DSSCs fabricated using squaraine dyes under 1 Sun simulated solar irradiation (A) and photocurrent action spectra of the same after monochromatic light illumination (B).

It can be seen from this figure-17 and table-3 that DSSC fabricated using SQ-162 bearing dual anchoring groups i.e., acrylic acid and phosphonic acid shows the best performance with the PCE of 2.87% having Jsc of 8.28 mA/cm^2, Voc of 0.56 V, and FF of 0.62. This high Jsc is associated with very good photon harvesting mainly in the far-red to NIR wavelength region with maximum incident photon to the current conversion efficiency of

55.2 % at 670 nm as reflected by the photocurrent action spectra shown in the Figure-17 (B). This could be attributed to the good energetic matching (Figure-16) very good ICT and the highest diversion of the electron density clouds in LUMO (Figure-8). Apart from the good PCE SQ-162 which bearing dual anchoring groups shows very good stability on TiO_2 as well. Other sensitizers like SQ-148 (cyano phosphonic acid) and Phosphonate based (SQ-151 and SQ-157) anchoring group although exhibited very good and strong binding with TiO_2 but relatively poor ICT and non-planer nature of the anchoring group, enhanced dye aggregation are bottlenecks of the facile electron injection leading to hampered photon harvesting. Although, alkyl substation in phosphonate anchoring group (SQ-151 and SQ-157) resulted in suppressed dye aggregation leading to improved PCE supported by enhanced IPCE but their relatively slow rate of dye adsorption and hampered binding strength with TiO_2 poses a question mark on the implementation of this concept for design and development of novel NIR dyes with improved efficiency and stability.

Dye	JSC (mA/cm^2)	VOC (V)	FF	PCE (%)
SQ-151	5.38	0.57	0.57	1.77
SQ-148	3.24	0.51	0.55	0.93
SQ-157	6.25	0.58	0.56	2.07
SQ-162	8.28	0.56	0.62	2.87

Table-3 Photovoltaic parameters for DSSCs fabricated using various unsymmetrical squaraine dyes under 1 Sun solar irradiation.

Unsymmetrical squaraine dye SQ-162 bearing acrylic acid and phosphonic acid as anchoring groups seems to be a good balance in terms of favorable ICT, relatively good electronic coupling with TiO_2 for facile electron injection, and good binding strength with TiO_2. At the same time, it a good PCE of about 2.87 %, which is although higher than all other dyes considered in this work. TD-DFT calculations for this dye shown in Figure-8 also exhibited a slightly lower diversion of electron density in the LUMO as compared to that SQ-148, which is attributed to slightly hindered electron injection. SQ-162 bearing double anchoring group exhibited extremely high binding with TiO_2, which >550 times stronger than cyano acrylic anchoring group. At the same time, observed PCE of about 2.87 % is highly boosted as compared to SQ-148 with free Phosphonic acids (0.9 %) and slightly lower than SQ-139 bearing single acrylic acid. Therefore, the design of SQ-162 offers

good hope for the further refinement of the molecular structure utilizing the main molecular framework with extended π-conjugation design and development of novel NIR sensitizers with further improvement in PCE while maintaining the stronger binding strength with TiO_2 leading stable and efficient DSSCs.

5.4 Conclusion

In summary, novel unsymmetrical squaraine dyes bearing different anchoring groups with special emphasis on phosphonate anchoring groups were successfully synthesized, characterized, and subjected to Photophysical investigation utilizing, electronic absorption spectroscopy, fluorescence emission spectroscopy, cyclic voltammetry, construction of energy band diagram. Investigation of dye adsorption behavior on the mesoporous revealed introduction of ethyl substituent in the phosphonate anchoring group resulted in hampered dye adsorption rate. Estimation of adsorption rate under identical experimental conditions on mesoporous TiO_2 exhibited the dye adsorption rate following the order of SQ-162> SQ-148>SQ-157>SQ-151. Anchoring group-dependent binding strength indicated that these dyes exhibit binding strength following the order SQ-162>SQ-148>SQ-157>SQ-151. Newly designed dye SQ-162 bearing phosphonic acid and acrylic acid double anchoring groups highest binding strength at TiO_2 surface, which is >550 times stronger than best-performing dye SQ-140 bearing cyanoacrylic acid functional group. Finally, SQ-162 has emerged as one of the potential dyes with extremely high binding strength without having serious compromise at the cost of loss in PCE.

References

1. H. Lund and B. V. Mathiesen, *Energy*, 2009, 34, 524.
2. A. M. Omer, *J. Agric. Ext. Rural Dev*., 2010, 2, 001.
3. N. F. Voudoukis, *European Journal of Electrical and Computer Engineering*, 2018, 2, 1.
4. M. Freitag, J. Teuscher, Y. Saygili, X. Zhang, F. Giordano, P. Liska, J. Hua, S. M. Zakeeruddin, J-E. Moser, M. Grätzel and A. Hagfeldt, *Nature Photonics*, 2017, 11, 372.
5. B. O'Regan and M. Grätzel, *Nature,* 1991, 353, 737-740.
6. M.S. Ahmad, A.K. Pandey, N. Abd. Rahim, *Renewable and Sustainable Energy Reviews*, 2017, 77, 89-108.
7. J. Wu, Z. Lan, J. Lin, M. Huang, Y. Huang, L. Fan, and G. Luo, *Chem. Rev.* 2015, 115, 2136–2173.
8. J. Wu, Z. Lan, J. Lin, M. Huang, Y. Huang, L. Fan, G. Luo, Y. Lin, Y. Xie and Y. Wei, *Chem. Soc. Rev.,* 2017, 46, 5975-6023.
9. A. Mishra, M.K.R. Fischer, P. Bäuerl, *Angew. Chem. Int. Ed. Engl*, 2009, 48, 2474–2499.
10. M. K. Nazeeruddin, F. De Angelis, S. Fantacci, A. Selloni, G. Viscardi, P. Liska, S. Ito, B. Takeru and M. Grätzel, *J. Am. Chem. Soc.* 2005, 127, 16835.
11. A. Yella, H.W. Lee, H. N. Tsao, C. Yi, A. K. Chandiran, Md. K. Nazeeruddin, E. W.G. Diau, C.Y. Yeh, S.M. Zakeeruddin, and M. Grätzel, *Science*, 2011, 334, 629-633.
12. K. Kakiage, Y. Aoyama, T. Yano, T. Otsuka, T. Kyomen, M. Unno and M. Hanaya, *Chem. Commun*., 2014, 50, 6379-6381.
13. S. Mathew, A. Yella, P. Gao, R. H. Baker, B. F. E. Curchod, N. A. Astani, I. Tavernelli, U. Rothlisberger, Md. K. Nazeeruddin and M.Grätzel, *Nature Chemistry*, 2014, 6, 242–247.
14. L. Zhang, X. Yang, W. Wang, G. G. Gurzadyan, J. Li, X. Li, J. An, Z. Yu, H. Wang, B. Cai, A. Hagfeldt, and L. Sun, *ACS Energy Lett*. 2019, 4, 943–951.
15. A. Islam, Md. Akhtaruzzaman, T. H. Chowdhury, C. Qin, L. Han, I. M. Bedja, R. Stalder, K. S. Schanze, and J. R. Reynolds, *ACS Appl. Mater. Interfaces*, 2016, 8, 4616–4623.
16. A. Pradhan, MS. Kiran, G. Kapil, S. Hayase, SS. Pandey, *Solar Energy Materials and Solar Cells*, 2019, 195, 122-133.
17. AK. Baranwal, T. Shiki, Y. Ogomi, SS. Pandey, T. Ma, S. Hayase, *RSC advances*, 2014, 4, 47735-47742.

18. G. M. Shivashimpi, SS. Pandey, R. Watanabe, N. Fujikawa, Y. Ogomi, Y. Yamaguchi, S. Hayase, *Journal of Photochemistry and Photobiology A: Chemistry,* 2014, 273,1– 7.
19. T.N. Murakami, E. Yoshida, N. Koumura, *Electrochimica Acta,* 2014, 131, 174–183.
20. L. Zhang and J. M. Cole, *ACS Appl. Mater. Interfaces,* 2015, 7, 3427–3455.
21. B.J. Brennan, M.J.L. Portole's, P.A. Liddell, T.A. Moore, A.L. Moore, D. Gust, *Phys. Chem. Chem. Phys*., 2013, 15, 16605–16614.
22. K. Hanson, M.K. Brennaman, H. Luo, C.R.K. Glasson, J.J. Concepcion, W. Song, T.J. Meyer, *ACS Appl. Mater. Interfaces*, 2012, 4, 1462.
23. K. Kakiage, M. Yamamura, E. Fujimura, T. Kyomen, M. Unno, M. Hanaya, *Chem. Lett.,* 2010, 39(3), 260.
24. T. Higashino, S. Nimura, K. Sugiura, Y. Kurumisawa, Y. Tsuji, and H. Imahori, *ACS Omega*, 2017, 2, 6958−6967.
25. A. K. Vats, A. Pradhan, S. Hayase, SS. Pandey, *Journal of Photochemistry & Photobiology A: Chemistry,* 2020, 394,112467.
26. D.G. Brown, P.A. Schauer, J.B. Garcia, B.R. Fancy, C.P. Berlinguette, *J. Am. Chem. Soc.,* 2013, 135, 1692–1695.
27. Kim S, Han S. High-performance aquarium dyes for high-tech use. Color Technol 2001; 117:61–7.
28. S.A. Archer, T. Keane, M. Delor, E. Bevon, A.J. Auty, D. Chekulaev, I.V. Sazanovich, M. Towrie, A.J.H.M. Meijer, J.A., Chem. Eur. J. 23 (2017) 8239–18251.
29. T. N. Murakami, E. Yoshida, N. Koumura, Electrochimica Acta 131 (2014) 174–183.
30. G.M. Shivashimpi, S.S. Pandey, R. Watanabe, N. Fujikawa, Y. Ogomi, Y. Yamaguchi, S. Hayase, Journal of Photochemistry and Photobiology A: Chemistry *273 (2014) 1– 7.*
31. W. Pham, W.-F. Lai, R. Weissleder and C.-H. Tung, *Bio conjugate Chem*., 2003, 14, 1048-1051.
32. Y.H. Chen, L.W. Qi, F. Fang and B. Tan, *Angew. Chem.,* 2017, 56, 16308-16312.
33. J. Li, C.Y. Chen, W.C. Ho, S.H. Chen, and C.G. Wu. *ORGANIC LETTERS*, 2012, 14, 5420–5423.
34. A. K. Vats, A. Pradhan, S. Hayase, SS. Pandey, *Journal of Photochemistry & Photobiology A: Chemistry,* 2020, 394,112467.

35. B. Su, H.H. Girault, Absolute standard redox potential of monolayer-protected gold nanoclusters, J. Phys. Chem. B 109 (2005) 11427–11431.
36. J. H. Yum, S. J. Moon, R. H. Baker, P. Walter, T. Geiger, F. Nüesch, M. Grätzel and Md. K. Nazeeruddin, *Nanotechnology*, 2008, 19, 424005.
37. G.M. Shivashimpi, SS. Pandey, A. Hayat, N. Fujikawa, Y. Ogomi, Y. Yamaguchi, S. Hayase, *J. Photochem. Photobiol. A: Chemistry*, 2014, 289, 53-59.
38. T.B Ren, W. Xu, W. Zhang, X.X. Zhang, Z.Y. Wang, Z. Xiang, L. Yuan and X.B Zhang, *J. Am. Chem. Soc*. 2018, 140, 7716–7722.
39. M. Pastore, S. Fantacci and F. D. Angelis, *J. Phys. Chem. C*, 117, 2013, 3685–3700.
40. M. K. Nazeeruddin, F. D. Angelis, S. Fantacci, A. Selloni, G. Viscardi, P. Liska, S. Ito, B. Takeru and M. Gratzel, *J. Am. Chem. Soc.,* 2005, 127,16835–16847.
41. R. Improta and V. Barone, *J. Chem. Phys*., 2006, 125, 054103.
42. SS. Pandey, T. Morimoto, N. Fujikawa and S. Hayase, *Sol.Energy Mater. Sol. Cells*, 2017, 159, 625–632.
43. A. Pradhan, T. Morimoto, M. Saikiran, G. Kapil, S. Hayase and SS. Pandey*, J. Mater. Chem. A*, 2017, 5, 22672.
44. V. Johansson, L. E. Gibbings, T. Clarke, M. Gorlov, G.G. Andersson and L. Kloo, Physical Chemistry Chemical Physics, 16,711-718 (2014).
45. A. C. Khazraji, S. Hotchandani, S. Das, and P. V. Kamat, J. Phys. Chem., 103 (22), 4693-4700 (1999)
46. T. Inoue, SS. Pandey, N. Fujikawa, Y. Yamaguchi, S. Hayase, , *J. Photochem. Photobiol. A: Chem.,* 2010, 213, 23–29.
47. Y. S. Kim, K. Liang, K. Y. Law, and D. G. Whitten, J. Phys. Chem., 98 (3), 984-988 (1994
48. Li, Z.X Li, Y.L Xie, H. Xu. T.M. Wang, Z.G. Xu, and H.L. Zhang, *J.Photochem. Photobiol. A*, 2011, 224, 25-30.
49. Y. Ogomi, T. Kato, S. Hayase, *J. Photopolym. Sci. Technol*., 2006, 19, 403–408.

6. General Conclusions and Future Scope

6.1 General Conclusions

Design and development of novel NIR dyes with facile dye adsorption and strong binding on the wide bandgap semiconductors is highly desired for the development DSSCs with high PCE in combination with high device stability. Sensitizing dyes are one of the most important integral parts of DSSCs and can be regarded as the heart of this type of solar cell. It is well known that the nature of the anchoring groups of the sensitizing dye molecules not only controls the PCE by controlling the electron injection but also influences the device stability by controlling the strength of binding. Since many designed organic dyes involve multiple step synthesis and consume time, and there are huge structural possibilities, Quantum chemical calculations play a pivotal role in the design and development of novel dyes. They have been successfully utilized for the prediction of energetics, electronic coupling, and electronic absorption spectra and emerged as a potential tool for the development of novel sensitizers.

For quantum chemical calculations, Gaussian has emerged as a powerful tool for the computational molecular design for the prior prediction of the various physicochemical properties of materials. It has been demonstrated that as the judicial selection of the computational cost and accuracy of the predicted results utilizing 6-311G as a basis set, DFT for electron-pair correlation and B3PW91 as functional using PCM solvent can reliably predict the energetics, electronic absorption spectra, and energy bandgap in the case of NIR dyes. Using unsymmetrical squaraine dyes with varying anchoring groups, it has been shown that there is an excellent correlation between the energy of the HOMO and absorption maximum with only a difference of ± 0.06 eV in the λmax and ± 0.05 eV in the HOMO energy level between the theoretically predicted and experimentally observed values validating the reliability of the theoretical prediction for the design and development novel functional dyes.

After getting the feedback from QC calculations, six unsymmetrical NIR squaraine dyes keeping the same main molecular mother core but different anchoring groups such as carboxylic acid, acrylic acid, cyano acrylic acid, hydroxyl, sulfonic acid, and phosphonic acid were synthesized

characterized, and performed their photophysical and photovoltaic characterizations. Investigation of adsorption behavior of these dyes on mesoporous TiO_2 revealed the rate of dye adsorption following the order SQ-139 > SQ-140 > SQ-138 > SQ-143 > SQ-141 > SQ-142, while desorption studies indicated that binding strength on the mesoporous TiO_2 follows the order SQ-143 > SQ-141 > SQ-139 > SQ-142 > SQ-138 > SQ-140. Squaraine dye with phosphonic acid anchoring group exhibited the strongest binding strength as compared to other anchoring groups. Theoretical MO calculation about the electron density distribution in HOMO and LUMO indicated good ICT and the possibility of strong electronic coupling with TiO_2 for the dyes bearing −COOH (SQ-138) and –SO3H (SQ-142) functional groups, which is also supported by their relatively improved photovoltaic performance as compared to other anchoring groups. Despite very good dye loading, very high binding strength, and favorable energetic cascade, SQ-143 exhibited highly hampered photovoltaic performance as compared to that of SQ-138, SQ-139, and SQ-140, which was attributed to poor ICT and electronic coupling with TiO_2 as indicated by theoretical MO calculations. SQ-140 bearing cyanoacrylic acid as anchoring group emerged as the champion sensitizer in terms of photoconversion exhibiting of about 6 % under 1 sun solar irradiation.

To address the contrasting impact of the phosphonic acid anchoring group on the photoconversion and binding stability, novel unsymmetrical squaraine dyes bearing different anchoring groups with special emphasis on phosphonate anchoring groups were successfully synthesized, characterized, and subjected to Photophysical investigations. Investigation of dye adsorption behavior revealed that the introduction of ethyl substituent in the phosphonate anchoring group resulted in a hampered dye adsorption rate. Estimation of adsorption rate under identical experimental conditions on mesoporous TiO_2 exhibited the dye adsorption rate following the order of SQ-162> SQ-148>SQ-157>SQ-151. Anchoring group-dependent binding strength indicated that these dyes exhibit binding strength following the order SQ-162>SQ-148>SQ-157>SQ-151. Newly designed dye SQ-162 bearing phosphonic acid and acrylic acid double anchoring groups exhibited the highest binding strength at TiO_2 surface, which is >550 times stronger than the best-performing dye SQ-140 bearing cyanoacrylic acid functional group. Finally, SQ-162 has emerged as one of the potential dyes with extremely high binding strength without having serious compromise at the cost of loss in PCE.

6.2 Future Prospects

Research conducted for this thesis has demonstrated the usefulness of QC calculations towards the design and development of novel sensitizers. Judicious selection of proper calculation parameters led to the very reliable prediction of the energy of HOMO and LUMO, electronic absorption spectra, and energy band diagram. This combined theoretical and experimental approaches for the design and development of sensitizing molecules with an excellent match between the theory and experimental results are very helpful for the fast development of novel dyes.

It has been demonstrated that phosphonic acid as anchoring group binds >70 and >550 times stronger binding compared to that of most commonly used carboxylic acid and cyanoacrylic acid anchoring groups, therefore, utilizing double and multiple anchoring groups with different roles that one for strong binding and other of facile injection could be one of plausible solution for the design and development of novel dyes with improved PCE and stability. The design of novel dye SQ-162 bearing phosphonic acid and acrylic acid double anchoring groups with improved binding and electron injection is one of the demonstrations for this proof of concept.

The recent past has shown that anchoring groups like silatrane and silyl ester bind even stronger than phosphonic acid on the mesoporous TiO_2 and do not desorb for a very long time even after putting the dye adsorbed TiO_2 in water. Therefore, utilizing such a concept of multiple anchoring group's discrete and different roles could pave the way for further development of novel functional sensitizers with very stability while maintaining a good PCE. At the same time, utilization of the main dye mother core with more extended π-conjugation in combination with strong binding and efficiently injecting anchoring groups could pave the way for the realization of NIR dyes with high stability and high efficiency.

ACHIEVEMENTS

List of Publications:

1- **Ajendra Kumar Vats**, Anusha Pradhan, Shuzi Hayase, and Shyam S. Pandey* ***"Synthesis, Photophysical characterization and dye adsorption behavior in unsymmetrical squaraine dyes with varying anchoring groups"*** Journal of Photochemistry & Photobiology A: Chemistry.

2- **Ajendra Kumar Vats**, Anusha Pradhan, Shuzi Hayase, Shyam S. Pandey ***"Molecular Design of NIR Dyes with Varying Anchoring Groups: Photophysical Characterizations and Dye Adsorption Behavior on TiO_2"*** NICE Proceedings 2019.

3- Ali Khalifa, Suhaidi Shafie, WZWHasan, H.N.Lim, M.Rusop, S.S. Pandey, **Ajendra K. Vats**, HusseinA. AlSultan, Buda Samaila ***"Comprehensive performance analysis of dye-sensitized solar cells using single layer TiO2 photoanode deposited using a screen printing technique"*** Optik 223 (2020) 165595.

Title of Papers to be published:

4- **Ajendra Kumar Vats**, Linjun Tang, Shyam S. Pandey **"Unraveling the Bottleneck of Phosphonic Acid Anchoring Groups towards Stability and Efficiency by Logical Molecular Design using Squaraine based NIR Dyes"**, Journal of Materials Chemistry-A (Submitted).

5- **Ajendra Kumar Vats**, Linjun Tang, Gururaj M. Shivashimpi, Shuzi Hayase and Shyam S. Pandey, "***Synthesis and Photovoltaic Characterization of Symmetrical Squaraine Dyes with Extended π-conjugation for Dye-Sensitized Solar Cells"***, ChemSusChem (Under process).

Conference Presentations:

1- **Ajendra Kumar Vats**, Anusha Pradhan, and Shyam S. Pandey: ***Prediction of Nature of Anchoring Groups on Electron Density Distribution in NIR Dyes by Quantum Chemical Calculations***; 55th Kyushu Branch Chemical Society, Meeting, Kokura International Conference Centre, Kokura, Kitakyushu, Japan, 30 Jun 2018.

2- **Ajendra Kumar Vats,** Anusha Pradhan, Shuzi Hayase, and Shyam S. Pandey ***"Synthesis and Photophysical characterization of far-red sensitive squaraine dyes bearing different functional groups for anchoring on mesoporous TiO_2"*** The Japan Society of Applied Physics 2018, Nagoya, Japan

3- **Ajendra Kumar vats,** Anusha Pradhan, Shuzi Hayase & Shyam S Pandey ***"Implication of Dye Molecular Structure on Adsorption Behavior and Anchoring Stability Using NIR Sensitive Squaraine Dyes"*** 6th International Symposium on Applied Engineering and Sciences (SAES2018) Kyushu Institute of Technology, 15th – 16th Dec 2018.

4- **Ajendra Kumar Vats**, Anusha Pradhan, Shuzi Hayase, and Shyam S. Pandey *"**Synthesis, Characterization and Adsorption behavior of Unsymmetrical Squaraine Dyes Bearing Varying Anchoring Groups on Mesoporous TiO_2"*** Materials Research Society of Japan 2018, Kokura, Japan.

5- **Ajendra Kumar vats,** Anusha Pradhan, Gaurav Kapil, Shuzi Hayase & Shyam S Pandey *"**Synthesis and Characterization of NIR Dyes with Varying Anchoring Groups for Dye-Sensitized Solar Cells"*** The Chemical Society of Japan The 99th CSJ Annual Meeting, 2019, Okamoto Campus, Konan University, Kobe, Japan.

6- **Ajendra Kumar Vats**, Shuzi Hayase, and Shyam S. Pandey "***Implication of the Nature of Anchoring groups on Photophysical Behavior of NIR Dyes for Dye-Sensitized Solar Cells"*** EM-NANO 2019, JUNE 19-22, 2019 NAGANO JAPAN.

7- **Ajendra Kumar Vats**, Gaurav Kapil, Shuzi Hayase, and Shyam S. Pandey *"**Sensitization of Wide Band Gap Oxide Semiconductors by NIR Dyes with Varying Anchoring Groups for Molecular Photovoltaics."*** International Conference on Materials for Advanced Technologies (ICMAT)-2019 and IUMRS-ICA 2019 at Marina Bay Sands, Singapore, June 23- June 28 on dated 27 June 2019, Sym-h-09, (Flash Presentation followed by Poster).

8- N. Kumari, M. Pandey, R. K Gupta, **A. K. Vats**, S. Nagamatsu, S. Hayase and S. S. Pandey "***Alkyl-Chain Length Dependent Optical and Electronic Properties of Donor-Acceptor Copolymers"*** ICMAT 2019 and IUMRS-ICA 2019 at Marina Bay Sands, Singapore, June 23- June 28 on dated 27 June 2019, Sym-h-09, (Poster).

9- **Ajendra Kumar Vats**, Gaurav Kapil, Shuzi Hayase, and Shyam S. Pandey ***"Synthesis and Photovoltaic Characterization of NIR Sensitive Squaraine Dyes with Extended π-conjugation for Dye-Sensitized Solar Cells".*** Kyushu Branch Chemical Society 2019, Kokura, Japan

10- **Ajendra Kumar Vats**, Shyam S. Pandey *"**Design and Synthesis of Novel NIR Dyes with Phosphonic Acid-based Anchoring Groups for Dye-Sensitized Solar Cells"*** The Chemical Society of Japan 2020, Kobe, Japan

11- **Ajendra Kumar Vats**, Shuzi Hayase and Shyam S. Pandey ***"Design and Synthesis of Novel NIR Dyes with Phosphonic Acid Derivative Anchoring Groups Aiming Towards Stable Dye-Sensitized Solar Cells."*** Pacific Rim Meeting on Electrochemical and solid-state science (PRiME) 2020, October 4-9 2020 (Online)

12- **Ajendra Kumar Vats,** Pritha Roy, Linjun tang, Shyam S. Pandey ***"Design of Novel NIR Dyes Aiming Towards Improved Stability and Efficiency for Dye-Sensitized Solar Cells"*** 8th International Symposium on Applied Engineering and Sciences (SAES2020) Virtual Conference / 12th–19th December 2020

13- **Ajendra Kumar Vats**, Pritha Roy, Linjun Tang, and Shyam S. Pandey *"**Synthesis and Photophysical Characterizations of Novel NIR Dyes bearing Different Anchoring Groups with Extended π-Conjugation for Dye-Sensitized Solar Cells**"* Materials Research Society of Japan-2020

14- Epifanio D.R. Balane*, **Ajendra K. Vats** and Shyam S. Pandey ***"Natural Dye Extract using Blueberry as Dye Sensitizer for the Clean Solar Energy Harvesting"*** 8th International Symposium on Applied Engineering and Sciences (SAES2020) Virtual Conference / 12th–19th December 2020.

15- Epifanio D.R. Balane, **Ajendra K. Vats** and Shyam S. Pandey Natural ***"Dye-based Dye-Sensitized Solar Cells using Egg Plant and Cabbage Extracts"*** Materials Research Society of Japan-2020.

16- Linjun Tang, **Ajendra K. Vats** and Shyam S. Pandey ***"Highly Sensitive Pb^{2+} Ion Chemo-Sensor based on Newly Designed NIR Squaraine Dye"*** Materials Research Society of Japan-2020.

17- Linjun Tang, **Ajendra Kumar Vats**, Shyam S. Pandey ***"Synthesis and Photophysical Characterizations of Novel Dyes with Multiple Glycol Units Aiming Towards Chemical Sensing"*** 8th International Symposium on Applied Engineering and Sciences (SAES2020) Virtual Conference / 12th–19th December 2020.

18- Shubham Sharma, Nikita Kumari, **Ajendra K. Vats**, Moulika Desu, Shuichi Nagamatsu & Shyam S. Pandey ***"Investigating Influence of the Molecular Self-assembly on the Performance of Schottky Diodes Fabricated using Poly(3-Hexylthiophene)"*** Materials Research Society of Japan-2020.

19- Shubham Sharma, Nikita Kumari, **Ajendra Kumar Vats**, Yuki Kurokawa, Shuichi Nagamatsu, and Shyam S. Pandey ***"Unraveling the Impact of Molecular Orientation on the Device Performance in Organic Electronic Devices"*** 8th International Symposium on Applied Engineering and Sciences (SAES2020) Virtual Conference / 12th–19th December 2020.

20- Pritha Roy, **Ajendra Kumar Vats**, Shyam S. Pandey ***"Semitransparent Dye-Sensitized Solar Cells using Novel Blue Colored Unsymmetrical Squaraine Dyes"*** The Chemical Society of Japan 2020, Kobe, Japan.

21- Pritha Roy, **Ajendra Kumar Vats**, Shyam S. Pandey "***See Through and Transparent Dye-Sensitized Solar Cells Fabricated by Judiciously Selecting Sensitizers to Disguise the Eye Sensitivity***" Materials Research Society of Japan-2020.

22- Pritha Roy, **Ajendra Kumar Vats**, Shyam S. Pandey "***Influence of Color of Sensitizing Dyes on Transparency and Efficiency of Dye-Sensitized Solar Cells***" 8th International Symposium on Applied Engineering and Sciences (SAES2020) Virtual Conference / 12th–19th December 2020.

Awards:

1- **Best Presentation Award in Materials Research Society of Japan (MRS-J) 2018, Kokura, Japan-"***Implication of the Nature of Anchoring groups on Photophysical Behavior of NIR Dyes for Dye-Sensitized Solar Cells."*

2- **Best Presentation Award in Kyushu Branch Chemical Society (KBCS) 2019, Kokura, Japan-** *"Synthesis and Photovoltaic Characterization of NIR Sensitive Squaraine Dyes with Extended π-conjugation for Dye-Sensitized Solar Cells."*